

Colour Gamut Expansion with Spectral Imaging



Athanasios Papathanasiou

TECHNICAL UNIVERSITY OF CRETE

SCHOOL OF ELECTRICAL AND COMPUTER ENGINEERING

ELECTRONICS LABORATORY

OPTOELECTRONICS AND IMAGING DIAGNOSTICS

RESEARCH GROUP

This dissertation is submitted for the Master of Science diploma.

Chania, December 2018

THESIS COMMITTEE

Professor Costas Balas, *Supervisor*

Professor Minos Garofalakis

Professor Dionisios Pnevmatikatos

Acknowledgments

I would like to thank my supervisor Professor Costas Balas, firstly for the opportunity he gave me to join and work in his research group and secondly for his continuous support and scientific guidance during my Master thesis work. In addition, I would like to thank professor Minos Garofalakis and Dionisios Pnevmatikatos for participating in committee charge and for evaluating the scientific soundness of the thesis. I am also very grateful to my fellow colleagues and friends in Optoelectronic & Imaging Diagnosis Research Group, Kastinakis M., Dr. Kortsalioudakis N., Markelos D., Rossos C., Tsapras A., Vardoulakis E., Zografos P., for their guidance, support suggestions and cooperation.

Finally, yet most importantly, I wish to thank my family and close friends for their advice and support during my time of study.

In memory of my mother

Abstract

Latest developments in hyperspectral imaging devices, such as operational speed, size, accuracy and convenient use, has led to a broader range of applications involving such technologies. Colour reproduction is a critical procedure since colour is used in a wide variety of applications in order to communicate information. Colour capturing is the first and probably most crucial step in colour pipeline procedures. In order to achieve good performance on colour processing and rendering, consistent raw data are required. In this thesis, the colour capturing capabilities of image acquisition devices are discussed and evaluated. By performing experiments based on standardised methods we were able to compare the amount of digital colour inputs to the total chromaticities an average person sees. A spectral-based modification is proposed for improving the conventional colour capturing systems such as trichromatic colour cameras. This modification achieves higher scores, in terms of shape matching and common area coverage, of the transformed camera colour space versus the standardised human colour space. Moreover, a new procedure for calculating hyperspectral imager's colour gamut has also been proposed. By using this method, it is possible to measure the colour space of a hyperspectral device and optimise it in order to match perfectly the human-observable colour space. Finally, the results presented here made clear the dominance of the hyperspectral imaging procedure -as opposed to the conventional colour cameras- in capturing and interconnecting colour.

Table of contents

List of Abbreviations	8
List of Figures	9
List of Tables	11
1. Introduction	12
1.1 The Electromagnetic spectrum	12
1.2 Colour	14
1.2.1 The Eye – Colour Perception	14
1.2.2 CIE standards	17
1.2.3 Illuminants	20
1.2.4 Colour Spaces	20
1.2.5 Colour Gamut.....	23
1.2.6 Metamerism	24
1.3 Digital Still Cameras.....	26
1.3.1 Photoelectric Effect.....	26
1.3.2 CCD-CMOS	26
1.3.3 Operational Characteristics.....	28
1.3.4 Colour Digital Still Cameras	29
1.4 Spectral Imaging.....	30
1.5 Overview of the thesis.....	32
2. Measuring Digital Camera Spectral Sensitivity	33
2.1 DSC Acquisition Model	33
2.2 ISO 17321-1	34
2.3 Experimental Setup.....	35
2.4 Results	39
2.4.1 Camera Alone Results	39
2.4.2 DSC with Triple Bandpass Results.....	40
2.4.3 DSC with custom White Balance Setting	41
3. Calculating Digital Camera’s Colour Gamut	41
3.1 Luther condition.....	42
3.2 Gamut Calculation	43
3.3 Current Literature.....	45
3.3.1 Camera Gamut calculation through Colour matrix approximations.....	45

3.3.2	Expanding Colour Gamut by adding new colour channels.....	47
3.4	Methodology	48
3.4.1	Experiment Data - Processing	48
3.4.2	Gamut Calculation Conditions	48
3.4.3	Error Measures	48
3.5	Results	50
3.5.1	Camera-Alone Colour Gamut.....	50
3.5.2	Camera coupled with a Triple Bandpass Filter.....	55
3.5.3	Camera coupled with a Triple Bandpass Filter without channel crosstalk	57
3.5.4	Summary.....	60
4.	Spectral Imaging and Colour Gamut Expansion	63
4.1	Introduction	63
4.2	Why Colour from spectra is needed.....	64
4.3	Calculation of Tristimulus Values using Spectral Data.....	66
4.4	Methodology for Hyperspectral Imager Gamut Calculation.....	68
4.5	Colour Gamut of an Ideal Hyperspectral Imaging Device	69
4.6.1	The Muses9-HS.....	74
4.6.2	Experimental Setup.....	75
4.6.3	Results.....	76
4.6.4	Applying Luther condition to Muses9-HS	78
5.	Conclusion and Future Work	80
6.	References	82

List of Abbreviations

- EM:** Electromagnetic
- EMR:** Electromagnetic Radiation
- PE:** Photon Energy
- DSC:** Digital Still Camera
- SI:** Spectral Imaging
- NIR:** Near Infrared
- CCD:** Charge Coupled Device
- CMOS:** Complementary Metal Oxide Semiconductor
- CFA:** Colour Filter Array
- CMF:** Colour Matching Functions
- SPD:** Spectral Power Distribution
- FWHM:** Full Width Half Max
- FOV:** Field Of View
- ROI:** Region Of Interest
- LS:** Least Squares
- L1:** Manhattan Norm
- ED:** Euclidean distance
- ADC:** Analog to Digital Converter
- SMI:** Sensitivity Metamerism Index
- HS:** Hyperspectral
- MMB:** Metamer Mismatch Body
- PDF:** Probability Distribution Function
- TFM:** Tunable Filter Module

List of Figures

Figure 1.1: The electromagnetic spectrum	12
Figure 1.2: Specular and diffuse reflection	14
Figure 1.3: Basic illustration of eye's retinal anatomy	15
Figure 1.4: Normalised Cones and rods absorbance.	16
Figure 1.5: Diagram of the opponent process stage.	16
Figure 1.6: Approximate spectrum of colour for each colour processing stage.	17
Figure 1.7: Field of View for 2° and 10° Standard Observers.	18
Figure 1.8: CIE Standard Observer Experiment Overview.	18
Figure 1.9: Left: CIE 1931 RGB CMF. Right: CIE 1931 Standard Observer CMF [5]..	19
Figure 1.10: Normalised SPD per CIE Illuminant and Photopic Eye Response.	20
Figure 1.11: CIE 1931 colour space chromaticity diagram.	21
Figure 1.12: Various Colour Spaces relative to CIE's 1931 chromaticity diagram.	22
Figure 1.13: XYZ triangle coordinates and CIE'31 RGB primaries plotted on CIE'31 chromaticity diagram.	24
Figure 1.14: An example of metamerism. Different spectra could result to the same colour stimuli.	25
Figure 1.15: Metameric colours on different light sources.	25
Figure 1.16: Illustration of photoelectric effect. Different photon energies result to different electron escape velocities.	26
Figure 1.17: Photodetector Material Responsivities vs. Wavelength.	27
Figure 1.18: CCD and CMOS sensor differences on charge to voltage operation.	28
Figure 1.19: Relative Spectral Responses of Sony's IMX124 (Solid line) and IMX 135 (dashed line).	30
Figure 1.20: A Spectral Cube acquisition illustration from satellite imaging.	31
Figure 2.1: Illustration of the acquisition chain of a digital imaging system.	33
Figure 2.2: Certified Reflectance Standard from Ocean Optics.	36
Figure 2.3: ZWO ASI178MC colour DSC with Sony's IMX178 digital image sensor.	36
Figure 2.4: ThorLabs OSL-1-EC SPD.	37
Figure 2.5: ThorLabs OSL-1-EC Halogen with fiber optic.	37
Figure 2.6: Edmund Mini-Chrom Monochromator.	37
Figure 2.7: Edmund Mini-Chrom Transmittances. This work measurements proceed with Model C restricted to 800nm.	38
Figure 2.8: Colour DSC Spectral Sensitivity measurement setup.	38
Figure 2.9: ZWO ASI178MC Spectral Sensitivities as measured in Optoelectronics Lab.	39
Figure 2.10: Chroma 69010m Triple Bandpass filter transmission spectrum.	40
Figure 2.11: ZWO ASI178MC coupled with Chroma 69010m triple bandpass filter Spectral Sensitivities.	40
Figure 2.12: ZWO ASI178MC Spectral Sensitivities with custom WB setting.	41
Figure 3.1: Colour Gamut calculation results using indirect method[15].	44
Figure 3.2: ASI178MC Transformed Spectral Sensitivities T_{CAM} as calculated with LS method.	51
Figure 3.3: ASI178MC Transformed Spectral Sensitivities T_{CAM} comparing to CIE '31 CMF.	51

Figure 3.4: ASI178MC Colour Gamut plotted with CIE '31 Chromaticity diagram	52
Figure 3.5: The overlapped area between CIE '31 Chromaticity diagram and ASI178MC Colour Gamut.....	53
Figure 3.6: Colour gamuts of the same DSC with different WB settings.....	54
Figure 3.7: ASI178MC coupled with Chroma 69010m Triple Bandpass filter Transformed Spectral Sensitivities T_{CAM} comparing to CIE '31 CMF.....	55
Figure 3.8: The overlapped area between CIE '31 Chromaticity diagram and ASI178MC coupled with Chroma 69010m triple bandpass filter Colour Gamut.....	56
Figure 3.9: ASI178MC coupled with Chroma 69010m Spectral Sensitivities without channel crosstalk.	58
Figure 3.10: ASI178MC Transformed Spectral Sensitivities T_{CAM} comparing to CIE '31 CMF.	58
Figure 3.11: ASI178MC Transformed Spectral Sensitivities T_{CAM} comparing to CIE '31 CMF.	59
Figure 3.12: The overlapped area between CIE '31 Chromaticity diagram and ASI178MC coupled with Chroma 69010m triple bandpass filter Colour Gamut and crosstalk free channels.	59
Figure 3.13: Plot of all calculated colour gamuts with CIE'31 chromaticity diagram.....	61
Figure 3.14: Selected colour gamuts from DSC measurements and Standardised colour spaces.	62
Figure 4.1: Acquisition procedure for calculating HS imager colour gamut	69
Figure 4.2: Simulated Spectral Bands with 5nm FWHM and 10nm band step interval..	70
Figure 4.3: Colour gamut of an ideal HS imaging device. The boundary layer matches CIE '31 chromaticity diagram's spectral locus.	71
Figure 4.4: The FWHM values that were used for the various HS gamut calculations....	72
Figure 4.5: As the FWHM of an HS imaging device increases, the spectral colours are getting further from CIE '31 chromaticity diagram spectral locus.....	72
Figure 4.6: CIE'31 Chromaticity Diagram coverage from spectral cubes with different FWHM values.....	73
Figure 4.7: The Muses9-HS camera that has been used for colour gamut calculation.....	75
Figure 4.8: Spectral cubes acquired for Muses9-HS colour gamut calculation plotted together.....	76
Figure 4.9: Muses9-HS colour gamut as calculated from matrix $SM9$	77
Figure 4.10: Muses9-HS transformed Spectral Sensitivities derived from Luther Condition.....	78
Figure 4.11: Colour gamut of Muses9-HS after applying Luther condition.	79

List of Tables

Table 1: sRGB Colour Space chromaticity coordinates.....	23
Table 2: RMSE and Manhattan Distance errors for T_{CAM} vs CIE '31 CMF.....	52
Table 3: Colour Correction Matrix M for converting camera R, G, B responses to X, Y, Z tristimulus values.....	52
Table 4: Total Area Characteristic Values for ASI178MC colour gamut and CIE '31 Chromaticity Diagram.....	53
Table 5: Min, Max and Mean Euclidean Distances of ASI178MC and CIE '31 Chromaticity Diagram spectral locus.....	54
Table 6: RMSE and Manhattan Distance errors for T_{CAM} vs CIE '31 CMF.....	55
Table 7: Total Area Characteristic Values for ASI178MC coupled with Chroma 69010m triple bandpass filter colour gamut and CIE '31 Chromaticity Diagram.....	56
Table 8: Min, Max and Mean Euclidean Distances of ASI178MC and CIE '31 Chromaticity Diagram spectral locus.....	56
Table 9: RMSE and Manhattan Distance errors for T_{CAM} vs CIE '31 CMF.....	59
Table 10: Total Area Characteristic Values for ASI178MC coupled with Chroma 69010m triple bandpass filter without channel crosstalk colour gamut and CIE '31 Chromaticity Diagram.....	60
Table 11: Min, Max and Mean Euclidean Distances of ASI178MC and CIE '31 Chromaticity Diagram spectral locus.....	60
Table 12: Gamut area values of ideal HS colour gamut and CIE '31 chromaticity diagram.....	71
Table 13: Area measures for different FWHM values.....	73
Table 14: Gamut area values of Muses9-HS colour gamut and CIE '31 chromaticity diagram.....	77
Table 15: RMSE and Manhattan distance errors for Muses9-HS transformed Spectral Sensitivities and CIE'31 CMF.....	79
Table 16: Gamut area values of Muses9-HS colour gamut after applying Luther condition and CIE '31 chromaticity diagram.....	79

1. Introduction

1.1 The Electromagnetic spectrum

The electromagnetic (EM) spectrum is the range of all types of EM radiation (EMR). Radiation is a form of energy that travels and expands as it propagates. For example, visible light that comes from a light bulb or the radio waves emitted from a radio station are two types of EMR. The other types of EM radiation that make up the electromagnetic spectrum are microwaves, infrared light, ultraviolet light, X-rays and gamma-rays as it is shown in Fig. 1.1. Electromagnetic waves that form EMR are synchronised oscillations of electric and magnetic fields which propagate perpendicular to each other at the speed of light. These oscillations are characterised by their own frequency and wavelength. Visible light spectrum starts from violet light at 380nm, and ends in red light at 700nm. The visible spectrum, that is the EM spectrum that the human eye can see, is a very small portion of the whole EM spectrum.

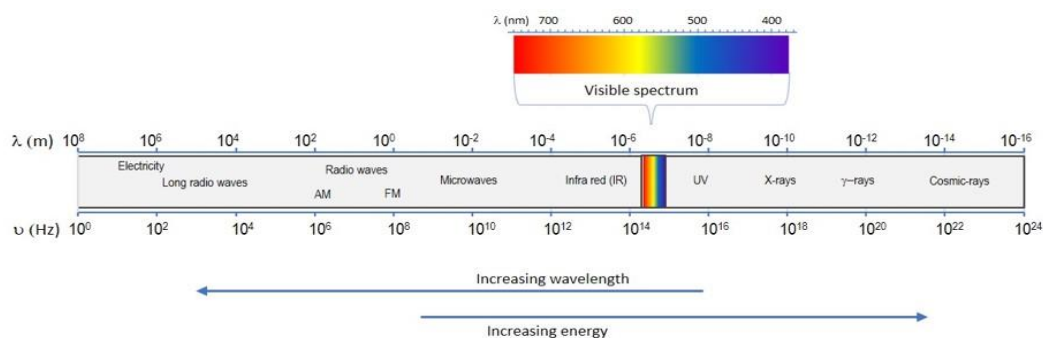


Figure 1.1: The electromagnetic spectrum¹

As on every force in the universe, EM force carrier is an elementary particle called photon. Photon has zero rest mass and propagates at the speed of light within a vacuum, as EM waves do. Many discussions have been made for light duality, if it is a particle, wave or both. By far the most acceptable answer in scientific community is the pilot wave model[1], originally developed by Louis de Broglie and further developed by David Bohm. This model states that there is no duality, but rather a system which exhibits both particle and wave properties simultaneously. This claim is, however, disputed by other physicists[2].

A single photon carries a specific amount of energy called Photon Energy (PE). PE is directly proportional to each photon's electromagnetic frequency and inversely proportional to its wavelength. The longer the wavelength, the lower the energy. Contrariwise, s energy. The equation for photon energy is::

$$PE = hc/\lambda,$$

¹ https://www.engineeringtoolbox.com/electromagnetic-spectrum-d_1929.html

where h refers to Planck constant, c is the speed of light in a vacuum and λ is photon's wavelength. Since c and h are both constants, PE changes in inverse relation to its wavelength λ . Since $c/\lambda = f$, where f is frequency the PE equation can be simplified to:

$$PE = hf,$$

known as Planck-Einstein relation².

EMR of different wavelengths has very different effects upon interaction with matter. For the long radio waves the human body is transparent. As we move on the EM spectrum towards higher frequencies such as microwaves, infrared and visible light, absorption becomes bigger whilst the transparency becomes lower.

When light encounters a surface or passes through a medium, inevitable interaction occurs between the light and the electrons of the atoms and molecules of the material. All molecules have resonant frequencies at which they trap particular EM wavelengths. The electronic transitions that result in heat or radiation of a photon depend on the complex molecular structure and the variety of electron orbitals in an atom, as well as from their shape characteristics.

There are three ways that light interacts with matter:

- *Absorption*
When a light wave with an identical frequency to an electron's natural frequency "impinges" upon an atom, the electrons begin to vibrate as a result. The electrons absorb the light wave with the same vibrational frequency and turn it into a vibrational motion. The electrons, in turn, bump up against neighboring atoms, which changes the vibrations into thermal energy. However, this thermal energy does not turn back into light energy. The light wave does not leave the object.
- *Reflection*
This occurs when the frequency of the incoming light wave does not match that of the electrons' natural frequency. If the object is opaque, the electron vibrations are not "passed down" such as they are during absorption. Rather, the surface-level electrons vibrate briefly before emitting the wave back out as light. Light undergoes one of two types of reflection – diffuse or specular.
 - In diffuse reflection light is emitted in all directions due to irregularities on the surface of the material.
 - In specular reflection all the reflected rays are parallel to each other.

² http://www-inst.eecs.berkeley.edu/~cs191/fa08/lectures/lecture8_fa08.pdf

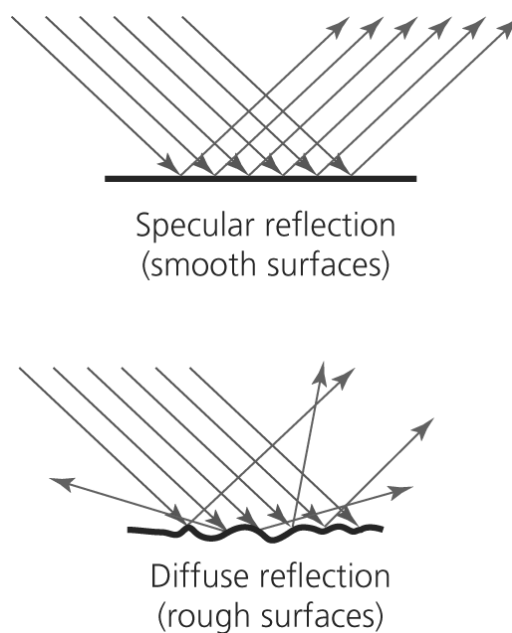


Figure 1.2: Specular and diffuse reflection³

- *Transmission*
Transmission follows the same interaction as reflection, except it involves transparent or semi-transparent objects. The atoms take in the wave, vibrate briefly, transfer the vibrations throughout the body of the material, and then re-emit the wave as light from the other end.

1.2 Colour

1.2.1 The Eye – Colour Perception

Human vision is a complicated process which is not completely understood, despite the extensive research effort that has been conducted towards its understanding. Human colour vision is defined as a physiophysical process consisting of two parts, the eyes and the brain. Eyes act as image receptors that convert light into electrical signals which are then transmitted to the brain. Processing by the brain consists partly of simple image processing and partly of higher functions, which build and manipulate an internal model of the outside world. It should be mentioned that eye-brain division is not clear-cut since both of them cooperate in order to interpret colour.

³ https://connect.collins.co.uk/repo1/Content/Live/JI/Leckie/AQA-GCSE-Physics-SB-Free-Site-13-Jan-V1/Contents/58774_gcse_physics_ch2_p22_2.html

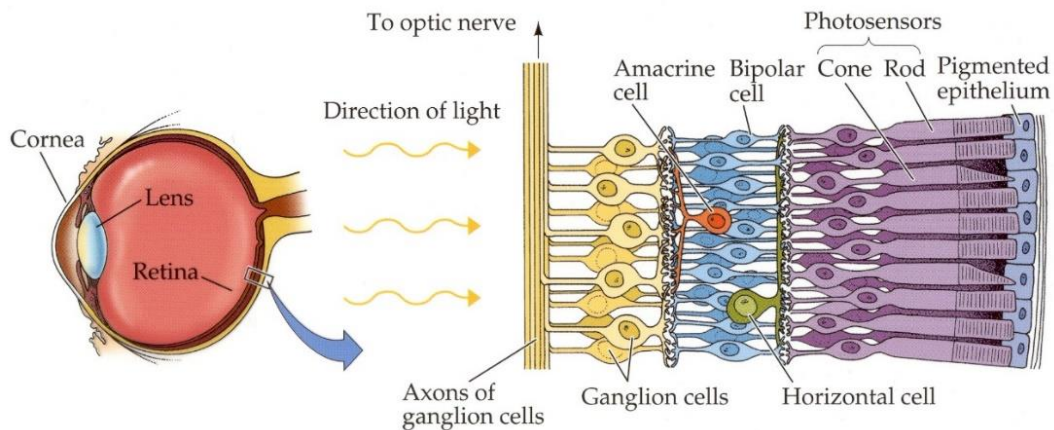


Figure 1.3: Basic illustration of eye's retinal anatomy⁴

Colour is the characterisation of the human visual perception property that can be identified as red, blue, green or other. It derives from the light spectrum in the range of $\sim 400\text{nm}$ to $\sim 700\text{nm}$. Eye light receptors have a certain spectral sensitivity, but it is not directly related to the colour perception as humans experience it. Most of living species on earth could perceive colour by having variations of the same physiological mechanism. Colour is not a property of natural objects and scenes, but a way that living organisms apprehend light and matter interaction. In other words, there is no colour in nature, only spectral properties that living species perceive as colour.

There are specialised retinal cells that are responsible for colour vision the cone cells. There exist three types of cone cells, each one with different spectral sensitivity. There are also rod cells that are colour blind. However, these cells are around $\times 100$ times more sensitive to a single photon than cones. Both rods and cones are interconnected, through intermediate cells, to ganglion cells that are responsible for the transmission of the light stimuli electrical signals to the optic nerve. Rods do not participate to colour sensation. They are responsible for the peripheral and scotopic vision which is the vision of the eye in low light levels. The spatial resolution of the image product from the rod cells is low, mainly due to the many-to-one connection with the ganglion cells. On the other hand, cone cells are responsible for the photopic vision which refers to well-lit conditions. The image product of the rod cells is characterised from high spatial resolution as the cone-ganglion relationship is one-by-one. Cones are mostly populated in retina's fovea (which is a small portion of total retina's area) where rods are sparsely distributed. Conversely, rods are in high population on the remaining retina region.

⁴ <http://www.lifeinharmony.me/anatomy-of-eye-cones-and-rods/anatomy-of-eye-cones-and-rods-three-dimensional-retinal-ganglion-cell-google-search-totem>

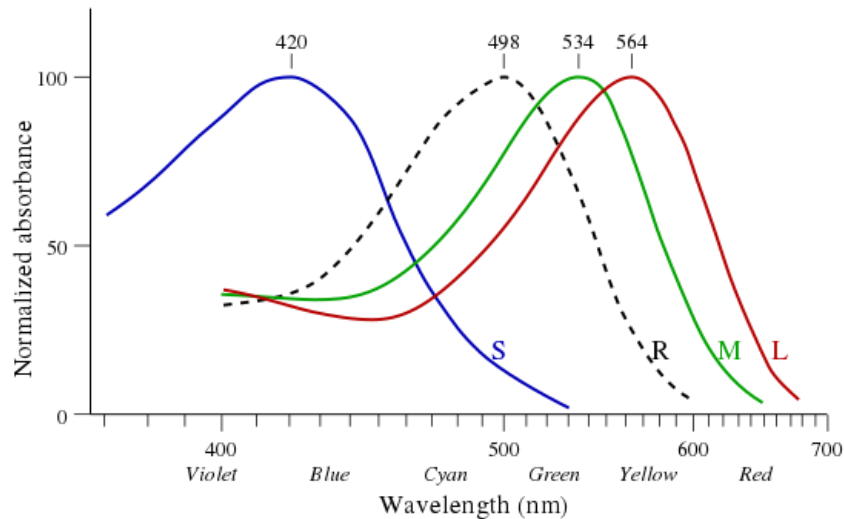


Figure 1.4: Normalised Cones and rods absorbance.⁵

Two complementary theories of colour vision exist: the Trichromatic theory and the Opponent Process theory. The Trichromatic theory assumes that three independent channels of cone cells are conveying the colour information. The Opponent Process theory states that the visual system interprets colour in an antagonistic way: red vs. green, blue vs. yellow, black vs. white. This theory is based on the fact that optical signals from cones are multiplexed as opponent colours pathways in ganglion cells. The described opponent process is clearly shown in Fig. 1.5.

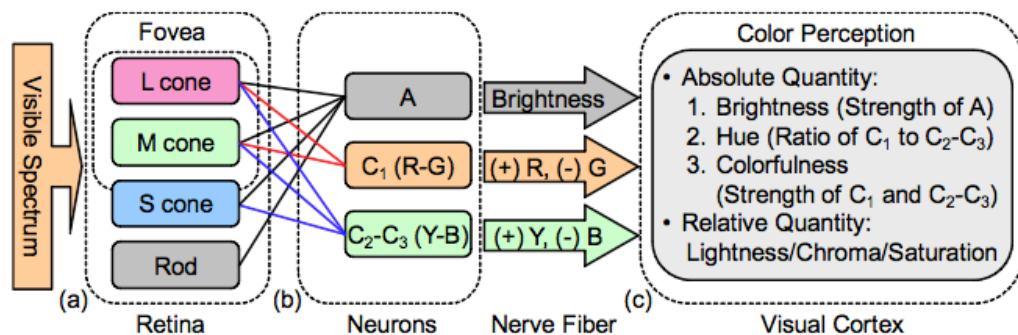


Figure 1.5: Diagram of the opponent process stage⁶.

As already mentioned, eye processing is fused with brain colour processing. This is the reason why both trichromatic and colour opponent theories do not perfectly match human colour experience. If colour processing was the product of either the trichromatic or opponent process theory, then the approximate spectrum should look like Fig. 1.6.

⁵ Bowmaker J.K. ; and Dartnall H.J.A., "Visual pigments of rods and cones in a human retina." J. ; *Physiol.* 298: pp501-511 (1980)

⁶ https://commons.wikimedia.org/wiki/File:Diagram_of_the_opponent_process.pngC4 Model

Eventually, both of theories are now accepted as valid in describing different stages in visual physiology, hence they are also described in combination as stage theory[3].

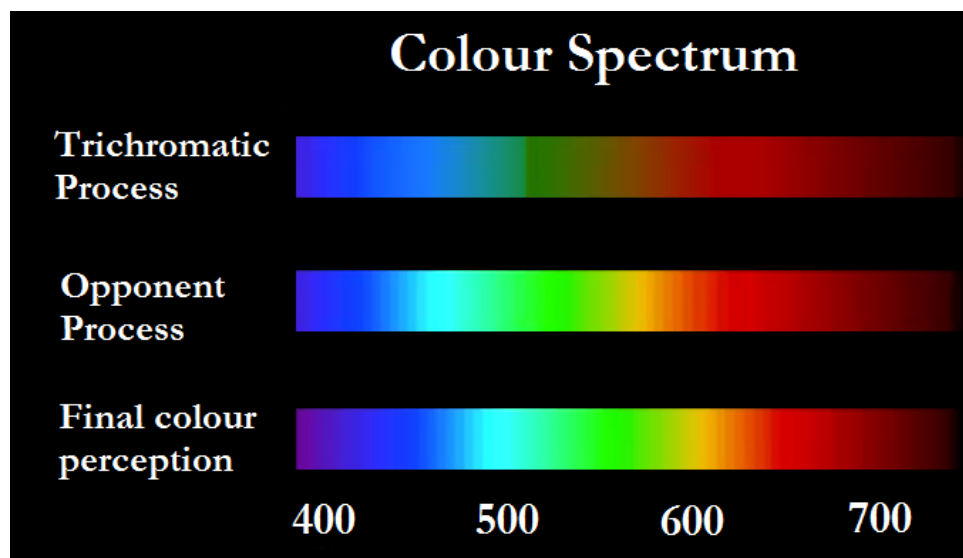


Figure 1.6: Approximate spectrum of colour for each colour processing stage.

Studies have shown that cone receptors mosaics differ dramatically among people [4]. Despite that, people with different cone population appear to perceive colours the same way. For example two individuals shown in *H. Hofer's* study have cone ratios: 3.8:1 and 1.15:1 although they were both classified as normal. This fact endorses the existence of non-linear processes in human colour perception.

1.2.2 CIE standards

As already mentioned in previous subsections, human colour perception is a subjective process. Beyond human eye physiology, colour perception also depends on the spectral distribution of the colour stimuli, size, shape, structure and surroundings of the stimulus area. Furthermore, it also depends on the state of adaptation of the observer's visual system, and on the observer's experience of the prevailing and similar situations of observation.

For the aforementioned reasons colour perception varies even for the same observer. This is due to conditions such as different light sources or variations in scene geometry that are continuously subject to change. This subjectivity often leads to inconsistencies when either evaluating or communicating colour internally or throughout the supply chain. In order to combat this subjective perception of colour, researchers in academia and industry have established functions to standardize and validate colour in a way to make it independent from various conditions.

The International Commission on Illumination⁷ -abbreviated as CIE from its French title "*Commission Internationale de l'Éclairage*" - is an organisation devoted to international cooperation and exchange of information among its member countries on all matters

⁷ <http://www.cie.co.at/>

relating to the science of light, illumination, colour and vision, photobiology and image technology. It was established in 1913 and is responsible for all current work for colour and standard illuminants.

The main goal was to standardise the “average” human colour perception. To achieve this, CIE followed a top-down approach without taking into account most of the physiological and psychological parameters. CIE 2° Standard Observer and CIE 10° Supplementary Standard Observer⁸ are two experiments that were published in 1931 and 1964 accordingly. The experiments resulted in the functions that are representative of how humans perceive colour.

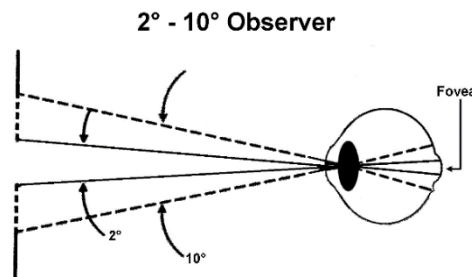


Figure 1.7: Field of View for 2° and 10° Standard Observers.

The experiments were conducted by using a circular split screen (a bipartite field) 2° in diameter for Standard Observer '31, which is the angular size of the human fovea and 10° for Standard Observer '64. On one side of the field, a test colour was projected and on the other side, an observer-adjustable colour was projected. The adjustable colour was a mixture of three primary colours, each with fixed chromaticity but with adjustable brightness.

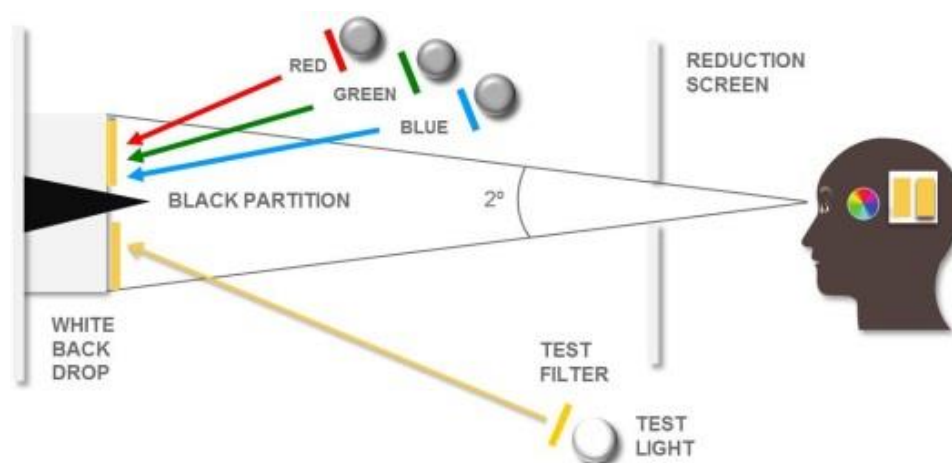


Figure 1.8: CIE Standard Observer Experiment Overview⁹.

⁸ All CIE standards could be found here: <http://www.cie.co.at/publications/international-standards>

⁹ <https://www.hunterlab.com/blog/uncategorized/human-observers/>

Red, Green, Blue colours are obtained using three monochromatic primaries at wavelengths of 700 nm (red), 546.1 nm (green) and 435.8 nm (blue). They defined as primaries because any combination of any subset of them could not derive to the third one. The resulting primary mixture coefficients are shown in Fig. 1.9 where Colour Matching Functions (CMF) are presented. The negative values on the red curve of CIE 1931 RGB CMF, corresponds to the addition of red primary illuminant on the Test Light side. There was a non-match in the conventional way between monochromatic light and RGB mixtures and that lead to the described action.

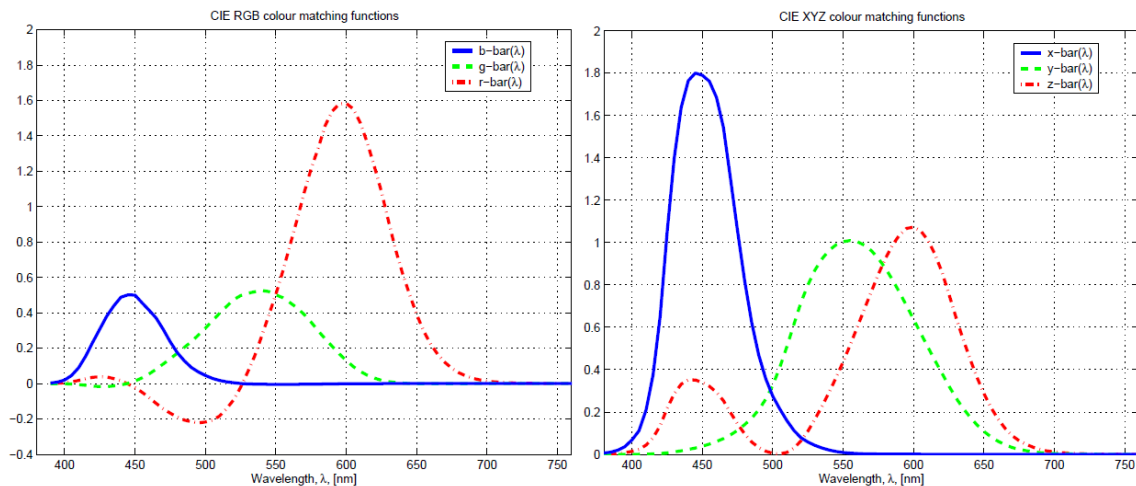


Figure 1.9: Left: CIE 1931 RGB CMF. Right: CIE 1931 Standard Observer CMF [5].

There are also “unofficial” Standard Observers [6] based on variables such as age, time of day gender, etc. These experiments are not recognised as standards from CIE.

Due to the problems revealed by the RGB primaries, CIE scientists performed a linear transformation resulting in new Colour Matching Functions. This new set of values, called X, Y, and Z, or tristimulus values, have the following properties:

1. They always produce positive tristimulus values.
2. It is possible to represent any colour in terms of these primaries.
3. Equal values of X, Y, and Z produce white.
4. They were arranged so that a single parameter Y determines the luminance of the colour.
5. They are related to the sensitivity of the human eye by the use of colour matching functions which match to the CIE 1931 Standard Observer.

In contrast to the R, G, B primaries described before, the new ones, have no physical meaning. These new values are the numerical description of the chromatic response of the observer. The x, y, z values do not correspond directly to R, G, B sensitivities, although they define a colour space known as XYZ Colour Space.

1.2.3 Illuminants

Light is the most significant reason for colour perception. Light sources are characterised from their Spectral Power Distribution (SPD). SPD describes the photometric quantity (radiant energy, intensity, luminous flux etc.) as a function of wavelength. Each light source emits different amounts of energy at each wavelength which results in different colour representations. CIE has standardised many Illuminants, in such a way, to describe physical light sources. In Fig. 1.10 are shown their normalised SPDs according to CIE's standardisation procedures and as a reference to the human eye's photopic response.

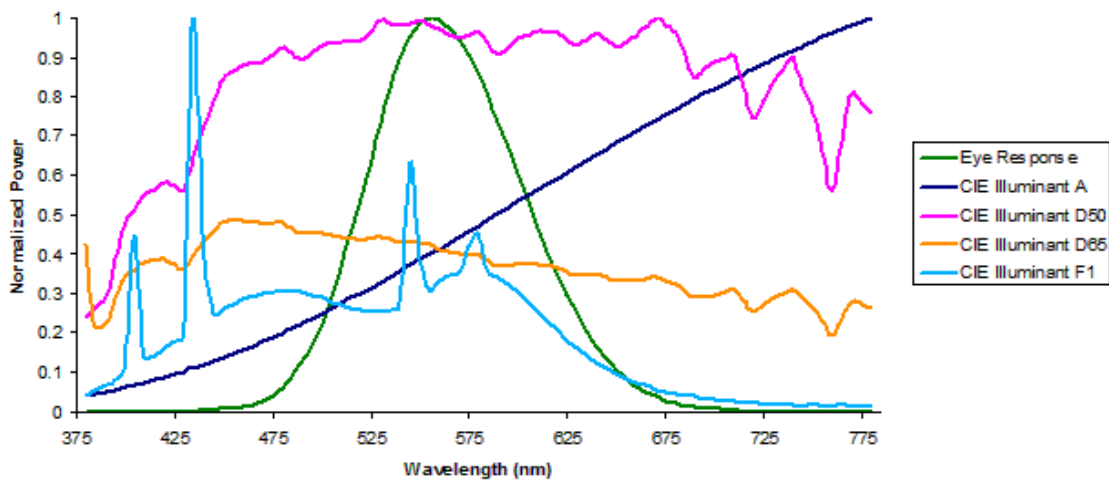


Figure 1.10: Normalised SPD per CIE Illuminant and Photopic Eye Response¹⁰.

Most Illuminants are Black Body Radiation exports, meaning that they are measured from thermal radiators that emit light, such as sun, candle, incandescent lamps etc.

Illuminant D65¹¹ is the most common one and refers to average daylight with a correlated colour temperature of 6504K. F Illuminants refer to Fluorescent light sources accordingly.

1.2.4 Colour Spaces

CIE defines colour as a combination of pure spectral colours (in the visible range). Since there are, in principle, infinitely many distinct spectral colors, the set of all physical colours may be thought of as an infinite-dimensional vector space [7] e.g. a Hilbert space¹². By defining a colour space, colours can be identified numerically by coordinates. CIE's 1931 XYZ colour space is the first quantitative link between distributions of wavelengths in the electromagnetic visible spectrum, and perceived colours for human colour vision. It is the common colour space that industry use in

¹⁰ https://commons.wikimedia.org/wiki/File:NormSPD_with_eye.png#/media/File:NormSPD_with_eye.png

¹¹ files.cie.co.at/204.xls

¹² https://en.wikipedia.org/wiki/Hilbert_space

order to communicate colour. All other known colour spaces are products from the XYZ colour space, meaning that the transition from one space to another is a linear transformation operation.

The CIE XYZ Colour Space was explicitly designed so that parameter Y is a measure of the luminance of a color. XZ plane stands for chromaticity at given luminance Y. In order to isolate brightness, the chromaticity of a colour is then specified by the derived parameters x and y, two of the three normalised values being functions of all three tristimulus values X, Y, and Z:

$$x = \frac{X}{X + Y + Z},$$

$$y = \frac{Y}{X + Y + Z},$$

$$z = \frac{Z}{X + Y + Z} = 1 - x - y.$$

In principle, the tristimulus values of X, Y, and Z, namely x, y, and z, are defined on a unit plane, and everywhere on this plane their sum equals one.

By replacing X, Y, Z the values for each wavelength with CMF '31, 2° and then project the products on the unit plane, it results in the convex hull of CIE chromaticity diagram, which is shown in Fig. 1.11.

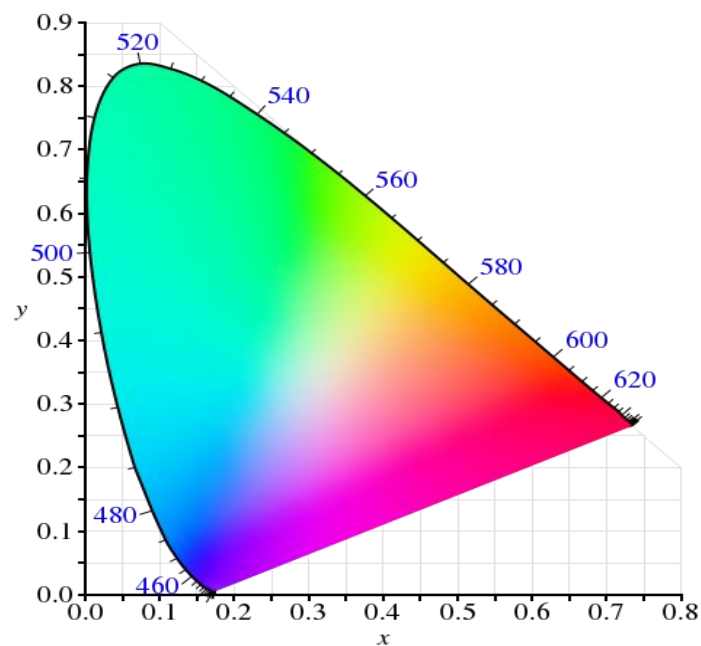


Figure 1.11: CIE 1931 colour space chromaticity diagram.

The outer curved boundary is called “Spectral Locus” and defines the coordinates of every spectral colour. The inner area represents all Non-Spectral colours that only can be created from mixtures of primary spectra. Outside the spectral locus there are only imaginary colours with no meaningful use. The line connecting the violets with the reds is called line of purples and represents the non-spectral purple colours.

The X and Z tristimulus values can be calculated back from the chromaticity values x and y and the Y tristimulus value:

$$X = \frac{Y}{y}x,$$

$$X = \frac{Y}{y}(1 - x - y).$$

There are various colour spaces, each one serving a specific purpose for industry needs, from printing colour accuracy to photography applications. These colour spaces are mostly certain complete subsets of colour in relation to XYZ colour space. Many of them are plotted on Fig. 1.12.

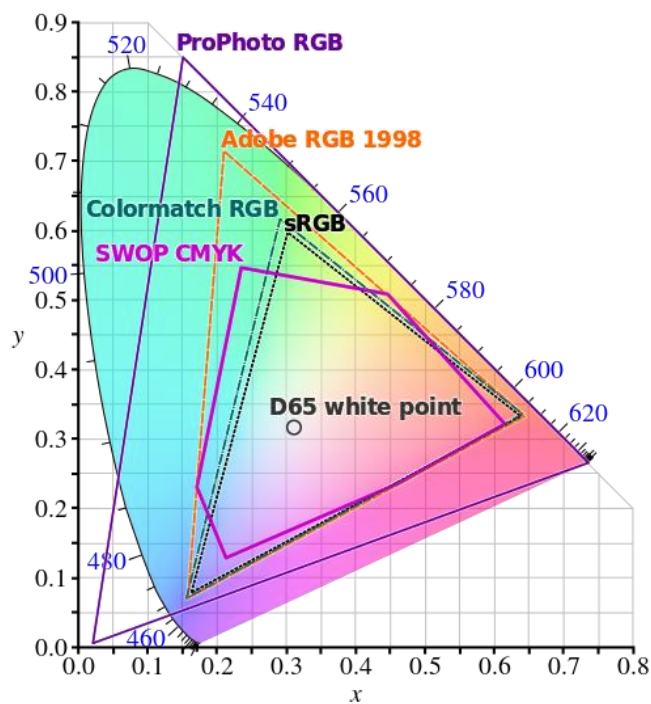


Figure 1.12: Various Colour Spaces relative to CIE's 1931 chromaticity diagram¹³.

In Figure 1.12 it could be easily noticed that most of the colour spaces have a triangular shape whilst others have manifold shapes. The vertices for each shape are the xy coordinates of the primary colours of the corresponding colour space. For example sRGB colour space¹⁴ primaries refer to coordinates as shown in Table 1.

Chromaticity	Red	Green	Blue	White Point
x	0.6400	0.3000	0.1500	0.3127
y	0.3300	0.6000	0.0600	0.3290
Y	0.2126	0.7152	0.0722	1.0000

¹³ http://commons.wikimedia.org/wiki/File:CIE1931xy_blank.svg

¹⁴ www.color.org/srgb.pdf

Table 1: sRGB Colour Space chromaticity coordinates.

In order to convert from industry standard XYZ Colour Space to common, web used, sRGB Colour Space, a linear transformation should be performed. This is done by vector-matrix multiplication as shown:

$$\begin{bmatrix} R \\ G \\ B \end{bmatrix} = \begin{bmatrix} 3.2406 & -1.5372 & -0.4986 \\ -0.9689 & 1.8758 & 0.0415 \\ 0.0557 & -0.2040 & 1.0570 \end{bmatrix} \begin{bmatrix} X \\ Y \\ Z \end{bmatrix}$$

where R, G, B is the product colour vector from X, Y, Z colour tuple. Often, the resulted values are proceed to gamma correction transformation in order to better match human non-linear colour perception.

1.2.5 Colour Gamut

The colour subspace consisting of all these colours that either can captured or represented is called colour gamut. Each colour device, either input or output, has its own colour gamut. This is because of the physical characteristics of each unique device. Therefore, various colour spaces fit better to their given device. Thus, making it easier to transit from one device's colour space to another standardised colour space. For example, sRGB's colour gamut give acceptable colour representation for the majority of currently used computer monitors. On the other hand, more professional solutions like Wide Gamut Monitors¹⁵ are calibrated and manufactured, so they can support wider gamut ranges (i.e. more colours) such as ProPhoto RGB or Wide-Gamut RGB.

A lot of discussion has been made in several colour photography and colour science fora^{16, 17} about the existence of input device colour gamut. Considering CIE's definition¹⁸ of colour gamut and that the human eye as an input mechanism, already has a defined colour space, it can be concluded that every input device can be characterised by its ability to capture colour stimuli by defining its colour gamut in relation to the human eye (i.e. CIE'31 XYZ colour space). The aforementioned reasoning along with this research will improve colour accuracy and representation through expansion and optimisation of Digital Still Cameras (DSCs) and hyperspectral devices colour gamut.

As it is shown in Fig. 1.12, three real sources cannot cover the gamut of human vision since colour mixing can create new colours that lie between two or three starting colours. Geometrically stated, there are no three points within the spectral locus that contain the whole CIE XYZ gamut area. The only triangle that could perform such area, is the XYZ triangle as it is shown in Fig. 1.13. X, Y and Z base vectors lie outside

¹⁵ For example: https://www.amazon.com/NEC-Monitor-PA302W-BK-30-Inch-LED-Lit/dp/B00EZIP270W?tag=hawk-future-20&ascsubtag=tomshardware-thaus:en_US_18_Review_4612-20

¹⁶ <https://photo.stackexchange.com/questions/81808/why-dont-we-see-charts-of-the-colorspace-gamut-of-a-dslr>

¹⁷ <https://www.provideocoalition.com/camera-not-color-gamut/>

¹⁸ <http://eiv.cie.co.at/term/211>

the spectral locus as they do not represent physical quantities. On the other hand CIE's R, G, B primaries form a triangle that represent their colour gamut. That leaves a significant part of the blue-green region, which lies outside the RGB triangle and therefore cannot be matched. This area relates to the negative values that CIE'31 RGB CMF had, as it is shown in Fig. 1.9.

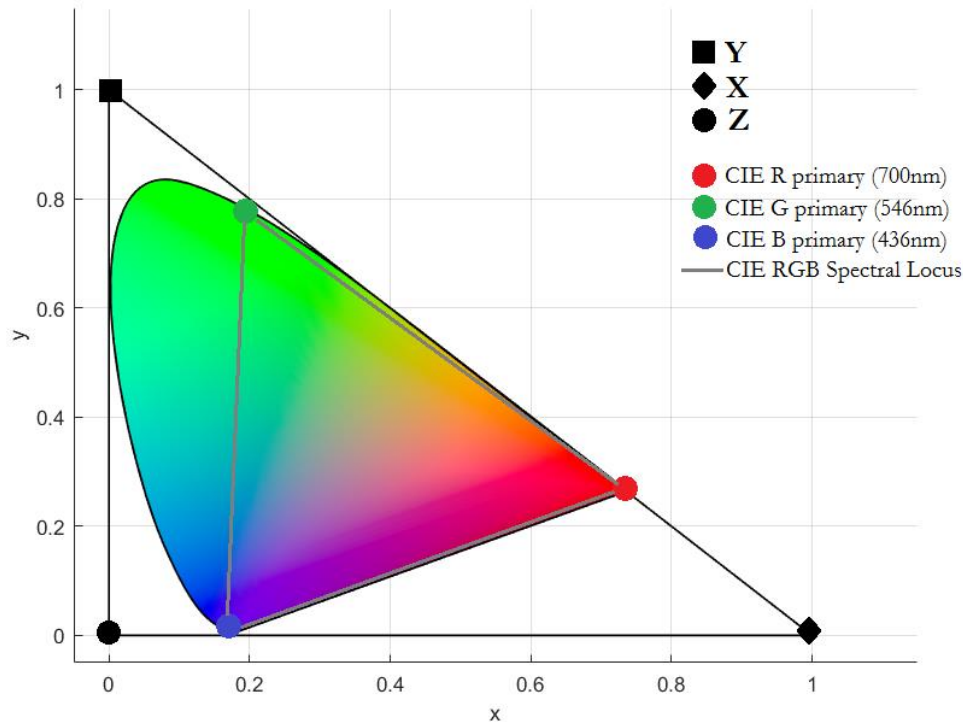


Figure 1.13: XYZ triangle coordinates and CIE'31 RGB primaries plotted on CIE'31 chromaticity diagram.

1.2.6 Metamerism

Colour stimuli is defined by a continuous characteristic spectrum that is perceived as colour from our partly trichromatic vision. Due to this, many colours with different spectra could appear the same in the human eye. Metamerism[8] is the perception of the same colours that consist from different Spectral Power Distributions (SPDs).

The existence of metamerism implies that there is a fundamental ambiguity in human visual perception. Given a triplet of cone responses -the eye's response to light from some surface- it is not possible for human eye to uniquely identify the physical properties of that surface but rather, there exist many surfaces consistent to the same response.

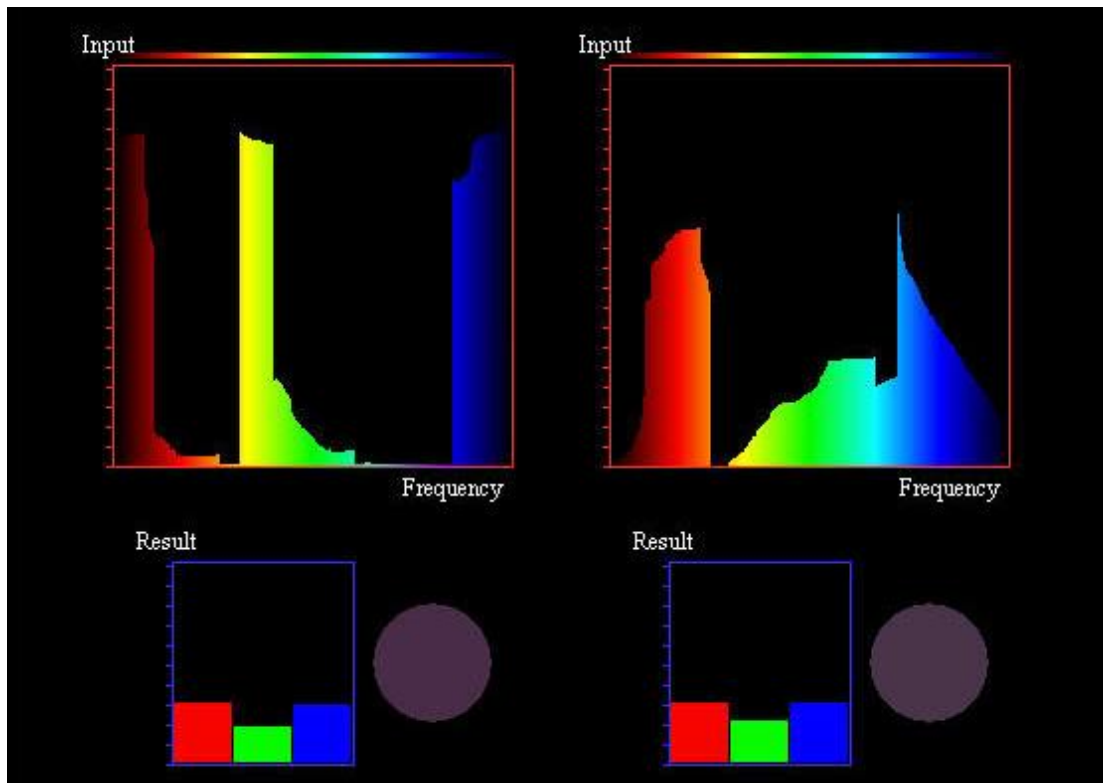


Figure 1.14: An example of metamerism¹⁹. Different spectra could result to the same colour stimuli.

Metamerism is a phenomenon that also depends on Illumination. Different Illuminants could reveal or hide metameretic colours as shown in Figure 1.14.

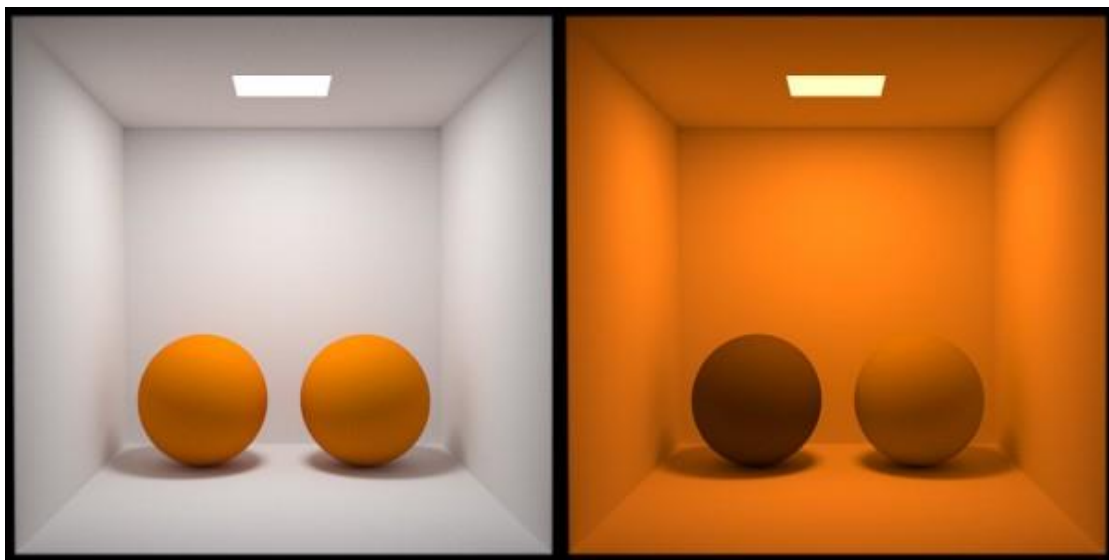


Figure 1.15: Metameric colours on different light sources²⁰.

Due to the metamerism phenomenon, attaining consistent and accurate colour of products can be a challenging task for the manufacturers. Especially, for those whose

¹⁹ Jeff Beall, Adam Doppelt and John F. Huges © 1995 Brown University and the NSF Graphics and Visualization Center.

²⁰ <https://www.eclat-digital.com/2013/02/22/metamerism/>

products are assembled using various parts that are supplied by different manufacturers where each of them has its own way of adding formulation. Any mismatch in the colours will not only generate unnecessary rectification cost but also affects the acceptance and buying behaviour of the customers. To prevent these issues, it is important to measure the colour of the objects and quantify the effect of metamerism.

1.3 Digital Still Cameras

1.3.1 Photoelectric Effect

In the early 1900's, Albert Einstein (1879-1955) worked on a phenomenon called photoelectric effect. Einstein showed that a quantum of radiant energy (a photon) could eject a negatively charged electron from the atoms in certain materials. As it can be seen in Fig. 1.16, depending on the energy gap of the material, different wavelengths produce different electron escape velocities i.e. kinetic energies.

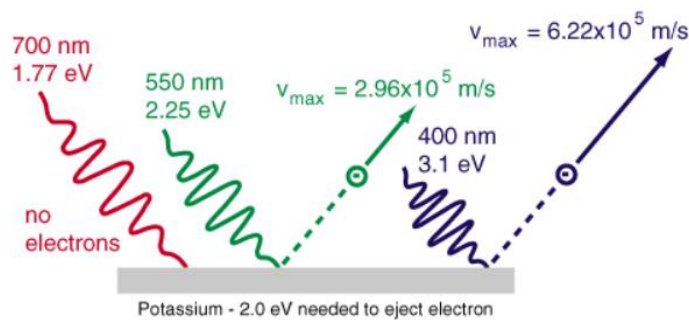


Figure 1.16: Illustration of photoelectric effect. Different photon energies result to different electron escape velocities²¹.

The increasing number of the same energy photons, or the increase of the intensity of the light beam, does not affect the energy of the emitted electrons but only the number of them. The ejected electrons are often called photoelectrons but there is no difference compared to the common electron. All quantum properties of the electron such as spin, magnetic moment, charge etc. remain identical.

1.3.2 CCD-CMOS

The photoelectric effect is the basic principle for the conception and design of today's digital camera sensors. In principle, a digital camera sensor is an array of individual photosensitive elements, called pixels (Picture Elements). Each one of which can absorb photons of light and utilise energy that releases electrons within the semiconductor. The processes of electronic design and integration take into account

²¹ <http://engineeringu.com/PhysiXcel/Chapter10.html>

the creation of an electrostatic field so as the emitted electrons to be trapped there. This method creates a storage region of holding many charges, which are proportional to the amount of photons that hit the photosensitive area.

The electronic element which is used for the photosensitive area is called photodiode. Photodiode Responsivity R_λ is defined as the ratio of the radiant energy (in watts), P , incident on the photodiode to the photocurrent output in amperes I_p . It is expressed as the absolute responsivity in amps per watt (A/W).

$$R_\lambda = \frac{I_p}{P}$$

For UV-VIS-NIR spectrum region, silicon or silicon admixtures are used for the construction of the photosensitive area because its bandgap (1.3ev to 1.8ev) meets the frequencies of the photons in the EMR part. As Fig. 1.17 shows, for different EMR areas, different photosensitive materials are being used.

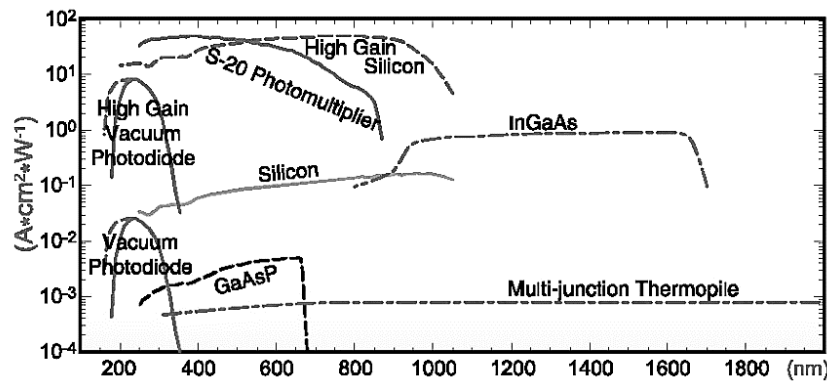


Figure 1.17: Photodetector Material Responsivities vs. Wavelength²².

CCD (charge couple device) and CMOS (complementary metal oxide semiconductor) are the main technologies for capturing digital images in UV-VIS-NIR EMR region. In a CCD sensor, every pixel's charge is transferred through a very limited number of output nodes (often just one) in order to be converted into voltage. It is then buffered and sent off-chip as an analog signal. However, in a CMOS sensor, each pixel has its own charge-to-voltage conversion. Latest developments in CMOS sensor design and fabrication include noise-correction and digitization circuits even for each independent pixel²³.

²² <https://depts.washington.edu/mictech/optics/me557/detector.pdf>

²³ <https://www.sony.net/SonyInfo/News/Press/201802/18-018E/index.html>

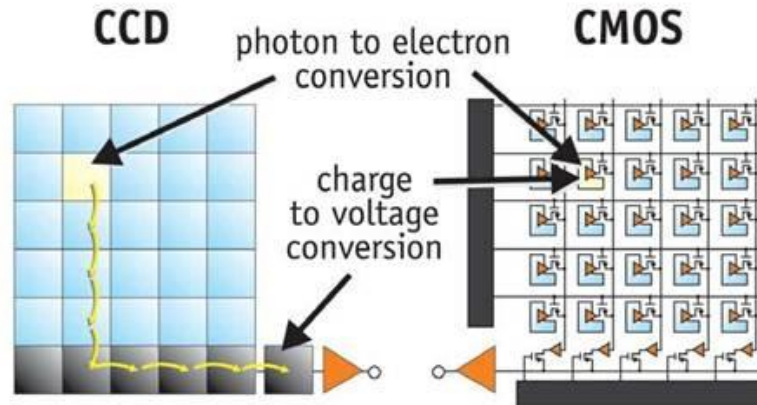


Figure 1.18: CCD and CMOS sensor differences on charge to voltage operation²⁴.

Today's CMOS area and line scan imagers outperform CCDs in most visible imaging applications. Developments in photolithography and fabrication techniques, in parallel with, the radical evolution of the mobile phone camera market, have resulted in CMOS sensor dominance [9].

1.3.3 Operational Characteristics

It could be assumed that a perfect imaging sensor converts each photon to electron and digitizes it without any loss. However, there are physical constraints which limit that possibility. For the current work, some of the most important properties of photon detectors are presented:

- Quantum efficiency
As discussed, different light frequencies result in different sensor responses. This relation is described from quantum efficiency property, usually with the plotted response values to the associated wavelength.
- Noise
Unwanted variations in pixel values derive a loss of image quality compared with the real image. Noise could be classified into two types: temporal and spatial. Temporal noise can be reduced by frame averaging, while spatial noise cannot. This is because temporal noise fluctuations have a zero mean value so by averaging the frames in time sequential order the system noise approaches zero. However, some amount of spatial noise can be removed by frame subtraction or gain correction techniques. Photon noise (or shot noise) emerge from the discrete nature of light. Since the time between photon arrivals is governed by Poisson statistics, the uncertainty in the number of photon collected during a given period of time is:

$$\sigma_{shot} = \sqrt{S},$$

²⁴ http://meroli.web.cern.ch/lecture_cmos_vs_ccd_pixel_sensor.html

where σ_{shot} is the shot noise and the signal, both expressed in electrons. Thermal noise is the random produced electrons (also called thermoelectrons) from the ambient temperature levels. Pixel non-uniformity is the result of imperfections between same pixels on an image sensor. There are slightly different light sensitivities and responses associated with these imperfections. This kind of noise is often eliminated from calibration procedures during manufacturing.

- **Dynamic Range**
The ratio between the highest and lowest grey level that a sensor can capture is defined as the dynamic range of that sensor. Usually, it is expressed in decibels and defined as Dynamic Range (DR):

$$DR = 20 \log \frac{N_{SAT}}{N_{noise}},$$

where N_{SAT} stands for maximum saturation level (expressed in electrons e) and N_{noise} stands for the Root Mean Square of read out noise.

1.3.4 Colour Digital Still Cameras

Colour Digital Still Cameras (DSCs) have certain built-in characteristics in order to achieve colour reproduction that approximates human colour perception. Silicon is sensitive in UV-VIS-NIR EMR continuous region. As a result, image sensors are colorblind, since they cannot discriminate between different colour bands i.e. different EMR divisions. To achieve colour reproduction, special microfilter arrays are placed above the sensor area in order to allow only particular spectral bands and finally construct color. The most common of such integrations is by using Colour Filter Arrays (CFAs) also called Bayer filter mosaic. Each pixel has its own bandpass filter usually for Red, Green or Blue EMR areas. Interpolation algorithms undertake these pixel values and through post-processing result in the colour signal on camera's output.

Alternative integrations use three or more different sensors (with the same specifications) coupled with the corresponding bandpass filter. Each filter enables specific colour bands to pass, resulting in the final colour output. A beam splitting optical element is responsible for the division of the incoming optical signal to three identical. Usually dichroic²⁵ instead of bandpass filters are used in order to perform better image separation. This technology is known as 3CCD²⁶ or 3CMOS, depending on the digital sensor's architecture. The number "3" could also variate according to the total sensor-to-channel combinations²⁷.

Foveon's X3 sensor²⁸, is using three photosensitive silicon layers that each one corresponds to a different colour channel. Thus, it is achieving colour reproduction without requiring interpolation techniques, improving the sharpness of the final colour

²⁵ <https://www.azooptics.com/Article.aspx?ArticleID=554>

²⁶ http://www.adept.net.au/news/newsletter/201203-mar/article_3ccd_colour.shtml

²⁷ http://www.adept.net.au/cameras/2CCD_3CCD_Cameras.shtml

²⁸ <http://www.foveon.com/article.php?a=67>

image. However, it is characterised by wide channel crosstalk areas and consequently loses in achieving saturated colours.

It is obvious that the values for the R, G, and B channels of a sensor are inherently dependent on its design. They are characterised by their spectral sensitivities, giving the proportion of incident photons that eventually reach the sensor for a given wavelength (as described before -quantum efficiency-). In Fig. 1.19, Relative Spectral Responses (normalised sensitivities) curves are shown, from two commercial CMOS colour image sensors. In particular, it should be noted that these curves are not the color-matching functions X, Y, Z.

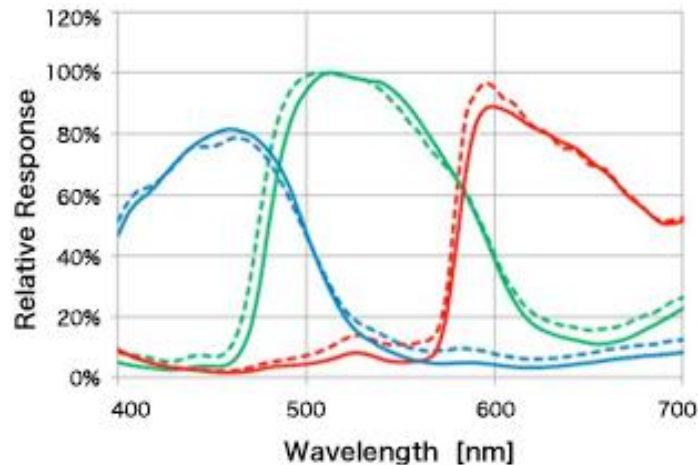


Figure 1.19: Relative Spectral Responses of Sony's IMX124 (Solid line) and IMX135 (dashed line)²⁹.

The RAW values in the R, G, and B channels on a uniform surface (ignoring noise for the time being) are not the sRGB values of this surface. In other words, the colour space of the sensor is not the sRGB colour space or any usual colour space. For that reason, industry use colour profile matrices to transform RAW R, G, B values into meaningful Standard colour spaces.

Because the XYZ CMF are not a linear combination of device spectral responses there are some colours which look the same to a device but have quite different XYZ tristimuli. Thus, colour cameras see different metamers than the human eye. The determination and analysis of such metamers has led to incremental progress[10], [11] in matching digital camera colour output with human colour perception.

1.4 Spectral Imaging

Spectrometers are scientific instruments/devices that measure the intensity of incoming light, either from reflection or transmission, as a function of wavelength also called spectrum. The spectrum can be used to identify and characterize a particular feature within the scene, based on unique spectral signatures. Spectroscopy is the study of interaction between matter and EMR with applications in colour science, biology,

²⁹ https://www.sony-semicon.co.jp/products_en/new_pro/april_2014/imx214_e.html

chemistry, astronomy and remote sensing. In its conventional configuration, spectroscopy uses single-point probes that cannot easily sample large areas or small areas at high spatial resolution. It is obvious that this configuration is clearly suboptimal when solid and highly heterogeneous materials, such as the biological tissues, are examined.

Spectral Imaging has the unique feature of combining the advantages of both imaging and spectroscopy (high spatial and spectral resolution) in a single instrument. In Spectral Imaging, light intensity is recorded as a function of both wavelength and location. The exported data structure from a Spectral Imaging device is three dimensional. The first two dimensions represent the spatial domain and the third one the spectral domain. This structure, called Spectral Cube could be perceived as a stack of images of the same area that each one represents a different spectral band. Each individual pixel refer to an N dimensional vector where N the number of spectral bands in spectral domain. The concept of Spectral Imaging and spectral cube is illustrated in Fig. 1.20.

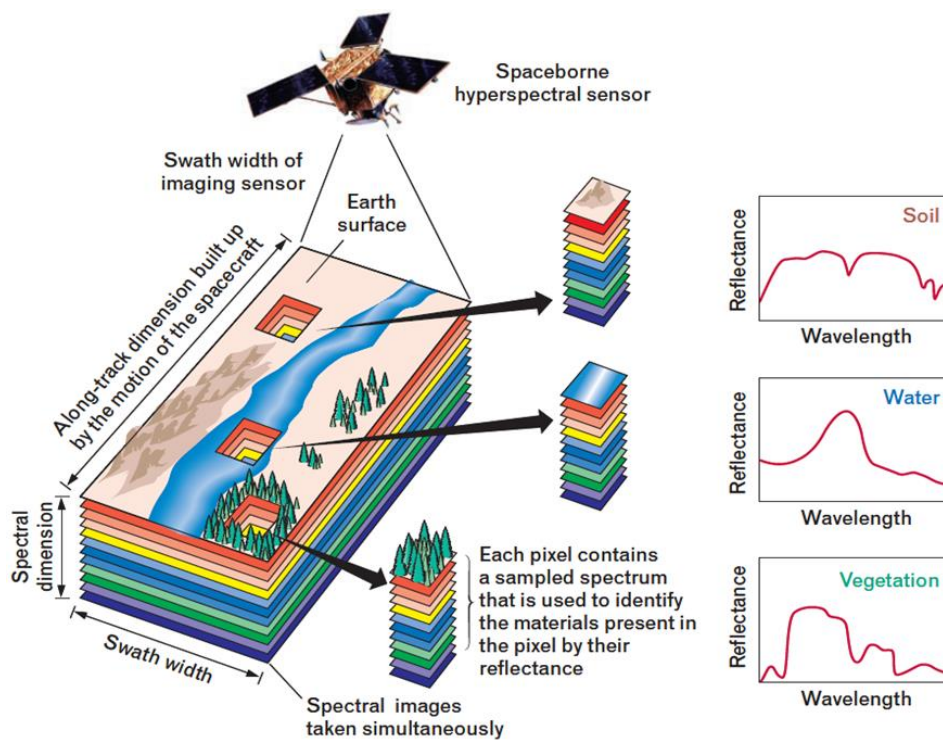


Figure 1.20: A Spectral Cube acquisition illustration from satellite imaging³⁰.

Spectral Imaging systems use monochrome sensors or sensor arrays, which can capture only two of the three spectral dimensions of the spectral cube at a time. To capture the third dimension, spatial or spectral scanning is required. Depending on the method employed for building the spectral cube, Spectral Imaging devices are classified as follows [12]: (a) whiskbroom SI devices, where a linear sensor array is used to collect the spectrum (λ dimension) from a single point at a time; the other two spatial coordinates are collected with (x, y) spatial scanning; (b) push broom Spectral Imaging devices in which a 2D sensor array is used, the one dimension of which captures the first spatial (x) coordinate and the other the spectral coordinate in each camera frame;

³⁰ <http://www.markelowitz.com/Hyperspectral.html>

the second spatial coordinate (y) is captured with line (slit) scanning; (c) staring Spectral Imaging devices, where a 2D sensor array is coupled with an imaging monochromator, which is tuned to scan the spectral domain and in each scanning step, a full spectral image frame is recorded. A tunable light source is also suitable for staring Spectral Imaging, but in that case, the possible contribution of the broadband ambient light should be eliminated

Spectral Imaging devices have been extensively used for accurate colour reproduction and colorimetry applications. Chapter 4, discusses the algorithmic procedure to extract colour from spectra and also proposed a colour gamut calculation procedure for Hyperspectral devices.

1.5 Overview of the thesis

DSCs spectral sensitivity data are essential for the calculation and determination of the colour gamut areas. The measuring preliminaries and procedure for acquiring DSC Spectral Sensitivities have been discussed, along with the experiments which were conducted in situ in the Optoelectronics Laboratory facilities, in Chapter 2. All measurements have been divided into three sections in order to examine whether and how they affect DSC colour gamut. The outcomes from this chapter have been exploited according to the measurement implementations in the following chapters.

In Chapter 3 the calculation and evaluation of DSC's colour gamut has been performed. The essential theoretical background and the current work have been discussed in the first section. Following that, the methodology with the experimental procedure have been presented. Based on Chapter's 2 results, the mentioned colour gamut areas have been calculated and correlated to the human eye colour gamut. Finally, it has been shown that with slight modifications referring to hardware components and processing steps, it is possible to achieve high scores of gamut expansion and matching.

Coming back to the results from the previous chapter, in Section 2 of Chapter 4, the reasoning for moving towards spectral based solutions has been discussed. After oppositional arguments to conventional colour reproduction procedures have been given, a new approach for measuring multi/hyperspectral camera device colour gamut have been proposed. The suggested measurement experiment has been implemented in two stages. Firstly, for simulated data in order to evaluate the theoretical considerations that have been made in the chapter's introduction. Secondly, to a commercial hyperspectral imaging camera which the hypothesised weaknesses have been exposed. An alternative process has been suggested, that is based on Chapter's 3 methodology, and has been implemented to an actual hyperspectral device. The proposed solution has been resulted in approximately 100% colour space matching between the hyperspectral device and human eye colour space.

2. Measuring Digital Camera Spectral Sensitivity

Measuring camera spectral sensitivity is not a trivial procedure. Most scientists with published work on spectral imaging and/or colour imaging are using simulations for their research. This, could easily bring researchers to inaccurate or false conclusions. For that reason, in this thesis we used the available Optoelectronics Laboratory equipment in order to conduct the physical experiments.

This chapter presents the measurement procedure for obtaining Spectral Sensitivity curves for commercial DSCs has been examined. The acquired measurements play a critical role for resolving and expanding DSC's colour gamut and also for improving the colour accuracy of a digital camera.

The chapter is divided in four sections. The first three refer to the theoretical background and the experimental setup of the measurements. In the final section, the measurement results are presented.

2.1 DSC Acquisition Model

The main components involved in image acquisition process are presented in Fig. 2.1. In its general definition (as described in this thesis), there is a linear relationship between each individual element of the whole process.

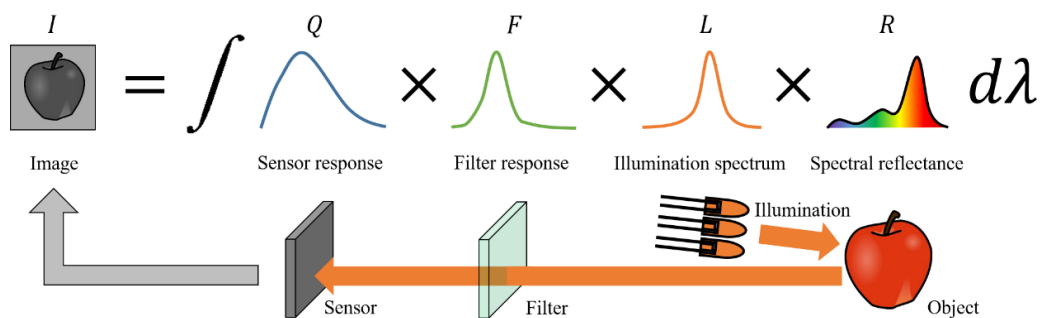


Figure 2.1: Illustration of the acquisition chain of a digital imaging system.

The acquisition chain in a multispectral imaging system with output vector d_k could be described as:

$$d_k = \int_{\lambda_{min}}^{\lambda_{max}} q(\lambda) f(\lambda) l(\lambda) r(\lambda) d\lambda + n_k,$$

where q describes the sensor response vector, f the filter transmission vector, λ is the corresponding wavelength, k is the colour DSC's channel (i.e. Red, Green, Blue),

I the illuminant spectrum vector, r the spectral reflectance of the target and n the system noise. The product of Q , F and L called Spectral Sensitivity S , and the product of Q and F called Spectral Responsivity T . In the measuring experiments that performed, noise was eliminated by preprocessing steps that will be discussed in Section 2.3. Therefore, assuming that system noise is nearly zero (both spatial and temporal noise) the described condition could be defined in matrix notations as:

$$I = S^T R,$$

where the superscript T denotes the matrix transpose.

The Spectral Sensitivity S^T for a conventional RGB DSC indicates a highly underdetermined system of equations as the corresponding matrix consists of k rows and N columns where $k \ll N$:

$$S = \begin{bmatrix} R(\lambda_1) & R(\lambda_2) & \dots & R(\lambda_N) \\ G(\lambda_1) & G(\lambda_2) & \dots & G(\lambda_N) \\ B(\lambda_1) & B(\lambda_2) & \dots & B(\lambda_N) \end{bmatrix}^T,$$

where λ_N indicates the n th wavelength and $R(\lambda)$, $G(\lambda)$, $B(\lambda)$ represent the red, green and blue channel's spectral sensitivities.

2.2 ISO 17321-1

As mentioned in 1.3.4, the spectral responses of the colour channels of DSCs do not, in general, match those of a typical human observer, such as defined by the CIE standard colorimetric observer. Nor do the responses of different DSCs ordinarily match each other. ISO 17321-1 is addressing these considerations by defining standard test procedures for measuring DSCs Spectral Sensitivities.

In the following, two alternative methods for obtaining these characterisations of data are described:

- *Method A*, the spectral method which uses spectral lights as stimuli.
- *Method B*, the target method which involves the use of a physical colour test target under specific lighting conditions.

In current work, Method A has been implemented because i) the results expected to be more accurate, and ii) the Optoelectronics laboratory's equipment was sufficient enough for first type of measurements. Method B was not chosen because it is an indirect measuring method (often involve linear and non-linear spectral sensitivities approximations[13]). Furthermore, the Optoelectronics laboratory's equipment which was available, was sufficient enough for the first type of measurements.

As specified in ISO 17321-1[13], spectral sensitivity-based characterisation measurements shall be obtained by using a light source and a monochromator. The output of the monochromator should evenly illuminate a diffuse reflective surface and

its emission spectrum should be limited to a range of wavelengths that the experiment defines.

The key components/settings for the measuring setup are:

1. A broadband lightsource with smooth SPD such as that obtained from a halogen source.
2. A monochromator for band pass spectral sampling. This device enables user-control wavelength selection with a very shallow Full Width Half Max (FWHM), under 5nm. The measurement's band step interval should be greater than the FWHM value so every wavelength measurement result should be independent from the previous one.
3. An illuminated Lambertian surface. Lambertian stands for an "ideal" diffuse reflective surface which reflects all incoming radiation homogeneously. ISO 17321-1 suggest that the illuminated surface should be the interior of an integrating sphere.
4. Camera settings should be fixed. All automatic DSC's procedures must be disabled and brightness levels should be between 50% and 90% of the total system's saturation.
5. DSC's output values must be in RAW mode, meaning that image data produced by, or internal to a DSC, has not been processed, except for A/D conversion. Any preprocessing step like demosaicing or digital gain should be avoided.

Each wavelength measurement value should be exported from the average of a 64x64 (or greater) pixel block of values in the center of Field Of View (FOV). This step is crucial in order to eliminate spatial noise that often results from non-uniformities on digital sensor's pixels. After averaging, the exported value should be multiplied with the monochromator's spectral response.

2.3 Experimental Setup

The implementation of the measurements is based on ISO 17321-1 setup, as described above. For illuminated Lambertian surface, Ocean Optics WS-1 Reflectance Standard has been used. This target consists of PTFE (Polytetrafluoroethylene³¹) diffusing material with >98% reflectivity from 250 to 1500nm. In order to avoid specular reflections, the primary axis of the incident illumination was approximately 45° to the center of the target area being imaged.

³¹ <https://link.springer.com/article/10.1007/s42114-018-0023-8>



Figure 2.2: Certified Reflectance Standard from Ocean Optics.

The DSC used for the described measurement was ZWO ASI178MC³². It has a 1/1.8" and 6.4M pixels sensor Sony IMX178. This sensor is back-illuminated, meaning that the photosensitive area is above each pixel's circuitry. This microelectronic design enables high quantum efficiency values and nearly absolute fill factor (usually above 95%). Pixel size is 2.4 μ m with Full Well capacity 15000e and Read Noise 1.4e. The communication interface is USB 3.0 enabling up to 60FPS in RAW mode.



Figure 2.3: ZWO ASI178MC colour DSC with Sony's IMX178 digital image sensor.

For illumination source ThorLabs OSL-1-EC with halogen lamp was used. The source's SPD was measured at the laboratory and it is shown in Fig. 2.4.

³² <https://astronomy-imaging-camera.com/product/asi178mc-color>

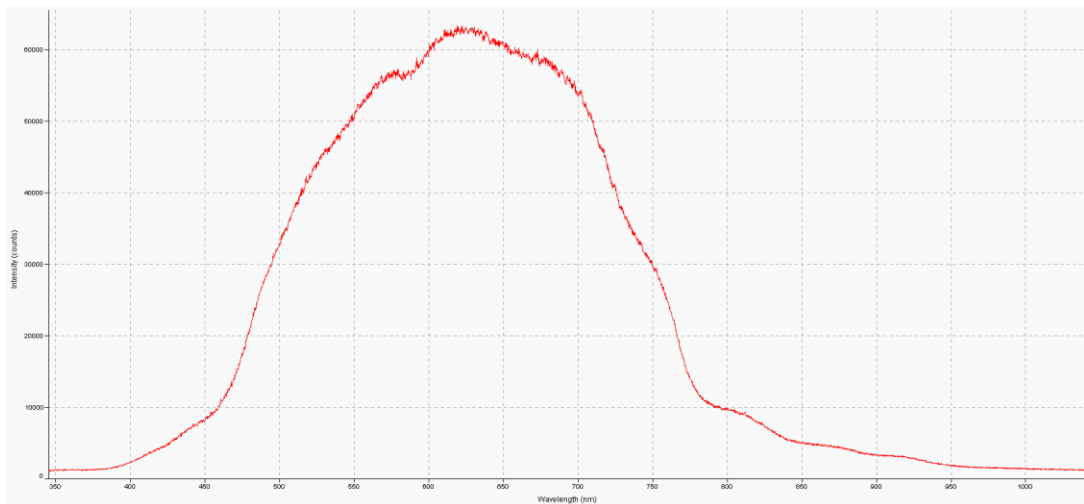


Figure 2.4: ThorLabs OSL-1-EC SPD.



Figure 2.5: ThorLabs OSL-1-EC Halogen with fiber optic.

The light source was coupled through a fiber optic with a manual Edmund Mini-Chrom monochromator³³ with spectral range from 300 to 800nm and FWHM 1nm. The monochromator's transmission spectrum is plotted on Fig. 2.7.



Figure 2.6: Edmund Mini-Chrom Monochromator.

³³ <https://www.edmundoptics.com/f/Manual-Mini-Chrom-Monochromators/11508/>

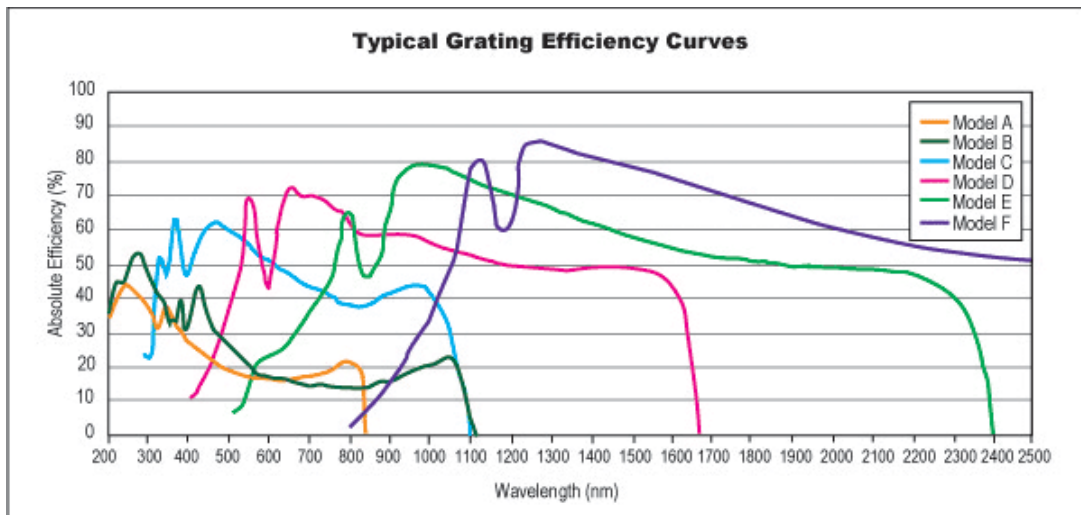


Figure 2.7: Edmund Mini-Chrom Transmittances. This work measurements proceed with Model C restricted to 800nm.

The target positioned at the center of DSC's FOV and the total illumination area width was about 500px. In Fig. 2.7 the discussed measurement setup is shown.

In front of DSC an Electrophysics 25mm C-Mount Lens was coupled. Iris setting was at f4 in order to achieve the appropriate Depth of Field.

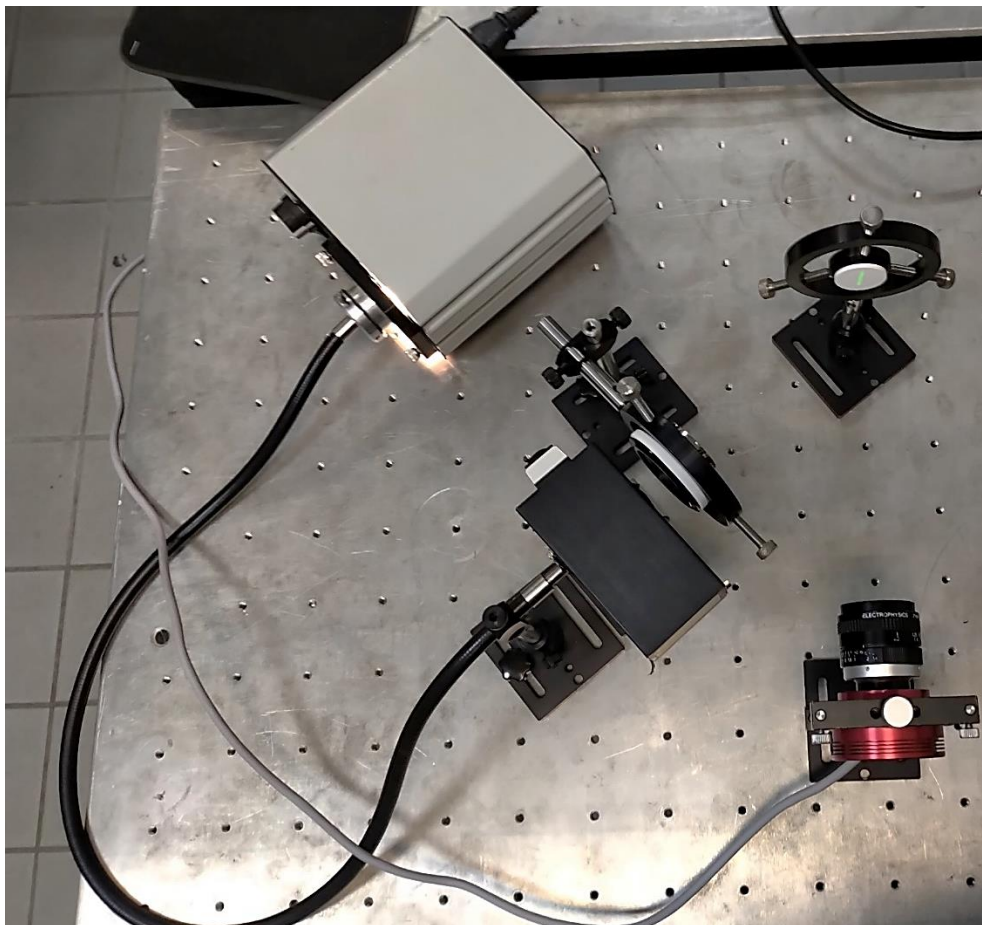


Figure 2.8: Colour DSC Spectral Sensitivity measurement setup.

2.4 Results

SharpCap 3.1 camera software was used in order to measure the system's output. As discussed in 2.2 the mean value of a 100x100 Region Of Interest (ROI) was used in order to eliminate spatial noise variations. The final value was determined by averaging 10 sequential frames, for minimizing the temporal noise fluctuations. Output format was set to RAW, Shutter speed to 200ms, Gain to 0dB. Every auto mode was switched off. It should be noted that the White Balance values were fixed at 64 for Red channel and 99 for Blue. These values were decided after the camera's automatic White Balance setting settled on those numbers. This automatic procedure performed in broadband setup (without the monochromator coupled). The band step interval was constant to 10nm.

2.4.1 Camera Alone Results

In Fig. 2.9 the ZWO ASI178MC Spectral Sensitivities are presented.

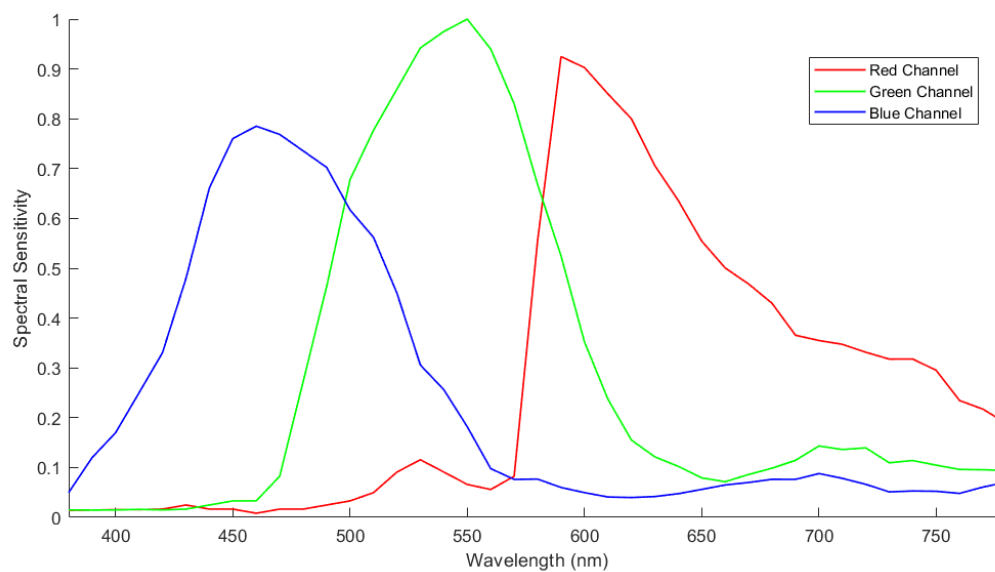


Figure 2.9: ZWO ASI178MC Spectral Sensitivities as measured in Optoelectronics Lab.

The sensitivities were normalised at measurement's max value on 550nm. The measurements took place from 380nm to 780nm such as they match CIE's CMF region limits.

2.4.2 DSC with Triple Bandpass Results

A second measurement was performed with Chroma 69010m Bandpass filter which coupled in front of the camera lens. The filter's transmittance spectrum is presented in Fig. 2.10.

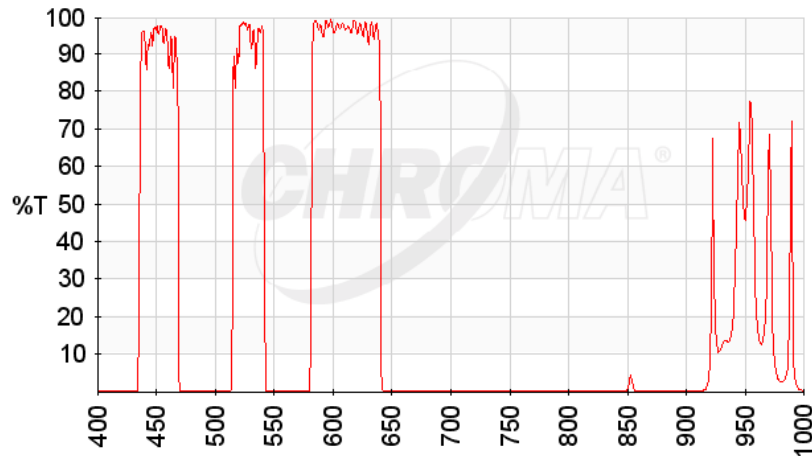


Figure 2.10: Chroma 69010m Triple Bandpass filter transmission spectrum.

The procedure was identical as that in 2.4.1. These three band regions are representative of the three colour channels Red, Green and Blue. The reason for performing this measurement was to compare the results with 2.4.1 in terms of linearity and use them to export DSC colour gamut in 3.4.3. The results are shown on Fig. 2.11.

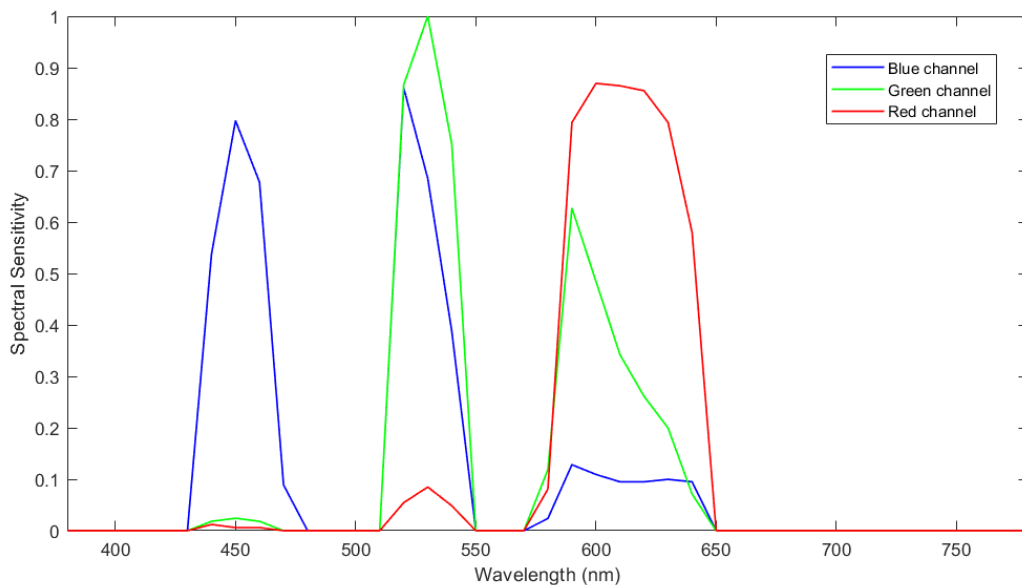


Figure 2.11: ZWO ASI178MC coupled with Chroma 69010m triple bandpass filter Spectral Sensitivities.

2.4.3 DSC with custom White Balance Setting

The third measurement was performed with custom White Balance setting 79 for Red channel and 79 for Blue channel. All other settings and procedures were identical to 2.4.1.

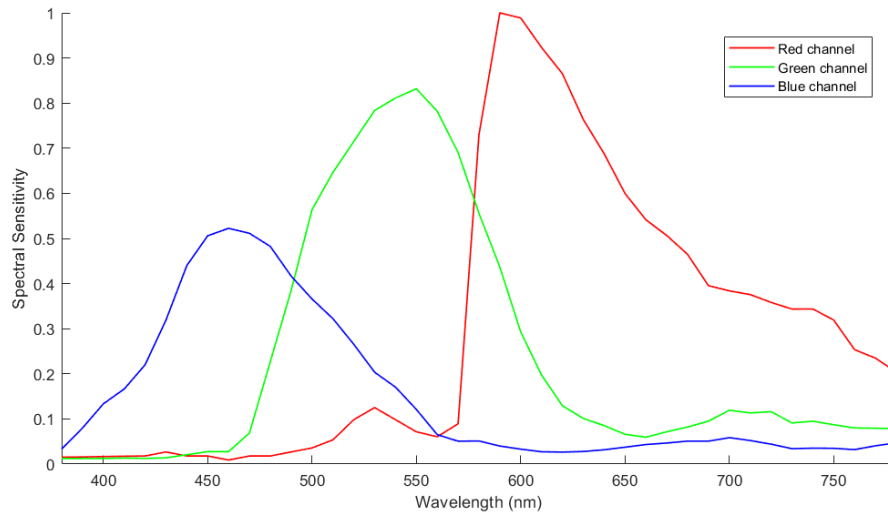


Figure 2.12: ZWO ASI178MC Spectral Sensitivities with custom WB setting.

It is noticeable that the channel's cross-sections are shifted comparing to Section 2.4.1 measurement. Blue-Green channel cross-section moved from $\sim 500\text{nm}$ to $\sim 490\text{nm}$. Green-Red channel cross-section moved from $\sim 590\text{nm}$ to $\sim 580\text{nm}$. WB setting affects each parameter R, G and B individually. Therefore, the contribution of one channel to another changes independently comparing to the constant values of CMF. This condition results in a non-linear relationship between them. Consequently, the colour matrix that maps from one colour space to another diverges for each WB setting, ending up to a different colour gamut area.

3. Calculating Digital Camera's Colour Gamut

A colour DSC provides a link between digital data and colour stimuli. This relationship between analog inputs and digital outputs depends on both physical properties (optics, spectral sensitivities, scene geometry etc.) and the processing of the acquired digital values (colour interpolation, white balance, tone mapping etc.). The main target is to reproduce colour as close to how the human eye perceives. By measuring the physical properties of a DSC, the processing of the digital colour values could be optimised to achieve that objective. Modifying the hardware of a DSC could also lead to the improvement of colour capturing capabilities.

Determining the gamut of input device (such as a colour DSC) is one of the main physical characteristics that has to be defined in order to achieve accurate colour.

However, the conceptual problems inherent to determining DSC's colour Gamut are numerous.

The calculation of colour Gamut, its complications and some practical examples are discussed in this chapter. Also, an improved alternative gamut approach is presented that outperforms the traditional linear correction methods.

3.1 Luther condition

As discussed in 2.1, colour DSC's Spectral Sensitivities S^T are described from highly underdetermined systems often with 3 (in case of a RGB DSC) linear equations for λ_N (N wavelengths) unknown variables. That matrix could lead to the same results with different inputs as noted in 1.2.6, where Metamerism was introduced. Namely spectrally different colour stimuli may give rise to identical RGB values. Therefore, it is very difficult to determine what colour-stimulus corresponds to a RGB tuple if the captured scene is not previously known.

If the captured target is known, for example XRite's³⁴ Macbeth SG Colorchecker®, the corresponding RGB values will be also known as well. After transforming the RGB tuple to XYZ tristimulus values then determines how the input device encodes these colour stimuli in comparison with the human eye. To do this, the DSC's colour profile must be applied to the RGB tuple to derive the corresponding XYZ values. Therefore, the colour Gamut of an input device depends on a colour transform. It is not clear a priori if any type of colour transform might be associated with the DSC's colour Gamut, or if it can be calculated by the means of alternative procedures.

In principle, the above procedure would not be necessary if there was a completely linear match between colour DSC's Spectral Sensitivities and CIE's CMF.

Luther condition[14] is satisfied when there is a linear relation between the Spectral Sensitivities of a digital input device and human colour responses as standardised by CIE's Standard Observer CMF.

Let $T_{RGB} = S^T$ for the DSC's Spectral Sensitivities, T_{XYZ} as a 3xN matrix for CIE's CMF and T_{CAM} the 3xN matrix for DSC's colour matching functions. According to Luther condition, the CMF and the DSC's Spectral Sensitivities can be expressed as a linear combination:

$$T_{XYZ} \approx T_{CAM},$$

where

$$T_{CAM} = MT_{RGB},$$

and M is the basic colour profile or colour connection matrix relating to both colour spaces (DSC colour space and CIE XYZ colour space). If the above approximation was satisfied (by becoming an equation), the XYZ tristimulus values derived from the

³⁴ <https://www.xrite.com/categories/calibration-profiling/colorchecker-digital-sg>

colour profile matrix would coincide with the real values, that where presented in the scene. In this state, the DSC would act as a colorimeter. A colour metameric for the eye must also be metameric for the camera and vice versa. However, in real life situations this approximation never reaches equality, mainly because of the non-linearities in an optoelectronic system pipeline. Consequently, due to the non-ideal optoelectronic performance and the nonfulfillment of the Luther condition, the input devices in RAW performance (without colour rendering to standard output-referred representations), will always show a colour Gamut different from that of the Colorimetric Standard Observer.

To summarise, the problem of colour correction is the problem of mapping RGB sensor responses to CIE XYZ tristimulus values. Unless device sensitivities are a linear transform of the XYZ colour matching functions (the Luther conditions apply) then perfect colour correction is not possible.

3.2 Gamut Calculation

The colour gamut of a DSC is defined as the range of the different colour stimuli that it can capture. These colours describe the device-specific colour space. In order to have a meaningful representation, the DSC colour space should be transformed to match CIE's XYZ colour space.

RGB triangles are often used to represent colour gamut of rendering devices such as displays and projectors. Consequently, three primaries contribute to colour mixing. They are also used to describe DSC's colour Gamuts, but these representations are actually crude and simplistic. Although, they are often used and are usually acceptable in the use of commercial devices, since the actual colour gamut of DSCs is approximately triangular.

This is not the case for real life measurements as also stated in Chapter 2. There are two main ways to calculate a DSC's colour gamut:

- By direct measurement of DSC's Spectral Sensitivities. After obtaining the measurements, the DSC Spectral Sensitivities are transformed related to CIE colour matching functions and according to the Luther condition.
- Indirectly, by measuring the colour coordinates of a known colour target and then mapping them to a CIE's standard colour space.

In this work the first approach has been investigated and implemented.

The indirect solution is a more practical approach that restricts the DSC colour gamut to the target colour space. An example of this approach[15] is shown in Fig. 3.1.

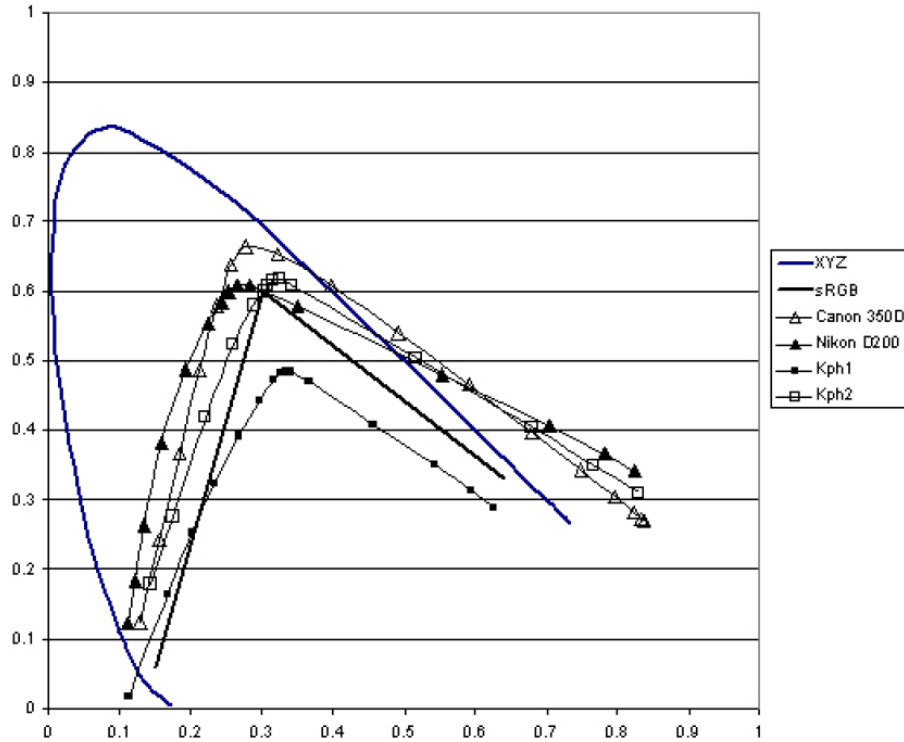


Figure 3.1: Colour Gamut calculation results using indirect method[15].

In the above implementation, a Gretag Macbeth Colorchecker³⁵ has been used, whose coordinates are limited in sRGB colorspace. It is obvious that the DSCs colour gamuts are placed close to the sRGB colour space, something which is not representative of the actual camera colour Gamut.

Based on the direct method, DSC's Spectral Sensitivity and CIE's CMF should be provided. In order to calculate the camera colour Gamut, colour matrix M should be firstly approximated. The easiest and most straightforward method for mapping RGB to XYZ is to use a linear transformation in the form of a 3×3 M matrix[16]. This matrix maps a RGB sensor response to the corresponding XYZ tristimulus values. This technique is also known as linear colour correction[17]. As it will be discussed (rather than implemented) later in 3.3.1, several optimisation approaches exist.

For this thesis, least squares approach is used. Using the equations in Section 3.1 and following the *least squares* sense by minimizing the root mean squared error and assuming that Luther condition is satisfied, the following condition has been derived:

$$\|T_{XYZ} - MT_{RGB}\|^2$$

Colour matrix M can be calculated from:

$$M = T_{XYZ}(T_{RGB})^+,$$

where notation “ $^+$ ” stands for pseudoinverse operation.

The transformation M matrix is a 3×3 matrix which is a function of device spectral sensitivities, illumination and, surface reflectance. These characteristic values are

³⁵ <https://www.xrite.com/categories/calibration-profiling/colorchecker-classic>

derived from T_{RGB} and have been calculated as defined in Section 3.1. By substituting to the estimated values of M matrix, the transformed spectral sensitivities T_{CAM} could be also calculated. It should be mentioned that the described procedure has many common characteristics with the linear colour correction methodology. However, in this particular implementation the DSC's spectral sensitivities have been explicitly modeled and played a crucial role of the colour matrix transformation.

After performing the discussed procedure the DSC's colour gamut could be plotted in the context of CIE chromaticity diagram. The transformed spectral sensitivities T_{CAM} describe the boundary layer of the camera colour space in relation to CIE XYZ colour space. In order to map the two dimensional plane of the specific colour space (as described in 1.2.4), the relative values $x(\lambda)$ and $y(\lambda)$ for each wavelength are computed as follows:

$$x(\lambda) = \frac{X(\lambda)}{X(\lambda) + Y(\lambda) + Z(\lambda)},$$

$$y(\lambda) = \frac{Y(\lambda)}{X(\lambda) + Y(\lambda) + Z(\lambda)},$$

where $X(\lambda)$, $Y(\lambda)$ and $Z(\lambda)$ are the first, second and third row, of the matrix T_{CAM} .

3.3 Current Literature

Many techniques have been developed in order to expand and optimize DSC's colour gamut. They could be classified into two categories. The first one refers to the improvement of estimating colour correction matrix M . These methods affect the processing procedure of the digital signal, as it goes through DSC's image pipeline. The second approach refers to the redesign of the colour channels by transforming and/or adding more than three. These methods usually affect the hardware components of the DSC.

3.3.1 Camera Gamut calculation through Colour matrix approximations

By calculating the M colour profile matrix with different approximations [15], [18], [19] (from the interpolation-based methods to best fitting methods), better colour fidelity results and/or colour gamut expansion could be achieved. Larger colour gamut does not necessary mean better colour accuracy. This realisation can be seen in [18] where various approximations have been used in order to estimate matrix M . These methods can be summarised [19] as:

- The Least Squares (LS) error minimization. LS fits the captured spectral sensitivity curves to the CIE 2° observer colour matching functions. It's the most common and simplistic approach. Errors at

each wavelength in XYZ space are minimised to derive the matrix that produces the smallest sum of squared errors. The matrix is independent of the scene adopted white.

- The White Preserving Partial Least Squares (WPPLS)[17] error minimization. It is a very common approach used by many related works. It is similar to the LS error minimization, but the matrix row sums are constrained to preserve equi-energy white.
- The RGB error minimization is a white point preserving least squares minimization of the spectral colours (monochromatic colors) performed in a colour space based on monochromatic primaries at 450, 540 and 620 nm, an equi-energy white point, the sRGB colour component transfer function, and with the spectral errors weighted by the adopted white spectral power distribution. With this method, the scene adopted white is mapped to equi-energy white in the error minimization colour space.
- The DNG matrices are the camera RGB to D65 XYZ matrices found in Adobe DNG³⁶ files for the Nikon and Canon cameras. It is assumed that these matrices are determined either by the camera manufacturer or by Adobe using unspecified methods.

All these methods can be easily extended to the case of multiple channels just by adding more rows to the colour matrix M . As mentioned in 3.2, in the current work only the LS minimization error has been implemented.

Based on these approaches of estimating matrix M values, the metamer space calculation plays an important role. As it is noted earlier in 1.2.6, the metamerism of a colour DSC does not match that of the human eye. The set of all possible X, Y and Z tristimulus values that match a single DSC RGB response synthesize a three-dimensional convex space usually named Metamer Mismatch Body (MMB)[20]. The ability to compute MMBs proved to be very useful in camera colour correction.

The usual method to calculate MMBs is by enforcing “physical realiseability” constraints[21], [22], such as:

- The MMB is a convex set.
- Linear Programming can be used to minimise or maximise a linear objective function over any convex set.
- The *linear form* of a direction vector can be used as an objective function that when minimised or maximised over a convex set yields points on the surface of the convex set, in that direction.

After calculating the convex hull of MMB the centroid[21] of that space is used to re-establish colour mapping between DSC’s colour space and CIE XYZ colour space. This solution has been proven to be the most effective one.

³⁶ <https://helpx.adobe.com/photoshop/digital-negative.html>

3.3.2 Expanding Colour Gamut by adding new colour channels

Researchers have considered using more than three colour channels to reduce DSC's colour space and CIE's XYZ mismatch. In [23], six colour channels were used for making the RGB colours derived from the six-channel data fit to the CIE XYZ colour space. Previous literature described in 3.3.1 considered the determination of a 3×3 linear transform between two colour spaces (one of which may be the CIE XYZ colour space)[18] and/or adding new colour channels. Cohen and Kappauf developed this concept further by proposing a matrix-R theory that uses an orthogonal projector, termed R (thus the name matrix-R), to decompose an incoming SPD into two components mathematically[24]. Accordingly, the incoming SPD from any point in a scene can be split into two components: a fundamental metamer and a metameric black vector. The fundamental metamer is unique to the channel responses. It is a definite linear combination of the CMF and responsible for the observed tristimulus response. The metameric black vector projects to $[0, 0, 0]$ in the colour space and lies completely in the space orthogonal to the CMF, thus does not contribute to the tristimulus response. The space orthogonal to the CMF is known as the metameric black space (MBS)[24].

Though previous work has recommended one or more extra channels for gamut expansion, they did not target the MBS of the camera and its overlap with the CIE XYZ colour space, which is the root cause of this problem. Also, they did not consider the design problem of the extra channels.

While metamerism and MBS has been used widely in colour research[21]–[23], [25], its use for the design of an additional channel is done for the first time from Dilip K. Psarad in [26]. This work proposes the design of an additional filter to be used with existing camera sensors. The filter design leverages on the matrix-R theory[24] that states that the space of metamerism of a sensor, known as MBS, can be determined directly from DSC's Spectral Sensitivities.

Although, most of the described works achieve good colour matching results they are not physical implementations i.e. they are based on simulation data. Moreover, new channels that are used do not have a physical meaning such as the small continuous regions of EMR spectrum R, G, and B.

3.4 Methodology

3.4.1 Experiment Data - Processing

The Spectral Sensitivities curves from Chapter 2 were used for implementing the experiments used in this thesis. The Gamut calculation is based on the fulfillment of Luther condition by using Least Squares approach to determine M colour matrix as described in 3.2.

The Colour Matching Functions that were used have been acquired from CIE's official website³⁷ and based on CIE '31 2° Standard Colorimetric Observer. The spectral range that has been used is from 380nm to 780nm with band interval 10nm.

Matlab 2018a has been used for data processing and plotting.

3.4.2 Gamut Calculation Conditions

All Gamut colour spaces are also represented in reference to CIE's 1931 chromaticity diagram. This illustration is used in order to examine the experiment's results isolated from brightness characteristics.

Three colour Gamuts have been calculated, each one based on different DSC's Spectral Sensitivities. These Gamuts are:

1. Camera Alone Gamut.
2. Camera coupled with a Triple Bandpass Filter.
3. Camera coupled with a Triple Bandpass Filter without channel crosstalk.

3.4.3 Error Measures

The results are presented in two main states. The first one is the calculated colour space of the DSC. The transformed Spectral Sensitivities of the DSC are correlated with the XYZ values of CIE '31 Standard Observer CMF. The second state refers to CIE's Chromaticity diagram and how DSC's colour gamut overlaps with it. For these two states, four different error measures are presented, two for each corresponding circumstance.

³⁷ <http://www.cie.co.at/technical-work/technical-resources>

3.4.3.1 Manhattan Distance (Normalised)

Also known as Taxicab norm or L1 Norm. Manhattan Distance is the sum of the magnitudes of the vectors in a space. It is the most natural way to measure the distance between vectors, by summing the absolute differences of their Cartesian coordinates. The L1 Norm between two vectors in an N -dimensional real vector space with fixed Cartesian coordinate system, is the sum of the lengths of the projections of the line segment between the points onto the coordinate axes as described in:

$$L1_n = \frac{\sum_{i=1}^N |\hat{\tau}_i - \tau_i|}{N},$$

where τ is the CIE's X or Y or Z tristimulus value, $\hat{\tau}$ is the DSC's corresponding X or Y or Z values. N is the total amount of individual wavelengths λ .

3.4.3.2 Root Mean Square Error (RMSE)

In statistics, the root mean square error or RMSE of an estimator is one of many ways to quantify the difference between an estimator and the true value of the quantity being estimated. RMSE is a risk function, corresponding to the expected value of the squared error loss or quadratic loss. RMSE measures the average of the square of the "error". The error is the amount by which the estimator differs from the quantity to be estimated. The difference occurs because of randomness or because the estimator does not account for information that could produce a more accurate estimate. More formally:

$$RMSE = \sqrt{\frac{\sum_{i=1}^N (\hat{\tau}_i - \tau_i)^2}{N}}.$$

In current work RMSE has been used column wise for DSC's transformed Spectral Sensitivities in comparison to CIE's '31 Standard Observer CMF. Every column of the estimated CMF, represents X, Y, Z tristimulus values of the camera's colour space for each wavelength λ .

3.4.3.3 Euclidean Distance

In mathematics, the Euclidean Distance (ED) or Euclidean metric is the "ordinary" distance between two points that one would measure with a ruler, and is given by the Pythagorean formula. By using this formula as distance, Euclidean space (or even any inner product space) becomes a metric space. The associated norm is called the Euclidean norm. In the Euclidean plane, then the distance is given by:

$$ED = \sqrt{(\hat{x}_\lambda - x_\lambda)^2 + (\hat{y}_\lambda - y_\lambda)^2},$$

where $\hat{x}_\lambda, \hat{y}_\lambda$ are the estimated chromaticity coordinates that represent the outer boundary of DSC colour gamut. Values x_λ, y_λ are the corresponding coordinates for CIE '31 chromaticity diagram. Mean, min and max values have been exported so as to attain a better overview of the final results. This error criterion refers to how good is the match between DSC colour gamut spectral locus and CIE'31 chromaticity diagram's spectral locus. In other words, it represents how close are the two examined colour gamuts in terms of shape, translation, rotation and stretch.

3.4.3.4 Gamut Area Difference

In order to achieve a more indicatory comparison, the difference between the common areas of two colour gamuts have been calculated. The overlapping area between CIE's chromaticity diagram and DSC's colour gamut represents how close the DSC's output is to the human colour perception. The lower the difference the better the match. Suppose that TA_C is the CIE's chromaticity chart total area and TA_D is the DSC's gamut total area. The difference DA between the common areas is:

$$DA = TA_C - (TA_C \cap TA_D).$$

The polygon for each colour gamut is calculated with Matlab's command "polyshape". After that "intersect" command is executed in order to calculate the overlapped gamut polygon. By using the command "intersect" for the corresponding colour gamut polygons (polyshape objects), the total area is calculated.

3.5 Results

3.5.1 Camera-Alone Colour Gamut

The DSC Transformed Spectral Sensitivities have been calculated with the measurements provided by 2.4.1. In Fig. 3.2 the results of the camera-alone setup are presented.

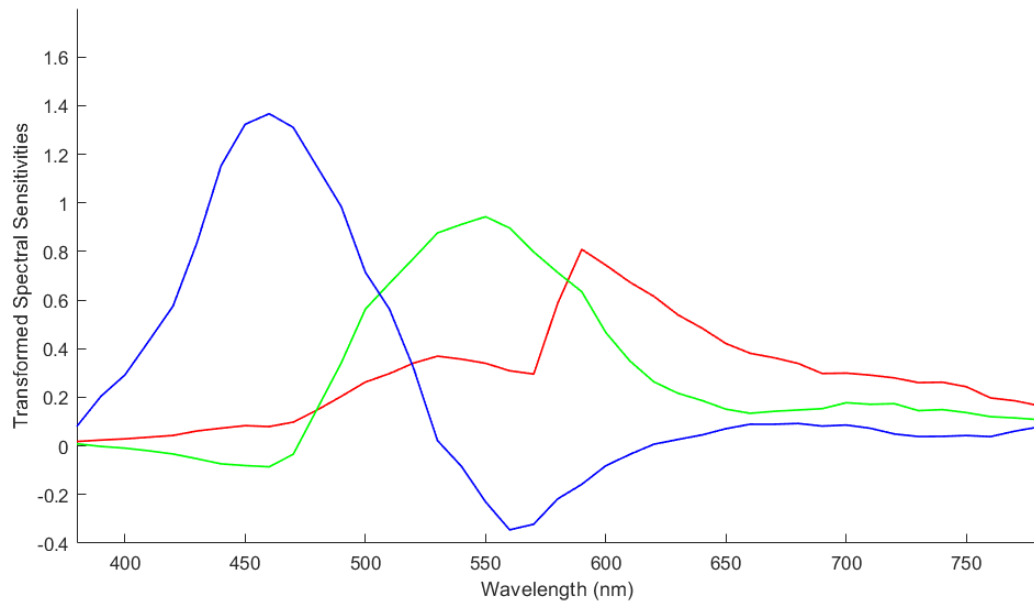


Figure 3.2: ASI178MC Transformed Spectral Sensitivities T_{CAM} as calculated with LS method.

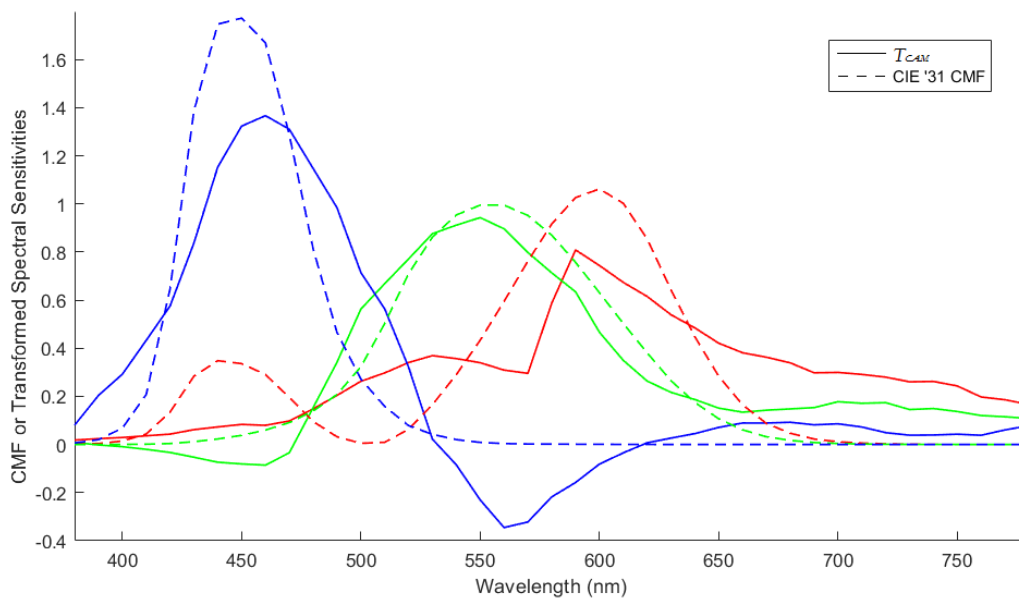


Figure 3.3: ASI178MC Transformed Spectral Sensitivities T_{CAM} comparing to CIE '31 CMF.

As it shown in Fig. 3.3, the transformed spectral sensitivities are far from matching CIE '31 Colour Matching Functions. The overall error results are shown in Table 2. It is clear that ASI178MC's chromaticity components \bar{x} and \bar{z} have significant variations compared to the corresponding ones of the CIE CMF. On the other hand, the illuminant component \bar{y} achieves better matching results.

	\bar{x}	\bar{y}	\bar{z}
RMSE	0.2284	0.1175	0.2389
L1	0.2025	0.1018	0.1751

Table 2: RMSE and Manhattan Distance errors for T_{CAM} vs CIE '31 CMF.

The colour matrix M values that transform DSC outputs to the corresponding X, Y and Z tristimulus values, are presented in Table 3.

	X	Y	Z
R	0.7111	0.2781	0.0823
G	0.1506	0.9606	-0.1512
B	0.0284	-0.5526	1.7638

Table 3: Colour Correction Matrix M for converting camera R, G, B responses to X, Y, Z tristimulus values.

The ASI178MC colour Gamut is plotted in comparison with CIE '31 chromaticity diagram in Fig. 3.4. Every point of measurement is presented with a diamond shape. The interconnection between them has been performed through linear interpolation. Each of the plotted “*diamonds*” correspond to a certain spectral colour from the spectral locus of the diagram.

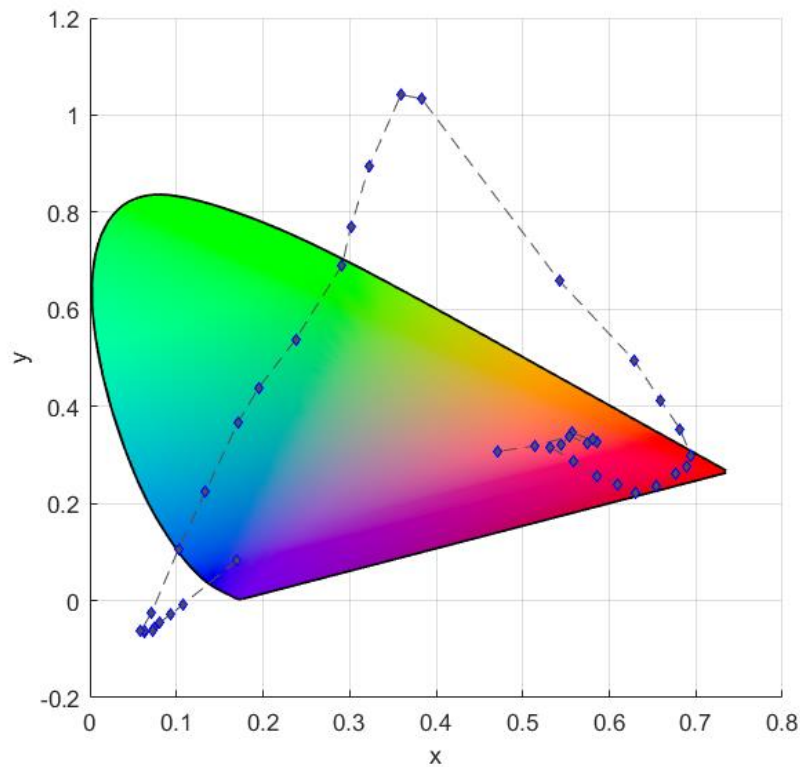


Figure 3.4: ASI178MC Colour Gamut plotted with CIE '31 Chromaticity diagram

It is useful to note that the shape of DSC's colour gamut tends to be triangular. This is in accordance with most of literature approaches that perform the same experiments.

As it is shown, ASI178MC colour gamut extends out not only the CIE '31 chromaticity diagram's spectral locus, but even outside XYZ primary triangle. The imaginary colours that DSC can capture are comparable to the amount of the real ones.

The common area between CIE '31 chromaticity diagram and ASI178MC colour gamut is presented on Fig. 3.5. This area represents the real colours that a DSC can capture according to the human eye colour perception. The non-highlighted region of DSC's colour gamut represents colours that are impossible for the human eye to observe.

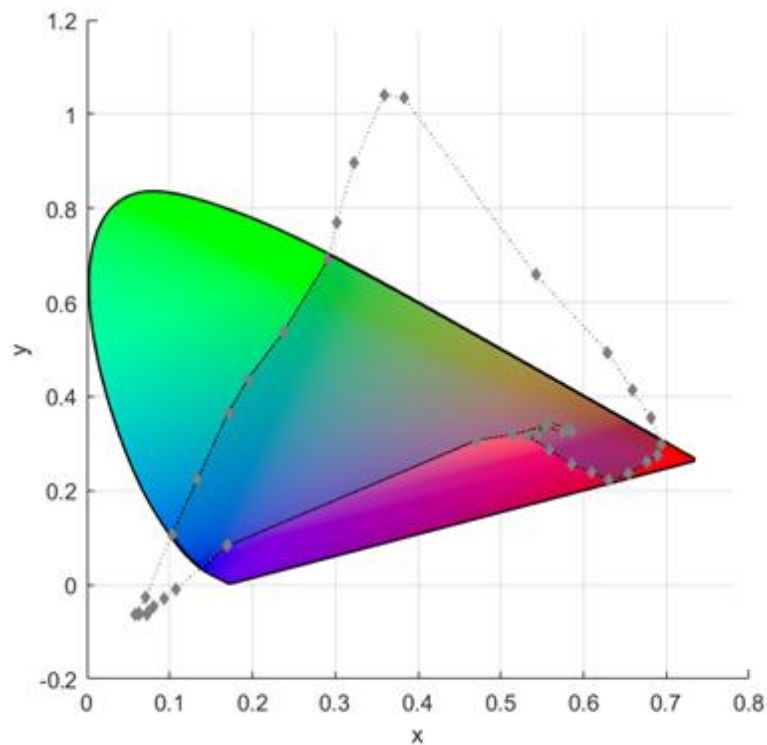


Figure 3.5: The overlapped area between CIE '31 Chromaticity diagram and ASI178MC Colour Gamut.

The total area characteristic values of the gamut comparison as it is shown in Fig. 3.5 are presented on Table 4.

Total Area

DSC	CIE '31	DA	Common Area	Common Area % - DSC	Coverage % - CIE '31
0.2561	0.3314	0.1726	0.1588	62.01%	48%

Table 4: Total Area Characteristic Values for ASI178MC colour gamut and CIE '31 Chromaticity Diagram.

The area mentioned as *Common Area % - DSC* represents the percentage of the whole DSC colour gamut to number of colour distinguishable to the human eye. The other measure *Coverage % - CIE '31* refer to the percentage of the total overlapped area compared to CIE '31 chromaticity diagram.

The spectral locus of each gamut is constructed by the corresponding wavelength in which the measurement took place. The closer each spectral colour tends to match CIE's spectral locus the better results in acquiring both gamut completeness and shape similarity. Table 5 shows the characteristic values min, max and mean for the Euclidean Distances between the two gamut spectral locus regions.

Euclidean Distance

Min	Max	Mean
0.0113	0.4831	0.1545

Table 5: Min, Max and Mean Euclidean Distances of ASI178MC and CIE '31 Chromaticity Diagram spectral locus.

By using the Spectral Sensitivities from 2.4.3 and performing the same procedure as proposed in this section the final colour gamut changes. This slight but noticeable change is shown on Fig. 3.6. The different white balance setting of the DSC seems to affect ASI178MC colour gamut. In this graph the XYZ triangle has been plotted in order to give a perception of the total mismatch of the calculated colour gamuts.

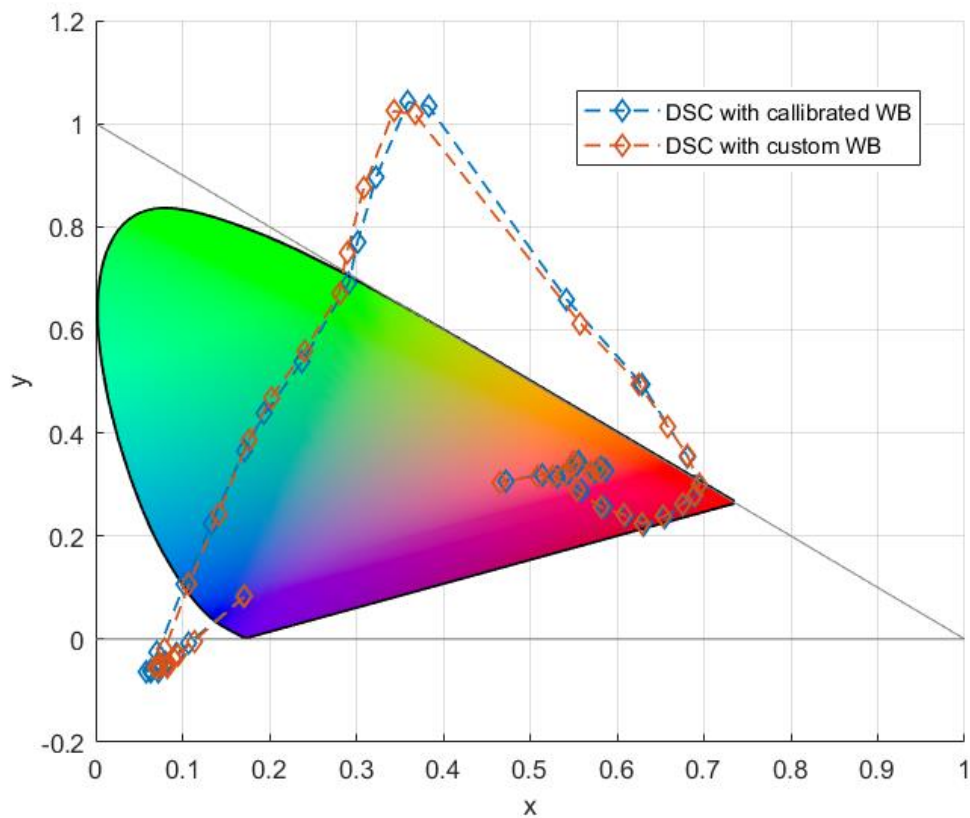


Figure 3.6: Colour gamuts of the same DSC with different WB settings.

3.5.2 Camera coupled with a Triple Bandpass Filter

In 2.4.2 ASI178MC Spectral Sensitivities were acquired with a triple bandpass filter coupled. These kinds of filters enable only certain frequencies of EM spectrum to pass through them. As a result, the final Spectral Sensitivity curves have zero values to the frequency-forbidden EMR regions. These curves are presented in Fig. 3.7.

If the Luther condition be applied in these Spectral Sensitivity curves, the total mismatch between them and CIE '31 CMF is considerable but not as broad compared to section 3.5.1.

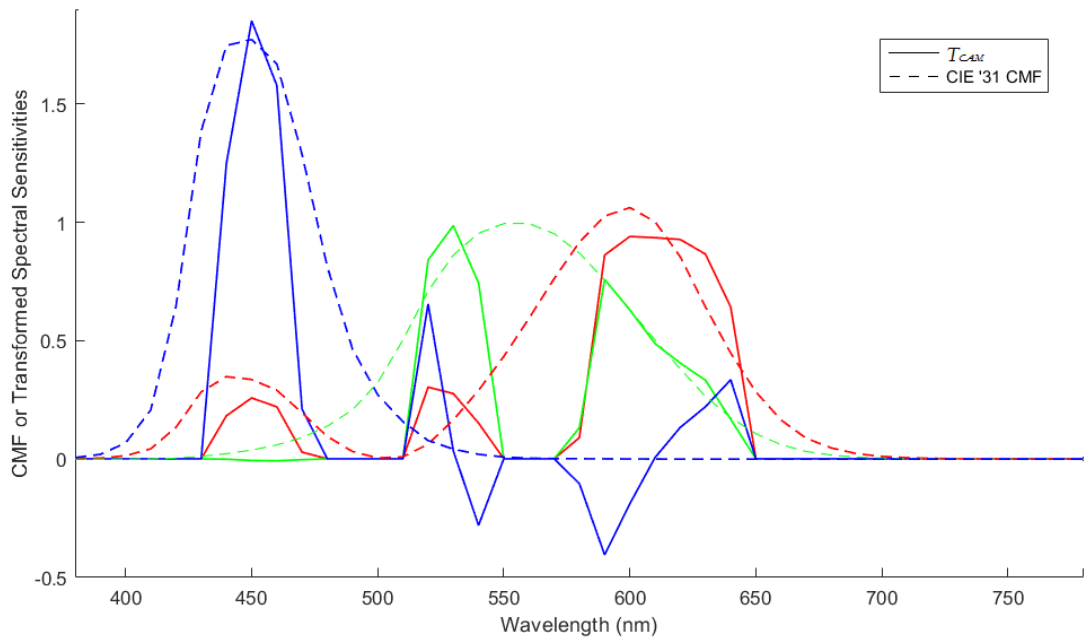


Figure 3.7: ASI178MC coupled with Chroma 69010m Triple Bandpass filter Transformed Spectral Sensitivities T_{CAM} comparing to CIE '31 CMF.

The results of total distances between the plotted curves (corresponding to each function) are shown in Table 6.

	\bar{x}	\bar{y}	\bar{z}
RMSE	0.1545	0.1253	0.2336
L1	0.0644	0.0378	0.0982

Table 6: RMSE and Manhattan Distance errors for T_{CAM} vs CIE '31 CMF.

As expected, the total gamut area of the mentioned setup diverges from CIE '31 chromaticity diagram. In Fig. 3.8 it is visually clear that ASI178MC with Chroma 69010m filter colour gamut area refers mainly to imaginary colours.

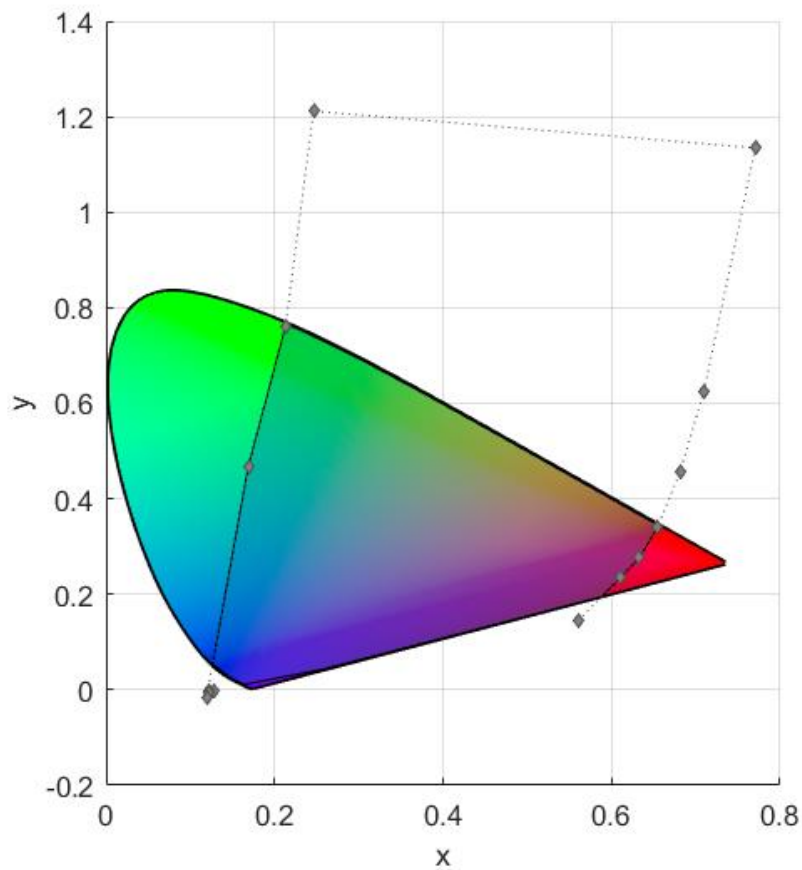


Figure 3.8: The overlapped area between CIE '31 Chromaticity diagram and ASI178MC coupled with Chroma 69010m triple bandpass filter Colour Gamut.

In Table 7 the total area characteristics between the two colour gamuts are shown. It is noticeable that the total overlapped area is wider than the *Camera Alone* setup on 3.5.1. Despite that fact, all other values are considerable out of reference. This reality is enhanced by the overall distance values of the spectral locus of two gamuts shown in Table 8.

Total Area

DSC	CIE '31	DA	Common Area	Common Area % - DSC	Coverage a % - CIE '31
0.5534	0.3314	0.1052	0.2262	40.87%	68%

Table 7: Total Area Characteristic Values for ASI178MC coupled with Chroma 69010m triple bandpass filter colour gamut and CIE '31 Chromaticity Diagram.

Euclidean Distance

Min	Max	Mean
0.0048	0.7502	0.2412

Table 8: Min, Max and Mean Euclidean Distances of ASI178MC and CIE '31 Chromaticity Diagram spectral locus.

3.5.3 Camera coupled with a Triple Bandpass Filter without channel crosstalk

Channel crosstalk or channel overlapping is an aftereffect of the design of the Bayer mosaic RGB filters. Colour cameras manufacturers use such filters in their CFA integrations in order to achieve good camera sensitivities and high levels of SNR. Although this consideration on colour DSC design results to better overall sensitivity it also affects colour reproduction. The crosstalk between different colour channels results to unwanted colour deviations from the observable scene colour. Many approaches have been implemented [27], [28] in order to preserve both high sensitivity and colour accuracy levels. Image processing algorithms in post-acquisition steps are used to compensate that effect.

It is noticeable that also the human's eye spectral sensitivities have sizeable crosstalk areas as it is mentioned in 1.2.1. Human colour perception is not a Linear Time Invariant (LTI) process -as stands for a DSC- but a highly complex procedure involving both the eye and the human brain. Arising from that fact, human colour perception could counteract the broad crosstalk characteristics in such a way as to preserve both high sensitivity and colour saturation.

In this section, crosstalk-free narrow band channels are presented. There is no proposed algorithm for achieving such a result since it is out of this thesis interests.

In Fig. 3.9 ASI178MC coupled with Chroma 69010m triple bandpass filter colour Spectral Sensitivities are shown. As noticed compared to 2.4.2 curves, the crosstalk between channels has been eliminated through simple subtraction.

This proposed modification is derived from spectral based camera integrations (multi/hyperspectral imaging devices) that use narrowband bandpass filters with linear independent channel responses. It is expected that these considerations derive better results compared to the conventional LS methods.

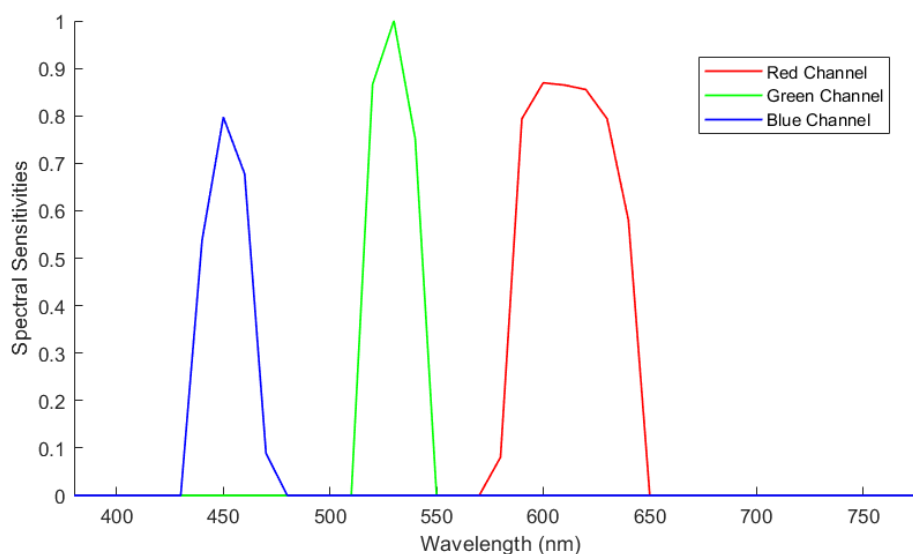


Figure 3.9: ASI178MC coupled with Chroma 69010m Spectral Sensitivities without channel crosstalk.

In Fig. 3.10 the transformed Spectral Sensitivities of Fig. 3.9 are presented. Comparing to the transformed Spectral Sensitivities from previous sections it is noticeable that no negative values exist.

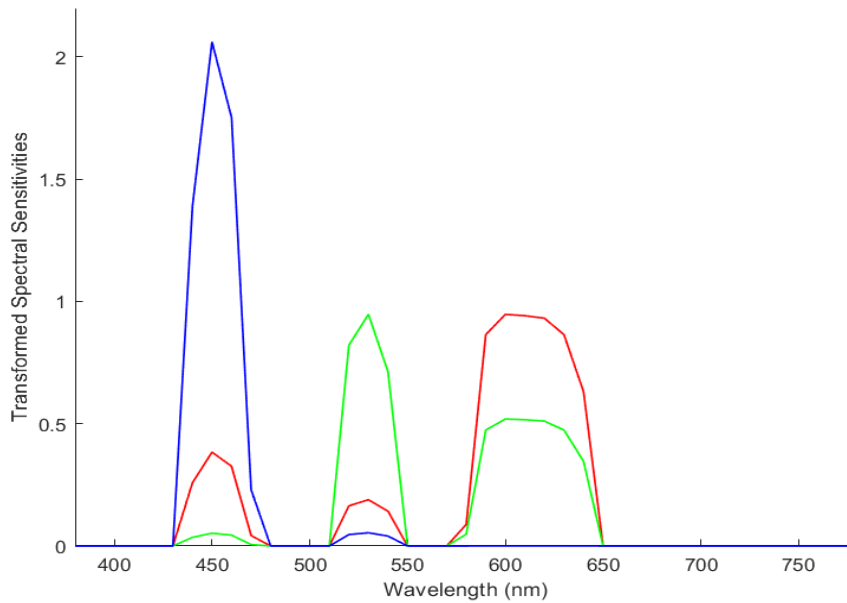


Figure 3.10: ASI178MC Transformed Spectral Sensitivities T_{CAM} comparing to CIE '31 CMF.

Comparing with CIE '31 CMF in Fig. 3.11, the transformed values tend to match the Standard Observer ones as it is numerically shown in Table 9.

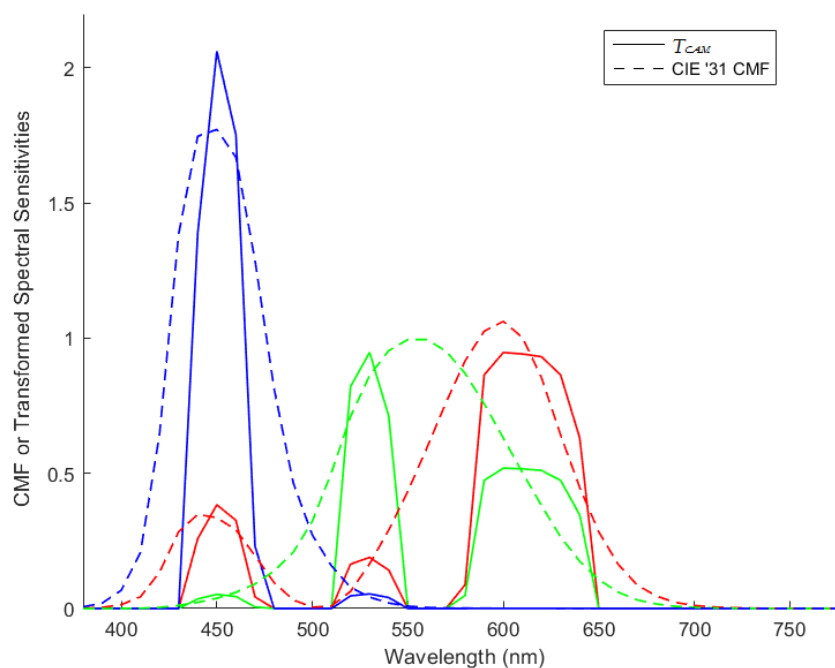


Figure 3.11: ASI178MC Transformed Spectral Sensivities T_{CAM} comparing to CIE '31 CMF.

	\bar{x}	\bar{y}	\bar{z}
RMSE	0.147	0.1517	0.1807
$L1$	0.0547	0.0562	0.0044

Table 9: RMSE and Manhattan Distance errors for T_{CAM} vs CIE '31 CMF.

The gamut of the Transformed Spectral sensitivities compared to CIE '31 chromaticity diagram is plotted in Fig. 3.12. The resulting colour gamut has an exact triangular shape with the cross points representing the system's primary colour channels. All ASI178MC gamut area is included in CIE '31 chromaticity diagram, thus this colour setup can capture only human observable colours.

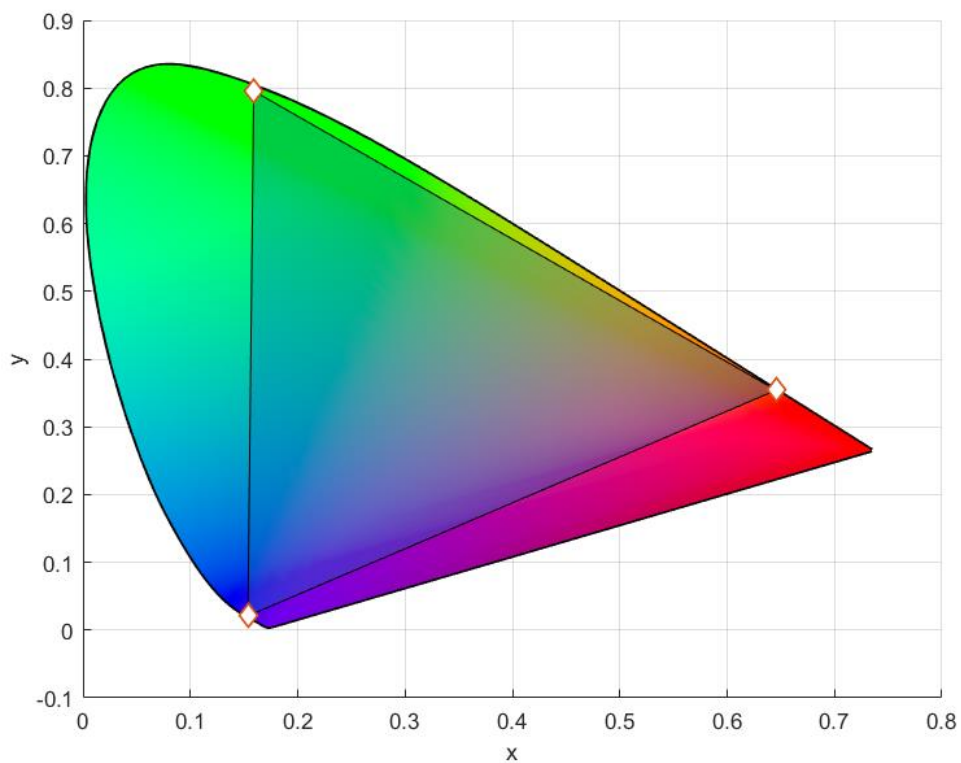


Figure 3.12: The overlapped area between CIE '31 Chromaticity diagram and ASI178MC coupled with Chroma 69010m triple bandpass filter Colour Gamut and crosstalk free channels.

The numerical results relating to the total area and spectral locus distances are shown in Table 10 and Table 11, accordingly.

Total Area

DSC	CIE '31	DA	Common Area	Common Area % - DSC	Coverage % - CIE '31
0.1897	0.3314	0.1417	0.1897	100.00%	57%

Table 10: Total Area Characteristic Values for ASI178MC coupled with Chroma 69010m triple bandpass filter without channel crosstalk colour gamut and CIE '31 Chromaticity Diagram.

Euclidean Distance

Min	Max	Mean
0.0112	0.156	0.0648

Table 11: Min, Max and Mean Euclidean Distances of ASI178MC and CIE '31 Chromaticity Diagram spectral locus.

3.5.4 Summary

In the tables bellow, all the examined colour gamuts are placed together in order to make the comparison more apparent.

RMSE

	\bar{x}	\bar{y}	\bar{z}
Camera Alone	0.2284	0.1175	0.2389
Camera with Triple	0.1545	0.1253	0.2336
Camera with Triple and no crosstalk	0.147	0.1517	0.1807

L1

	\bar{x}	\bar{y}	\bar{z}
Camera Alone	0.2025	0.1018	0.1751
Camera with Triple	0.0644	0.0378	0.0982
Camera with Triple and no crosstalk	0.0547	0.0562	0.0044

Total Area

	DSC	CIE '31	DA	Common Area	Common Area % - DSC	Coverage % - CIE '31
Camera Alone	0.2561	0.3314	0.1726	0.1588	62.01%	48%
Camera with Triple	0.5534	0.3314	0.1052	0.2262	40.87%	68%
Camera with Triple without crosstalk	0.1897	0.3314	0.1417	0.1897	100.00%	57%

Euclidean Distance			
	Min	Max	Mean
Camera Alone	0.0113	0.4831	0.1545
Camera with Triple	0.0048	0.7502	0.2412
Camera with Triple without crosstalk	0.0112	0.156	0.0648

In Fig. 3.13 all colour gamuts of this chapter are presented in comparison with CIE'31 chromaticity diagram.

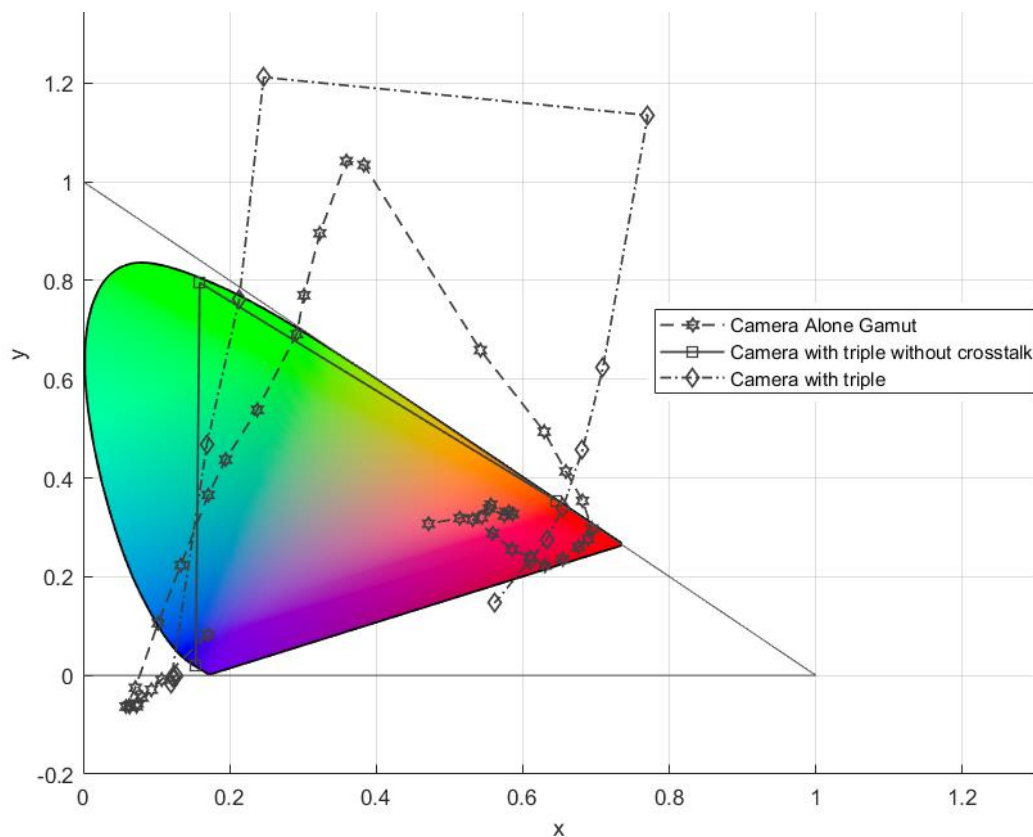


Figure 3.13: Plot of all calculated colour gamuts with CIE'31 chromaticity diagram.

This proposed modification led to better results both in CIE CMF comparison and CIE xy colour gamut completeness. The advantages compared to the conventional procedures could be summarised as follows:

1. The colour gamut of the DSC expanded in relation to CIE'31 chromaticity diagram. The expansion performed only within CIE gamut convex hull performing 100% common area score and enabling only human observable colours output. Further expansion within those limits could be achieved by changing the dominant wavelengths of each colour channel (by replacing the triple bandpass filter). The new spectral bands are just swift the triangle cross-sections according to the spectral locus.
2. The shape of colour gamut is triangular and matches most of commonly used colour spaces.

3. The White Balance setting should not affect the gamut area since there is no crosstalk between the colour channels. On the other side, the statistical approaches produce different colour matrix M for nearly every different WB setting.

To give a perspective of the coverage of various colour spaces, Fig. 3.14 includes NTSC and HDTV standard colour gamuts in comparison with the calculated ones. The colours that are out of the corresponding gamut region, for example between HDTV and ASI178MC colour gamut, become saturated, losing the colour information that the rendering colour space can describe.

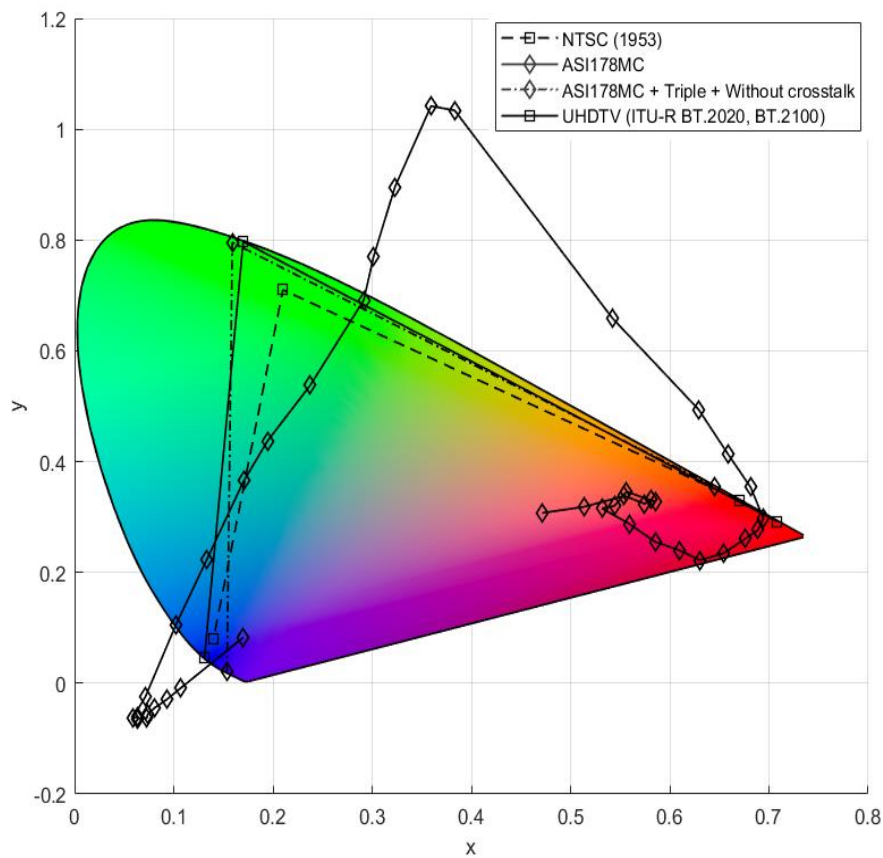


Figure 3.14: Selected colour gamuts from DSC measurements and Standardised colour spaces.

4. Spectral Imaging and Colour Gamut Expansion

4.1 Introduction

The number of applications that involve digital colour imaging, either for capturing or representing colour, is growing rapidly as technology evolves. Accurate colour reproduction is one of the major challenges that applied industries and scientific communities are facing. Due to the complex and vagueness in colour nature there is no clear-cut approach for accurate colour reproduction. Most conventional system integrations use computational and statistics-based solutions to achieve competent results^{38,39}. Marketing strategies usually affect system design and often lead to dropping the overall image quality[29]. Specifying the role and importance of each image process step, is a key element for improving the overall colour imaging performance.

It could be assumed that the digital colour imaging pipeline consists from three main procedures: image capturing, image processing/storage, and image rendering. The final two categories are highly dependent from the quality of the capturing output. Even if the most advanced procedures were used by the processing and visualizing steps, the main limitations are set by the capturing capabilities of the image acquisition device. Therefore, the consideration of a well performing capturing system is highly important for imaging applications.

Most of today's colour image capturing devices are based on trichromatic capturing such as RGB cameras. This is also the main limitation of these systems (further discussion can be seen in Section 4.2). An approach to break through this limitation is to go beyond the trichromatic boundaries, i.e., using spectrum-based colour reproduction systems. It has been reported that the use of multispectral imaging significantly improves colour accuracy [30], [31]. In the display industry, the multiprimary colour approach becomes one of the choices for expanding colour gamut[32], [33]. It is difficult, however, to take full advantage of multiprimary colour technology because a wide gamut image source is not available for such displays. A total system based on spectral information has not yet been established. A few papers [34]–[36] were devoted to multispectral systems, including both input and output, for hardcopy applications or still image displays, but no systematised implementations of the multispectral and multiprimary colour imaging technologies have been reported.

Multi and hyperspectral devices have been used extensively for art paintings restoration applications [5], [37]. The main purpose of such systems extends from pigment identification and classification operations to colorimetric level colour reproduction.

In this chapter, hyperspectral cameras as colour reproduction devices will be examined in terms of completeness of CIE XYZ colour gamut. An alternative procedure from

³⁸ <https://www.qualcomm.com/news/releases/2018/12/05/qualcomm-announces-new-flagship-snapdragon-855-mobile-platform-new-decade>

³⁹ <https://www.91mobiles.com/hub/ai-software-mobile-photography-overview/>

Chapter 3 will be proposed in order to define hyperspectral imager's colour gamut. Prerequisites for this chapter can be found in the introduction and Chapter 3.

4.2 Why Colour from spectra is needed.

It can be seen in the literature and in this thesis that many drawbacks of the common trichromatic colour reproduction approaches have been exposed. These limitations are briefly reviewed in this section in contrast with the spectrum-based advantages.

1. Many conventional colour imaging systems are designed for user preference, and the RGB values do not represent objective colour information. As it extensively discussed in Chapter 3, even if colorimetric colour calibration is applied and/or better performing colour matrices produced, most colour cameras do not satisfy the Luther condition. Thus, the RGB output does not have one-to-one correspondence to the tristimulus values perceived by human vision.
2. The primary colours that comply with a colour space, such as sRGB, AdobeRGB, CMYK etc. are defined under a reference white point (usually from CIE's standard illuminants). When the illuminant of the observation environment is different from that of image capture, the colour under the different illuminant should reproduce the colour as if the object were placed at the site of the observer. White Balance adjustment in conventional colour imaging is performed in the trichromatic device colour space, sometimes introducing a colour appearance model. But the colorimetric accuracy is not high, because the spectral reflectance of the object and the spectral distribution of illuminant are required in principle in order to calculate the colour under the different illuminant. As it was shown in 3.5.1, different White Balance settings resulting different gamut areas. Thus, system adaptation to different illuminants is not possible by using the trichromatic DSCs.
3. In the colour displays, the colour gamut does not cover all the existent colours. As a result, many high saturation colours cannot be reproduced. A display system has specific colour profile with a fixed gamut size that further produces limitations when used to define colour. To enlarge the colour gamut, the saturation of primary colours can be increased, but the gamut is still limited within a triangle. Monitors for professional photography and image editing that have been calibrated to use extended colour gamut areas, such as Adobe RGB, are currently available on the market. Multiprimary colour approach, i.e., using more than three primary colours, has been proposed in many works [33] for a larger colour gamut representations. Even though if the display device allows a wider colour gamut, conventional colour signals such as sRGB or ITU-R BT.709 are just stretched to the wider gamut colour area. Consequently, the variability of device colour profiles with different colour gamuts make difficult to communicate colour without losing accuracy.
4. The expansion of colour gamut on the conventional additive colour based systems such as RGB DSCs does not lead to better colour results. Many studies [18] have shown that colour gamut expansion reduce colour accuracy and

produce colour banding^{40,41} effects. These outcomes are due to the limitation of storing and representing colour information. Common DSCs bit depth for each colour channel is fixed at 8bits of information. Although the Analog to Digital Converters (ADCs) often produce digital signals with greater bit depth, the remaining bits are truncated in order to reduce unwanted noise⁴². Even though, there are remaining unwanted variations that tend to further decrease bit depth. For three colour channels the total amount of colours that could be described with a colour bit depth of 24 (8 bits per channel) is approximately 16.7 million. When the total area that include these number of colours grows, the colour coordinates are stretched up, thus the distance between individual colours is extended. Many professional cameras provide RAW colour data up to 16-bit depth per channel and allow to retain this extra information through specialised applications such as Photoshop.

5. As discussed in Chapter 3, spectrally different colour stimuli may give rise to identical colour data. As human eye colour space differs from that of a common DSC, the metamerism effect will also differ accordingly. This also refer to rendering devices such as screens and projectors. As the communication of colour has a solid base defined by CIE with X, Y and Z tristimulus values, the various colour profiles of input and output devices could not be inconsistent to colour acquisition. For this reason, Sensitivity Metamerism Index (SMI)[38] has been designed to give a measure for such potential colour error. On the other hand, the multi/hyperspectral approach solves this problem by means of spectral colour reproduction.
6. Analyses of spectral reflectances of standard colour specimens and natural objects [39]–[41] have indicated statistically that three channels, such as in tristimulus devices, are not sufficient for representing the spectral content of a scene very well. Hence the adequate dimensionality of the spectral information is larger than three. The general conclusion of [42]–[44] is that 4 to 10 known bases (equivalent to 4 to 10 colour channels) are needed for retaining sufficient spectral information. Based on these facts, researchers have considered the use of more than three colour channels tending to approach multi/hyper spectral imaging devices in order to capture accurate colour.

Spectrum-based colour reproduction provides the solution to these problems, but it is necessary to integrate such systems to the corresponding application field. Additionally, colour from spectra approach is the only way to achieve device and illuminant independency as the output of HS systems is not an arbitrary colour space but well-defined spectral data.

As mentioned in 2.1, DSC acquisition model could be described from a $k \times N$ matrix where k is the number of camera channels and N is the corresponding wavelengths λ . These matrices are highly rectangular ($k \ll N$) thus highly underdetermined. Additionally, the channel crosstalk adversely affects the independency of each row.

⁴⁰ https://en.wikipedia.org/wiki/Colour_banding

⁴¹ https://www.adobe.com/digitalimag/pdfs/phscs2ip_colospace.pdf

⁴² <http://theory.uchicago.edu/~ejm/pix/20d/tests/noise/noise-p3.html>

For hyperspectral imaging devices the equivalent matrix is:

$$S_{HS} = \begin{bmatrix} K_1(\lambda_1) & K_1(\lambda_2) & \dots & K_1(\lambda_N) \\ K_2(\lambda_1) & K_2(\lambda_2) & \dots & K_2(\lambda_N) \\ \vdots & \vdots & \vdots & \vdots \\ K_Z(\lambda_1) & K_Z(\lambda_2) & \dots & K_Z(\lambda_N) \end{bmatrix}^T,$$

where K is each individual spectral channel of total Z and $Z \leq N$. In this situation the matrix is approximately square and it is characterised from almost individual channel vectors. These conditions enable reversibility and accurate estimation procedures as the column space is approximately full-rank.

On the other hand, hyperspectral cameras are often bulky and hard to operate, especially in rapidly changing environments. The latest advances in CMOS design (back-illuminated sensors with high quantum efficiency, stacked electronic units etc.) and microelectronic integrations (Microelectromechanical systems –MEMS-, multiple cameras on a chip etc.) enable the construction of robust snapshot multi and hyperspectral imaging devices[45], [46]. These developments in relation to Artificial Intelligence advances in estimating illuminating sources[47], [48] and performing exceptional system adaptation in various environments, result in the miniaturization⁴³ and ease of use for hyperspectral imagers. For many applications, this reality could lead to the replacement of conventional trichromatic imaging systems with the more sophisticated and well performing multi/hyperspectral devices.

4.3 Calculation of Tristimulus Values using Spectral Data

Colour vision is an illusion created by the physiological interactions between retinal cells and neurons in the brain. There is no colour in the external world; the physical quantity that human eye perceives as colour is the interaction between matter and light -the spectrum of each individual element in a scene.

The way in which the human brain separates two properties of light, energy (equivalent to wavelength) and intensity, and then recombines them into colour perception is a complex mechanism. Even with the latest scientific and technological advances this mechanism has not revealed. Examination of the responses of single neurons or arrays of such neurons provides the best insights into the physiology of colour vision. Ultimately, the understanding of this process will allow scientists to model the neural circuits that underlie the perception of colour and form. Although still beyond reach, progress has been made in deciphering these sophisticated circuits that create the perception of the external world.

⁴³ <http://www.qcell.tech/products/>

As described in 1.2.2 the first quantitative links between human colour vision and EMR spectrum were CIE 1931 colour spaces. Though, colour is not a property of electromagnetic radiation, but a feature of visual perception by an observer. This mapping between wavelengths of light in the visual EM spectrum and human colour perception is consistent with the variety of colour applications that are used today.

The XYZ colour space is the common space that has been created in order to communicate colour. The tristimulus values X, Y and Z have to be calculated in order to enable the transition to each other colour space. These values could be computed from spectral data:

$$X = \frac{Q}{D} \int_{\lambda} S(\lambda)I(\lambda)\bar{x}(\lambda)d\lambda,$$

$$Y = \frac{Q}{D} \int_{\lambda} S(\lambda)I(\lambda)\bar{y}(\lambda)d\lambda,$$

$$Z = \frac{Q}{D} \int_{\lambda} S(\lambda)I(\lambda)\bar{z}(\lambda)d\lambda,$$

where

$$D = \int_{\lambda} I(\lambda)\bar{y}(\lambda)d\lambda,$$

with Q a scaling factor and λ stands for wavelength in nm. $S(\lambda)$ stands for spectral reflectance or transmittance and $I(\lambda)$ for the SPD (Spectral to Power Distribution) of given illuminant. As the spectral information of the scene is known the tristimulus values for a given illuminant could be acquired. The wavelength range could be from 380 to 780 nm as this is the EM area that CMF are defined. The band step interval could be 5nm or greater.

In this thesis, standard illuminant D65 is used for every colorimetric calculation. It is the most commonly used standard illuminant and corresponds roughly to the average midday light in Western Europe / Northern Europe, hence it is also called a daylight illuminant. D65 is a tabulated SPD in increments of 5 nm from 300 nm to 830 nm, using linear interpolation on the original data binned at 10 nm.

4.4 Methodology for Hyperspectral Imager Gamut Calculation

As discussed in 4.2 the acquisition matrix of a hyperspectral device is almost full-rank. Thus, Luther condition could apply nearly perfect. This condition means that for every output spectral vector δ_z there will be a $3 \times Z$ colour matrix M that maps with near one by one relationship between hyperspectral output and CIE XYZ colour space.

Although there is the conventional way, by using Luther condition, to determine an imaging system's colour gamut, it does not refer to Hyperspectral devices. The reason is that the output of HS devices is already scene reflectances, therefore by simple substitution to the spectrum-to-colour equations (defined by CIE), X, Y and Z tristimulus values will be derived. Each spectral reflectance measurement per wavelength to a Lambertian surface corresponds to the device response –the common DSCs do not have the capability for reflectance measurement-, consequently enabling the transition to CIE XYZ colour space directly. In other words, because the multi/hyperspectral imagers are coherently device and illuminant independent, there is no need for physical device characterization, and colour profile matrices in order to transform the output values from the device colour space to CIE XYZ colour space.

A different approach is proposed in order to determine accurately a Hyperspectral (HS) imager's colour gamut.

As mentioned in 1.2.4 the outer boundary of the CIE'31 chromaticity diagram, named spectral locus, describes the spectral colours that define the boundary layer of the presented colour space. All linear mixing between these colours, could result to all in-between chromaticities.

In order to define a HS imager colour gamut, the outer boundary needs to be calculated. This could be achieved by capturing independently for each spectral band the corresponding spectral cube on a Lambertian surface illuminated by the related wavelength. Then the final X, Y and Z tristimulus values could be computed by using the equations from Section 4.3. After that, chromaticities x, y could be also calculated in order to plot them against CIE '31 chromaticity diagram. The procedure is shown in Fig. 4.1.

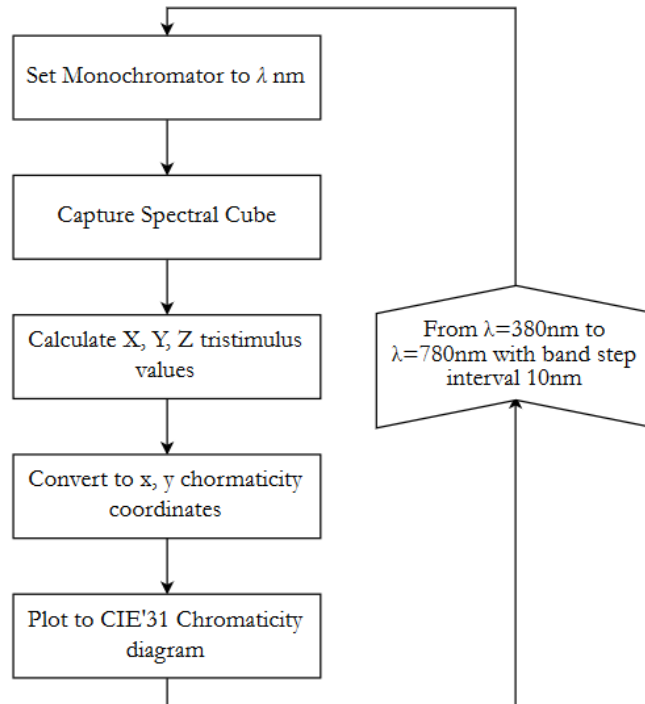


Figure 4.1: Acquisition procedure for calculating HS imager colour gamut

The starting and ending bands of the experiments should match CMF starting and ending points, from 380nm to 780nm as also the band step should not overcome 10nm. These considerations have been made in order to produce reliable results. All the experiments were conducted under these requirements.

The error measurements were limited to the area values since the Luther condition was not applied (no transformed sensitivities provided). Moreover, the ED error metrics didn't found useful as:

- HS colour gamut expand always inside the CIE'31 total area i.e. no imaginary colours are captured.
- Their shape deviations are tiny i.e. the spectral locus preserve the shape regardless the total area differences.

4.5 Colour Gamut of an Ideal Hyperspectral Imaging Device

The term “Ideal Hyperspectral Imaging Device” is an arbitrary selected title used to describe a HS device which:

- The FWHM value is constant.
- The FWHM value is half (or less) than the band step interval.
- Spectral range is from 380nm to 780nm.

- Band step interval is either 5 or 10 nm.

As these criteria are fulfilled, every column in S_{HS} should be linear independent from each other. As such device was not available, simulation of the total operation has been performed.

More specifically, using Matlab, normal Probability Distribution Functions (PDFs) with the above characteristics were created in order to simulate HS device responses for each spectral cube. The function "normpdf" was used assuming that the filter transmittances were Gaussian. The mean value for each PDF was selected according to the central wavelength of the corresponding spectral cube. The Standard Deviation was set to 2.5, assuming 5nm FWHM values. After this, the described procedure in Section 4.4 was followed to extract the final colour gamut.

The band step interval was fixed at 10nm. The total 41 spectral bands match 41 data points of each corresponding Colour Matching Function \bar{x} , \bar{y} and \bar{z} . The spectral bands that simulated are shown in Fig. 4.2.

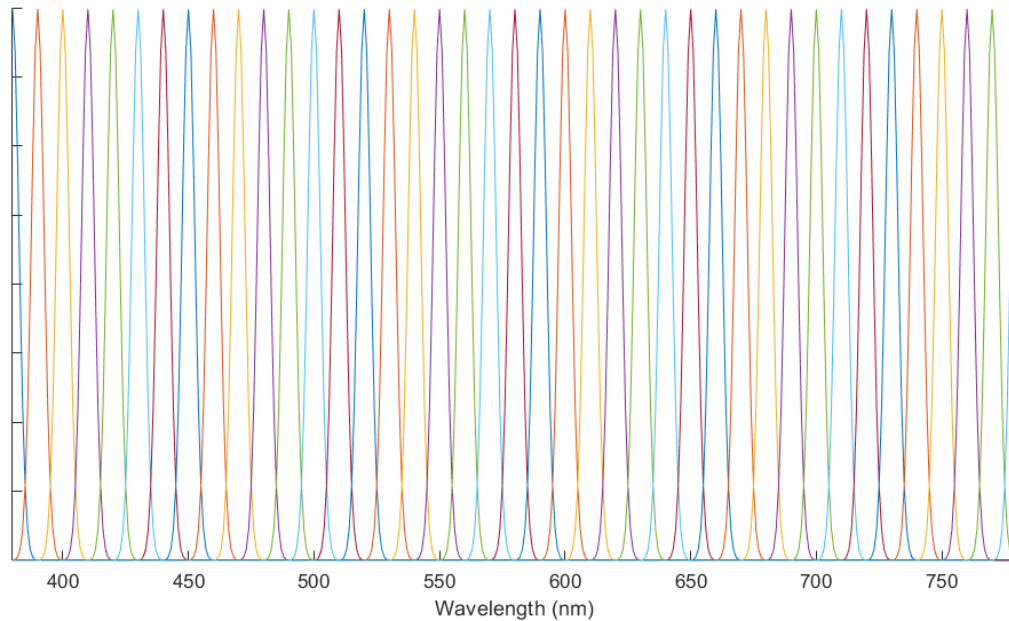


Figure 4.2: Simulated Spectral Bands with 5nm FWHM and 10nm band step interval.

The final colour gamut of the simulated spectral cube matches perfectly the whole CIE'31 chromaticity diagram as it is shown in Fig. 4.3. The total area values based on the error measurement of the previous chapter are presented in Table 12.

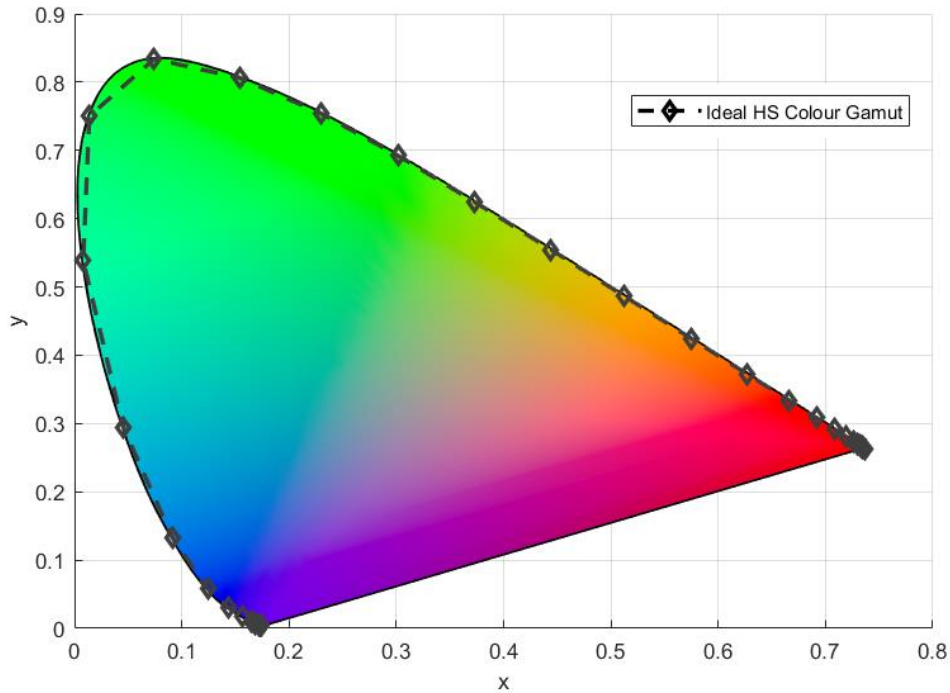


Figure 4.3: Colour gamut of an ideal HS imaging device. The boundary layer matches CIE '31 chromaticity diagram's spectral locus.

Total Area

DSC	CIE '31	DA	Common Area	Common Area % - HS	Coverage % - CIE '31
0.3314	0.3314	0	0.3314	100%	100%

Table 12: Gamut area values of ideal HS colour gamut and CIE '31 chromaticity diagram.

With the above results it could be assumed that the XYZ tristimulus values derived from this device would coincide with the real values of a hypothetical scene. This input device would also work as a colorimeter having the same metameric accuracy as the human eye does.

In real life scenarios though, the HS cameras struggle to achieve such “ideal” properties. The FWHM value is changing through wavelengths and neighboring channel crosstalk occurs differently at each spectral band. These drawbacks result in decreasing the rank of matrix S_{HS} and decreased colour saturation i.e. the spectral colour of the HS device deviate (to real colours area) from CIE '31 spectral locus.

To validate this consideration, various FWHM values were tested with the same procedure as described above. The only value that increased was FWHM leaving it constant (after the change) for all the other spectral bands. The FWHM values that were selected are presented in Fig. 4.4. The colour gamut results are shown in Fig. 4.5.

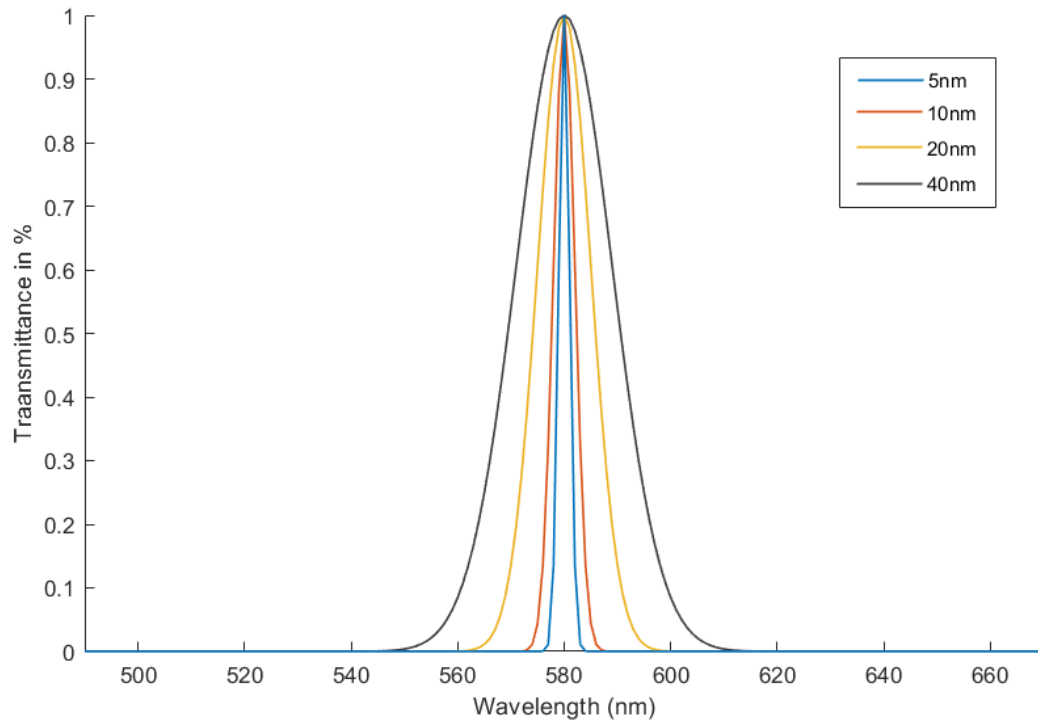


Figure 4.4: The FWHM values that were used for the various HS gamut calculations.

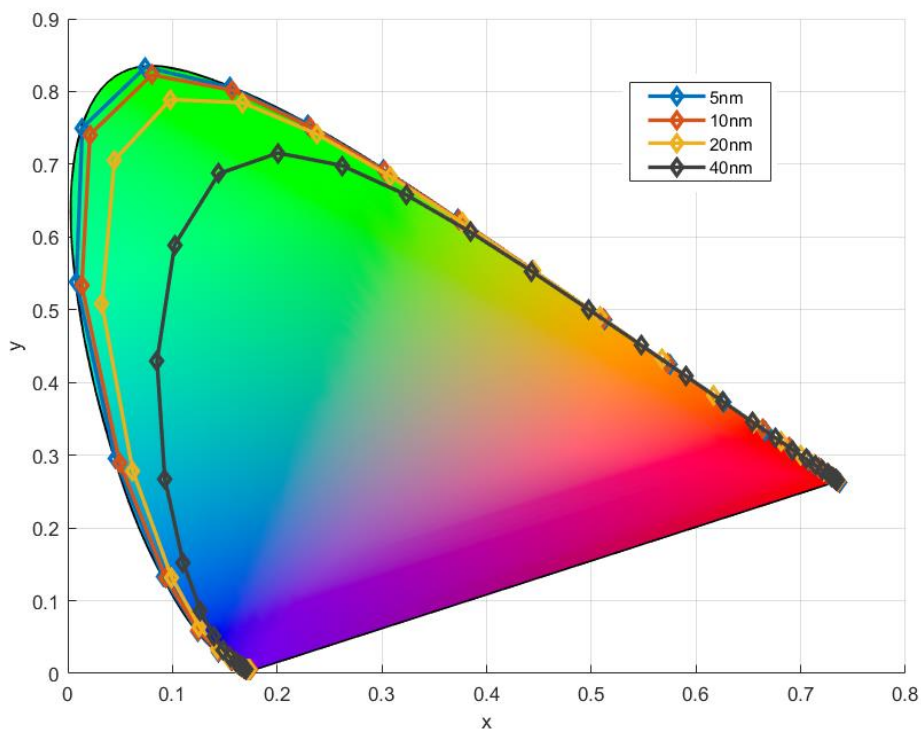


Figure 4.5: As the FWHM of an HS imaging device increases, the spectral colours are getting further from CIE '31 chromaticity diagram spectral locus.

It is obvious that the broader the channel crosstalk, the smaller the total gamut overlapping. The most affected spectral regions are from 480 to 570nm. In that EM region CMF coefficients have the greatest values overall.

In order to examine the tendency of gamut-shrinking relative to FWHM values, several measures were performed. The total results are shown in Table 13. The coverage percentages versus the FWHM values are plotted in Fig. 4.6. The continuous grey line that is plotted, is interpolated between 5nm and 200nm data points. It is noticeable that the trend of gamut reduction is almost linear.

FWHM (nm)	DSC	CIE '31	DA	Common Area	Common Area % - HS	Coverage % - CIE '31
5	0.3314	0.3314	0	0.3314	100%	100%
10	0.3264		0.005	0.3264		98%
15	0.3189		0.0125	0.3189		96%
20	0.3102		0.0212	0.3102		94%
25	0.3001		0.0313	0.3001		91%
40	0.2658		0.0656	0.2658		80%
100	0.1497		0.1817	0.1497		45%
200	0.0315		0.2999	0.0315		10%

Table 13: Area measures for different FWHM values

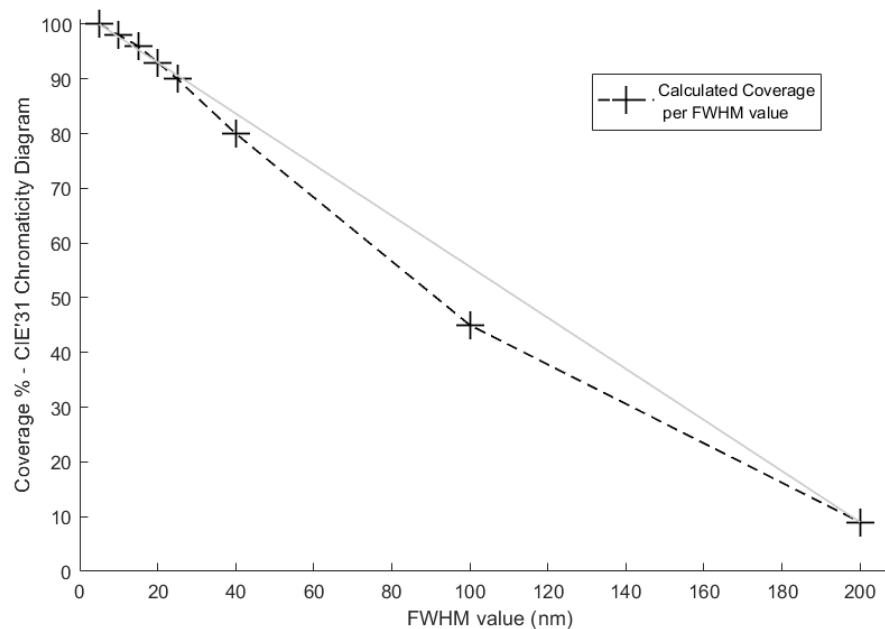


Figure 4.6: CIE'31 Chromaticity Diagram coverage from spectral cubes with different FWHM values.

4.6 Colour Gamut of a commercial Hyperspectral Imager

In this section, the colour gamut of a commercial HS device has been measured and presented. The procedure follows the same steps as described in Section 4.4. Physical device measurements are vital in order to give accurate results and avoid false conclusions. For this reason, the experiments have been accurately designed and contacted in Optoelectronics Laboratory facilities.

4.6.1 The Muses9-HS

Muses9-HS is a hyperspectral handheld camera provided by Spectricon⁴⁴. Muses9-HS is a HS camera capable of real time spectral imaging with high spectral and spatial resolution along with a high throughput ratio. The universal C-Mount threads located on the imager and lens positions, enable the usage on a huge variety of photographic lenses and multi-operational characteristics. It can be used as a standalone measurement camera for open field or laboratory measurements. It can be attached to a microscope as an analytical tool to perform both brightfield and fluorescence microscopy (either trans or epi luminescence). The real time spectral imaging feature is made possible by a computer-controllable, continuously tunable filter module (TFM). The calibration procedure is automatic and software controlled. All processes from spectral cube acquisition to the analysis steps are performed from the same software that comes with the device.

Muses9-HS specifications that has been used are:

- Wavelength tuning range: 400nm to 1000nm
- FWHM: 7-18nm
- Band step interval: 5-30nm
- Control: From provided application software
- Operation modes: Colour and Spectral Imaging
- Exposure range: 32ms – 10s
- Sensor type: Si-CMOS
- Thread: C-Mount
- Spatial resolution: 6.4 MP (3096x2080)
- Connection Interface: USB 3.0
- Weight: 350gr
- Dimensions: 200x100x50mm

⁴⁴ <http://www.spectricon.com/>

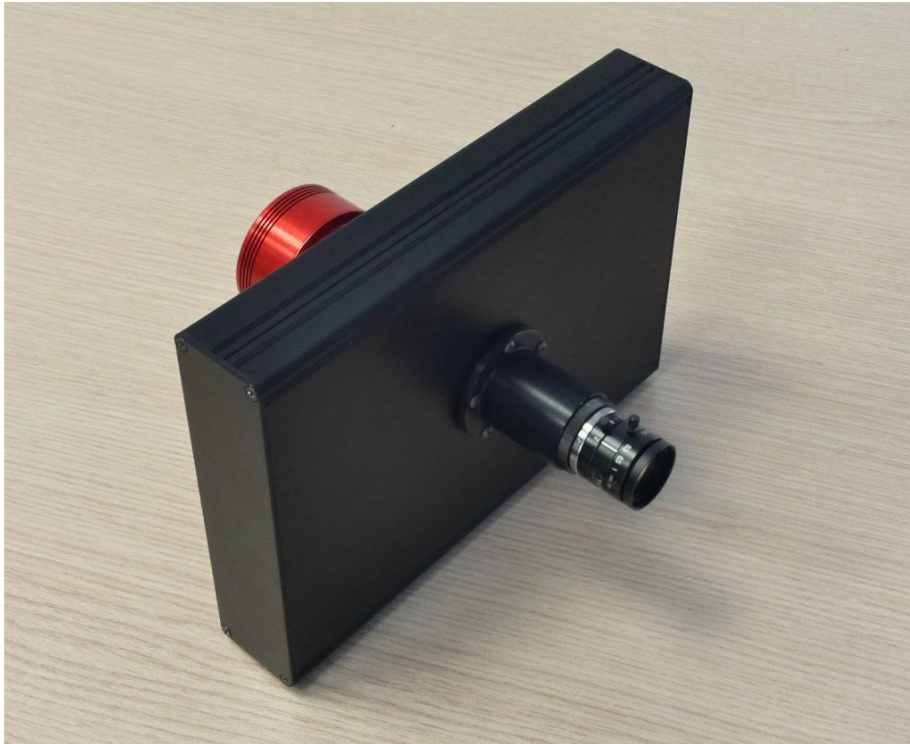


Figure 4.7: The Muses9-HS camera that has been used for colour gamut calculation.

4.6.2 Experimental Setup

For conducting the measurements, the described materials and devices were needed:

- A HS imaging device:
Muses9-HS has been used. The device was coupled with ASI178MM monochrome DSC. This camera has the same specifications as ASI178MC that was used in Chapter 3. The only difference is that ASI178MM is not a colour DSC.
- A tunable monochromator device:
Edmund Mini-Chrom monochromator was used.
- Illumination Source:
ThorLabs OSL-1-EC Halogen light source was used, coupled with a fiber optic to drive the light through the monochromator.
- Reflectance standard:
Ocean Optics WS-1 Reflectance Standard has been used on a 45° - 0° detector-illumination setup.

The Muses9-HS was facing Ocean Optics WS-1 reflectance target which act as the ideal Lambertian surface. The target was illuminated by monochromatic light from Edmund Mini-Chrom monochromator that was coupled with ThorLabs OSL-1EC halogen light through a fiber optic element.

39 spectral cubes were acquired, from 400nm to 780nm. The band-step was chosen to be 10nm as FWHM of Muses9-HS is variable from 7-18nm. For each spectral cube, the monochromator was tuned to the central wavelength increasingly from 400-780nm with 10nm interval. For example, the first cube monochromator setting was on 400nm, for the second one 410nm and so on till 780nm. There was no need for calibration procedure since the final colour gamut reference to chromaticity diagram.

The spectral data exported from a central region of the total FOV that correspond to the illuminated target. All processing tasks were performed in Matlab R2018a, like wise the plotted results.

4.6.3 Results

Each spectral cube which acquired is inherently the response of the corresponding channel of the HS imager. As mentioned, no calibration procedure was needed since the results relate to chromaticities. In Fig. 4.8, the spectra for each spectral cube are plotted. It is clear that the FWHM value differs for each spectral band.

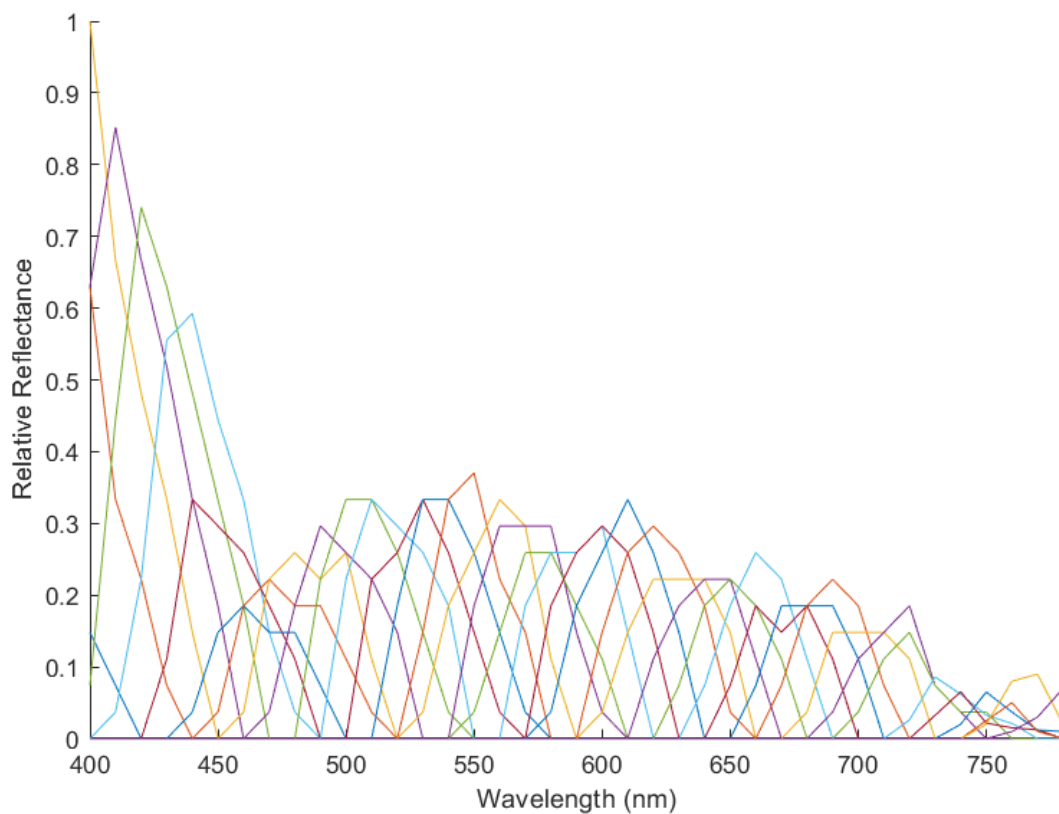


Figure 4.8: Spectral cubes acquired for Muses9-HS colour gamut calculation plotted together.

The acquired data compose the matrix S_{M9} with total dimensions 39x39. Each row represents a different spectral cube measurement and each column the response for each wavelength. By substituting the equations from Section 4.3, 39 tristimulus tuples X, Y, Z

were acquired. These values were converted to xyY coordinates in order to map the Muses9-HS colour gamut according to CIE'31 chromaticity diagram.

In Fig. 4.9, Muses9-HS colour gamut and CIE xyY colour space are plotted. The overlapped area is about 89% of the total CIE gamut area. The summary of total area values are shown in Table 14.

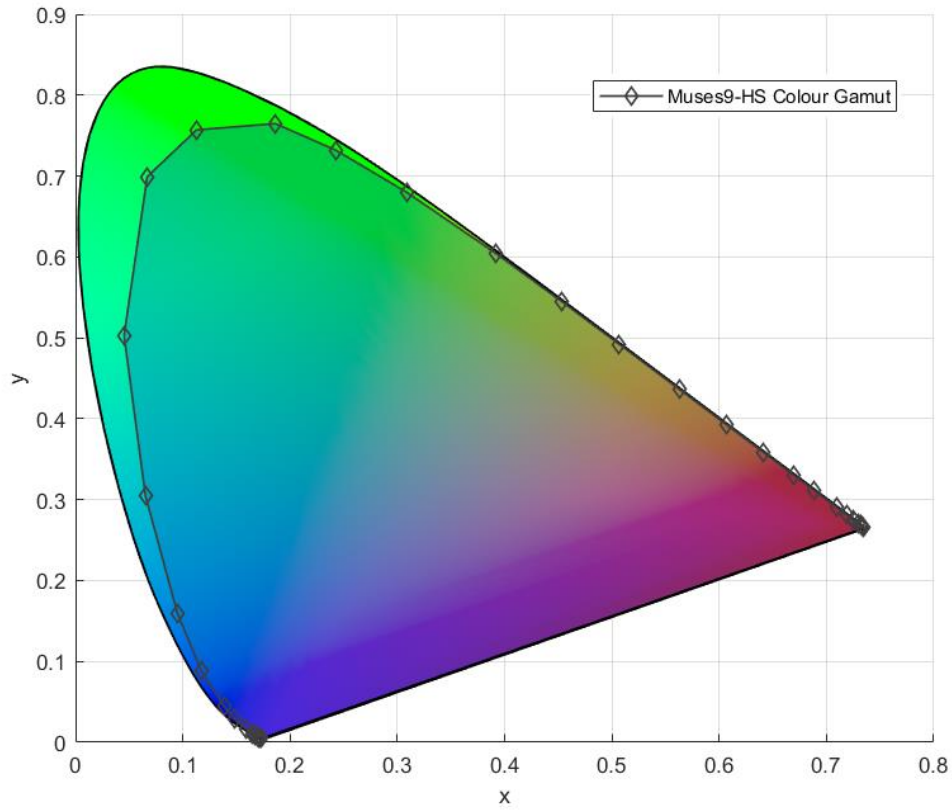


Figure 4.9: Muses9-HS colour gamut as calculated from matrix S_{M9} .

Total Area					
DSC	CIE '31	DA	Common Area	Common Area % - HS	Coverage % - CIE '31
0.2981	0.3314	0.0333	0.2981	100%	89%

Table 14: Gamut area values of Muses9-HS colour gamut and CIE '31 chromaticity diagram.

4.6.4 Applying Luther condition to Muses9-HS

As shown in Fig. 4.8, Muses9-HS spectral channels are not independent from each other. Therefore, Muses9-HS spectral cubes are characterised from a small error that is constant for each measurement since channel crosstalk is a constructional characteristic. This leads to an imperfect match of the total CIE'31 colour gamut. Contrariwise the simulated response of the ideal HS camera from Section 4.5 achieved 100% completeness of CIE's colour gamut. In order to achieve such performance with Muses9-HS, a transformation matrix is needed to map exactly the CIE XYZ colour space.

The same linear-mapping approach, as described in Chapter 3, was followed in this Section, by using Luther condition hypothesis. \bar{S}_{M9} is a 39x41 matrix was used to describe the Spectral Sensitivity of Muses9-HS. A new matrix S_{M9} has been used, where the first two columns that refer to spectral bands 380nm and 390nm have been filled with zeros since Muses9-HS was not capable to capture images in that EM region. The other column values were replaced with the corresponding ones from \bar{S}_{M9} matrix.

$$M_{M9} = T_{XYZ} S_{M9}^+,$$

where M_{M9} is the colour transformation matrix 3x41, T_{XYZ} the CIE'31 CMF and superscript "+" stands for pseudoinverse. The above equation is also presented in Section 3.1 where the Luther condition was described.

LS (Least Squares) were used for the calculation of the colour matrix M_{M9} . In Fig. 4.10 the resulting transformed Spectral Sensitivities are shown. The total difference from the CIE'31 CMF is approaching zero and shown in Table 15.

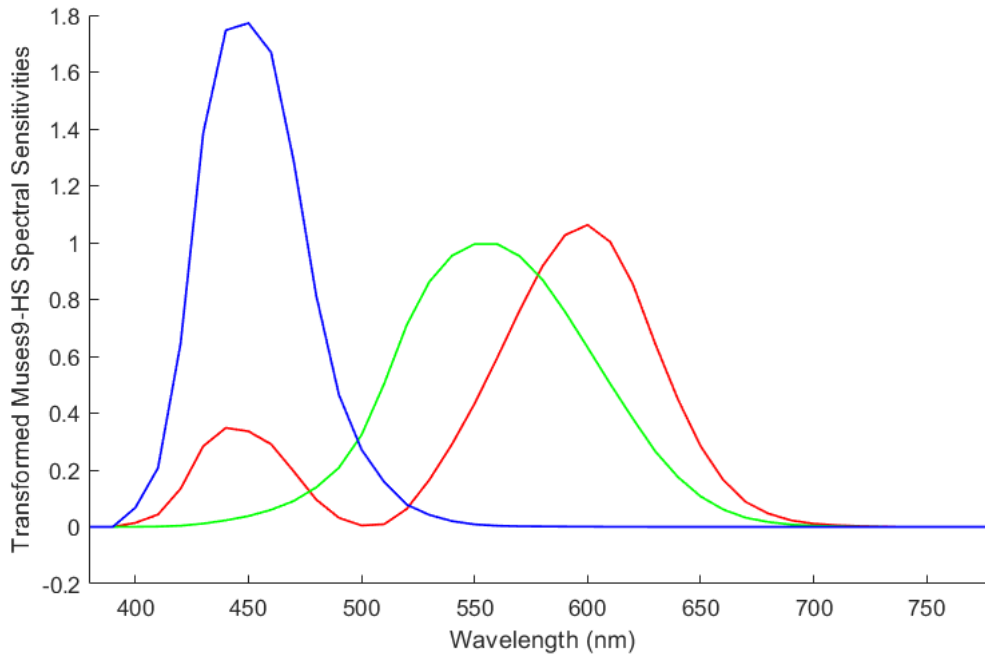


Figure 4.10: Muses9-HS transformed Spectral Sensitivities derived from Luther Condition.

	\bar{x}	\bar{y}	\bar{z}
RMSE	7.07e-04	4.86e-05	0.0033
L1	0.0069	6.33e-04	0.0265

Table 15: RMSE and Manhattan distance errors for Muses9-HS transformed Spectral Sensitivities and CIE'31 CMF.

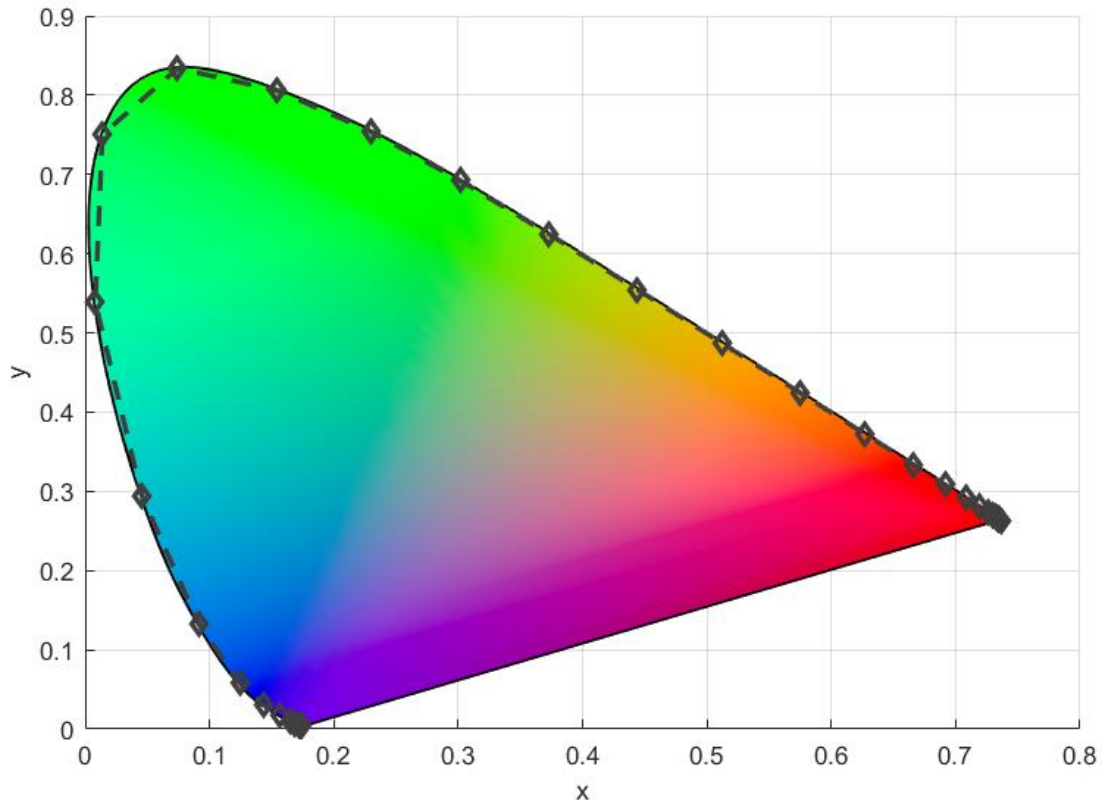


Figure 4.11: Colour gamut of Muses9-HS after applying Luther condition.

Total Area					
DSC	CIE '31	DA	Common Area	Common Area % - HS	Coverage % - CIE '31
0.3309	0.3314	0.0005	0.3309	100%	99%

Table 16: Gamut area values of Muses9-HS colour gamut after applying Luther condition and CIE '31 chromaticity diagram.

The coverage of CIE'31 chromaticity diagram is nearly perfect. It is declared that this implementation bypasses the classical method to extract X, Y and Z tristimulus values from the spectrum. The acquired spectral cube has to be multiplied with the matrix M_{M9} in order to produce the corresponding tristimulus values. If another standard illuminant needs to be used, then recalculation of the M_{M9} is essential (based on the new illuminant's values).

5. Conclusion and Future Work

The main concept of this thesis is the measurement and improvement of the colour gamut of DSCs and Spectral Imaging devices. All the implemented procedures, reference to global colour standards as described from CIE. The applications of these improvements have significant importance since colour is one of the main principles of how humans perceive and communicate information. From biomedical and art preserving applications to professional photography and consumer mobile cameras, colour constancy plays an important role. It's the first time to the best of our knowledge where a real Hyperspectral imager colour gamut measurement is conducted, based on the proposed methodological procedure.

The main advantages of this thesis can be summarised to:

- Hyperspectral imaging systems could achieve one-to-one match between captured information and the standardised colour which corresponds to the average human colour perception. This statement is strengthened by the fact that DSC camera acquisition is described by an ill-posed matrix in contrast with the well-defined hyperspectral data space. One-to-one colour match also affects metamerism which stays the same as the average person would perceive it.
- There are no concerns about different illuminants and scene conditions since spectral imagers are truly device and light independent. Each spectral cube refers to a physical measurement of the observed scene, thus the acquired values are constant and precise. In common colour DSCs, different operational settings result to different colour gamuts.
- As HS colour gamut has near 100% coverage of CIE colour gamut, all colour spaces could be described without loss of any colour information.
- By using a narrow multiband filter and performing crosstalk correction on a commercial DSC, the colour gamut of the camera has significant improvement. The colour gamut grows and fits better to the human eye colour space.
- Nevertheless, a real HS device does not have a perfect match with CIE'31 chromaticity diagram, it is possible to achieve 100% coverage by using Luther condition. Contrariwise, in common DSCs it is not possible to achieve such performance.

The most fundamental result of this thesis is the verification of the dominance of hyperspectral imaging devices instead of the conventional trichromatic DSCs, in terms of colour capturing capabilities. It is also worth to mention that these conclusions have been made based on real experimental data and not on simulated ones. The experimental procedure is a key component for evaluating the thesis results and in extracting safe conclusions about the findings of the thesis.

Further investigation with real Spectral Sensitivity data could also be done on the estimation of colour matrices that map DSC's colour space to CIE XYZ colour space. More DSCs and commercial HS devices could also be measured in order to validate

the proposed gamut expansion techniques. More DSC setting variations need to be investigated in order to examine the way that they affect DSC's colour gamut.

It would be also interesting to investigate the performance of a multichannel camera setup versus a hyperspectral imager, mentioned that spectral estimation algorithms perform well in regards to VIS-NIR signals. The questioning in this comparison is if the spectra-to-colour procedure and its variations overcome the standard matrix multiplication methodology.

The expansion and improvement of colour gamut overlapping between a capturing device and a standardised colour space affects the plurality of capturing colours without necessarily improving colour quality. Thus, in order to evaluate this thesis results in terms of colour accuracy and colour sensitivity, further work needs to be conducted that focuses on comparing and validating the colour fidelity of the proposed setups.

6. References

- [1] L. E. Ballentine, *Quantum Mechanics, A Modern Development*. World Scientific Publishing Co. Pte. Ltd.
- [2] R. Kastner, *Why the Afshar experiment does not refute complementarity*. 2005.
- [3] M. Kalloniatis and C. Luu, “The Perception of Color,” in *Webvision: The Organization of the Retina and Visual System*, H. Kolb, E. Fernandez, and R. Nelson, Eds. Salt Lake City (UT): University of Utah Health Sciences Center, 1995.
- [4] H. Hofer, J. Carroll, J. Neitz, M. Neitz, and D. R. Williams, “Organization of the human trichromatic cone mosaic,” *J. Neurosci. Off. J. Soc. Neurosci.*, vol. 25, no. 42, pp. 9669–9679, Oct. 2005.
- [5] A. R. Cortes, “Multispectral Analysis and spectral Reflectance Reconstruction of Art Paintings,” p. 250.
- [6] L. Beke, G. Kutas, Y. Kwak, G. Y. Sung, D.-S. Park, and P. Bodrogi, “Colour preference of aged observers compared to young observers,” *Colour Res. Appl.*, vol. 33, no. 5, pp. 381–394, Oct. 2008.
- [7] R. Lenz, “Spectral Colour Spaces: Their Structure and Transformations,” in *Advances in Imaging and Electron Physics*, vol. 138, Elsevier, 2005, pp. 1–67.
- [8] A. Akbarinia and K. R. Gegenfurtner, “Colour metamerism and the structure of illuminant space,” *JOSA A*, vol. 35, no. 4, pp. B231–B238, Apr. 2018.
- [9] “iSuppli: CCDs fall in image sensor market as CMOS surges.” [Online]. Available: <https://www.vision-systems.com/articles/2010/10/isuppli-image-sensors-market-2010.html>. [Accessed: 01-Dec-2018].
- [10] “Optimum spectral sensitivity functions for single sensor colour imaging.” [Online]. Available: <https://www.spiedigitallibrary.org/conference-proceedings-of-spie/8299/829904/Optimum-spectral-sensitivity-functions-for-single-sensor-color-imaging/10.1117/12.907904.short?SSO=1>. [Accessed: 01-Dec-2018].
- [11] “Sensor Transforms to Improve Metamerism-Based Watermarking,” *Zeeba TV*. [Online]. Available: <http://zeeba.tv/sensor-transforms-to-improve-metamerism-based-watermarking/>. [Accessed: 01-Dec-2018].
- [12] C. Balas, C. Pappas, and G. Epitropou, “Multi/Hyper-Spectral Imaging,” in *Handbook of Biomedical Optics*, CRC Press, 2011, pp. 131–164.
- [13] K. Barnard and B. Funt, “Camera characterization for colour research,” *Colour Res. Appl.*, vol. 27, no. 3, pp. 152–163, Jun. 2002.
- [14] R. Luther, “Aus dem Gebiet der Farbreizmetrik (On colour stimulus metrics),” p. 39.
- [15] F. Cao, F. Guichard, and H. Hornung, “Sensor spectral sensitivities, noise measurements, and colour sensitivity,” presented at the Electronic Imaging 2008, San Jose, CA, 2008, p. 68170T.
- [16] “(PDF) Exact Reproduction of Colored Images,” *ResearchGate*. [Online]. Available: https://www.researchgate.net/publication/222438967_Exact_Reproduction_of_Colored_Images. [Accessed: 03-Dec-2018].
- [17] G. D. Finlayson and M. S. Drew, *White-Point Preserving Colour Correction*. 1997.
- [18] S. Bianco, F. Gasparini, and R. Schettini, “Matrixing, number of colour channels, and colour gamut of camera devices,” presented at the Electronic Imaging 2007, San Jose, CA, USA, 2007, p. 650208.
- [19] “Capture colour analysis gamuts,” *ResearchGate*. [Online]. Available: https://www.researchgate.net/publication/290762223_Capture_color_analysis_gamuts. [Accessed: 03-Dec-2018].
- [20] G. Wyszecki, “A Measure for the Total Difference of Two Sets of Color-Mixture Functions,” *JOSA*, vol. 49, no. 8, pp. 811–814, Aug. 1959.

- [21] G. D. Finlayson and P. M. Morovic, “Metamer Constrained Colour Correction,” p. 6, 1999.
- [22] “A Simple Algorithm for Metamer Mismatch Bodies - Semantic Scholar.” [Online]. Available: <https://www.semanticscholar.org/paper/A-Simple-Algorithm-for-Metamer-Mismatch-Bodies-Centore/c1d18ae1676496946ed3a03ad5ad9cfc837b3678>. [Accessed: 03-Dec-2018].
- [23] “Characterization of novel three- and six-channel colour moire free sensors.” [Online]. Available: <https://www.spiedigitallibrary.org/conference-proceedings-of-spie/3648/0000/Characterization-of-novel-three--and-six-channel-color-moire/10.1117/12.334603.short?SSO=1>. [Accessed: 03-Dec-2018].
- [24] “Metameric colour stimuli, fundamental metamers, and Wyszecki’s metameric blacks. - PubMed - NCBI.” [Online]. Available: <https://www.ncbi.nlm.nih.gov/pubmed/7168455>. [Accessed: 03-Dec-2018].
- [25] P. Morovic and G. D. Finlayson, “Metamer-set-based approach to estimating surface reflectance from camera RGB,” *J. Opt. Soc. Am. A Opt. Image Sci. Vis.*, vol. 23, no. 8, pp. 1814–1822, Aug. 2006.
- [26] D. K. Prasad, “Gamut expansion of consumer camera to the CIE XYZ colour gamut using a specifically designed fourth sensor channel,” *Appl. Opt.*, vol. 54, no. 20, p. 6146, Jul. 2015.
- [27] G. Agranov, V. Berezin, and R. H. Tsai, “Crosstalk and microlens study in a colour CMOS image sensor,” *IEEE Trans. Electron Devices*, vol. 50, no. 1, pp. 4–11, Jan. 2003.
- [28] K. Hirakawa, “Cross-talk explained,” in *2008 15th IEEE International Conference on Image Processing*, San Diego, CA, USA, 2008, pp. 677–680.
- [29] T. Chen, P. B. Catrysse, A. El Gamal, and B. A. Wandell, “How small should pixel size be?” presented at the Electronic Imaging, San Jose, CA, 2000, p. 451.
- [30] “(PDF) Analysis Multispectral Image Capture,” *ResearchGate*. [Online]. Available: https://www.researchgate.net/publication/239666107_Analysis_Multispectral_Image_Capture. [Accessed: 03-Dec-2018].
- [31] S. Tominaga, “Multichannel vision system for estimating surface and illumination functions,” *JOSA A*, vol. 13, no. 11, pp. 2163–2173, Nov. 1996.
- [32] “(PDF) Expanded colour gamut reproduced by six-primary projection display,” *ResearchGate*. [Online]. Available: https://www.researchgate.net/publication/252231529_Expanded_color_gamut_reproduced_by_six-primary_projection_display. [Accessed: 03-Dec-2018].
- [33] “Multiprimary colour display using holographic optical element | Request PDF,” *ResearchGate*. [Online]. Available: https://www.researchgate.net/publication/241507621_Multiprimary_color_display_using_holographic_optical_element. [Accessed: 03-Dec-2018].
- [34] B. Hill, “Multispectral colour technology: a way toward high-definition colour image scanning and encoding,” in *Electronic Imaging: Processing, Printing, and Publishing in Color*, 1998, vol. 3409, pp. 2–14.
- [35] “Multispectral colour system with an encoding format compatible to conventional tristimulus model,” *ResearchGate*. [Online]. Available: https://www.researchgate.net/publication/243654498_Multispectral_color_system_with_an_encoding_format_compatible_to_conventional_tristimulus_model. [Accessed: 03-Dec-2018].
- [36] M. Rosen, F. H. Imai, X. Jiang, and N. Ohta, “Spectral reproduction from scene to hardcopy: II. Image processing,” in *Colour Imaging: Device-Independent Color, Colour Hardcopy, and Graphic Arts VI*, 2000, vol. 4300, pp. 33–42.

- [37] “Multispectral imaging targets art restoration.” [Online]. Available: <https://www.vision-systems.com/articles/print/volume-20/issue-3/features/multispectral-imaging-targets-art-restoration.html>. [Accessed: 03-Dec-2018].
- [38] P.-C. Hung, “Sensitivity metamerism index digital still camera,” in *Colour Science and Imaging Technologies*, 2002, vol. 4922, pp. 1–15.
- [39] “OSA | Vector-subspace model for colour representation.” [Online]. Available: <https://www.osapublishing.org/josaa/abstract.cfm?uri=josaa-7-4-725>. [Accessed: 03-Dec-2018].
- [40] H. S. Fairman and M. H. Brill, “The principal components of reflectances,” *Colour Res. Appl.*, vol. 29, no. 2, pp. 104–110, Apr. 2004.
- [41] “(PDF) Sensor Transforms to Improve Metamerism-Based Watermarking,” *ResearchGate*. [Online]. Available: https://www.researchgate.net/publication/228481453_Sensor_Transforms_to_Improve_Metamerism-Based_Watermarking. [Accessed: 03-Dec-2018].
- [42] C. P. Huynh and A. Robles-Kelly, “A Comparative Evaluation of Spectral Reflectance Representations for Spectrum Reconstruction, Interpolation and Classification,” in *2013 IEEE Conference on Computer Vision and Pattern Recognition Workshops*, 2013, pp. 328–335.
- [43] “Statistics of Real-World Hyperspectral Images.” [Online]. Available: <http://vision.seas.harvard.edu/hyperspec/>. [Accessed: 03-Dec-2018].
- [44] J. Cohen, “Dependency of the spectral reflectance curves of the Munsell colour chips,” *Psychon. Sci.*, vol. 1, no. 1, pp. 369–370, Jan. 1964.
- [45] G. Wong, “Snapshot hyperspectral imaging and practical applications,” *J. Phys. Conf. Ser.*, vol. 178, no. 1, p. 012048, 2009.
- [46] “SPIE | Optical Engineering | Review of snapshot spectral imaging technologies,” 20-Sep-2015. [Online]. Available: <https://web.archive.org/web/20150920195938/http://opticalengineering.spiedigitalibrary.org/article.aspx?articleid=1743003>. [Accessed: 03-Dec-2018].
- [47] D. An, J. Suo, H. Wang, and Q. Dai, “Illumination estimation from specular highlight in a multi-spectral image,” *Opt. Express*, vol. 23, no. 13, pp. 17008–17023, Jun. 2015.
- [48] T. Su, Y. Zhou, Y. Yu, X. Cao, and S. Du, “Illumination separation of non-Lambertian scenes from a single hyperspectral image,” *Opt. Express*, vol. 26, no. 20, pp. 26167–26178, Oct. 2018.